NASA Contractor Report 3753

Fracture Behavior of Unidirectional Boron/Aluminum Composite Laminates

James G. Goree and Walter F. Jones

GRANT NSG-1297
DECEMBER 1983

25th Anniversary
1958-1983

NASA

NASA Contractor Report 3753

Fracture Behavior of Unidirectional Boron/Aluminum Composite Laminates

James G. Goree and Walter F. Jones
Clemson University
Clemson, South Carolina

Prepared for
Langley Research Center
under Grant NSG-1297

National Aeronautics
and Space Administration

**Scientific and Technical
Information Branch**

1983

TABLE OF CONTENTS

ACKNOWLEDGEMENTS

The writers wish to thank the Fatigue and Fracture Branch, Materials Division of the NASA-Langley Research Center for their continued support of this study under NASA Grant NSG-1297. We are particularly grateful for the insight, interest, and assistance provided by the grant monitor Mr. Clarence C. Poe, Jr.

The second author completed much of this work while a Ph.D. student in Engineering Mechanics at Clemson. Dr. Jones is now an Assistant Professor of Engineering Science and Mechanics at the University of Tennessee in Knoxville.

LIST OF FIGURES

LIST OF SYMBOLS

A_F	Cross-sectional area of each fiber, m^2.
$A(\theta)$	Function defined in equation (29).
B_m	Coefficients of a Fourier cosine series.
COD	Crack opening displacement, m.
d	Spacing between fibers, m.
$D^2(\theta)$	Function defined in equation (23).
E_F	Young's modulus of the fiber material, Pa.
$f(\eta)$	Function defined in equation (19).
$g(\eta)$	Axial displacement difference defined in equation (36).
G_M	Shear modulus of the fiber-matrix region, Pa.
h	Shear transfer distance, m.
ℓ	Axial split length, m.
L	Total axial damage length, m.
m	Broken fiber index.
M	Index of the last constrained fiber.

n	Fiber index number.
N	Index number of the last broken fiber.
NBF	Number of fibers broken by the notch.
t	Lamina thickness, m.
T_o	Material parameter defined in equation (15), Pa.
$u(y)\|_n$	Transverse displacement of the nth fiber, m.
$v(y)\|_n$	Axial displacement of the nth fiber, m.
$V(\eta)\|_n$	Normalized axial displacement.
$\overline{V}(\eta,\theta)$	Transform function for the axial displacement as defined in equation (20).
y	Axial coordinate, m.
α	Normalized total axial damage length.
β	Normalized axial split length.
$\delta^2(\theta)$	Function defined in equation (23).
η	Normalized axial coordinate.
$\sigma_F(y)\|_n$	Axial fiber stress in the nth fiber, Pa.
$\sigma_M(y)\|_n$	Transverse stress within the matrix region bounded by the (n-1) and (n) fibers, Pa.
$\overline{\sigma}_n$	Stress concentration factor for the nth fiber.

σ_∞	Applied remote tensile stress, Pa.
$\tau(y)\|_n$	Shear stress within the fiber-matrix region bounded by the (n-1) and (n) fibers, Pa.
τ_o	Yield stress in shear for the fiber-matrix material, Pa.
$\overline{\tau}$	Normalized yield stress in shear.
$< \ >$	Unit step function.

CHAPTER I

INTRODUCTION

The desire for lighter and stronger structural materials has led to a rapidly growing use of fibrous composite materials in many modern applications. By combining the properties of more than one material having different strengths and weights, a structural member that is lighter and stronger than the isotropic material it replaces can be produced. An added benefit often gained is that due to this multiphase construction composites are frequently more insensitive to damage and damage growth than isotropic materials.

Many different types of composite materials can be found in use today such as short fiber composites, woven cloth composites, and composites with randomly placed fibers. The list of matrix materials used to support these fibers is at least as long as the list of different fibers. In advanced structures such as airframes, however, most structural members are made of multiple layers, each consisting of continuous, parallel fibers embedded in a matrix. These layers, each of which is referred to as a lamina, are bonded together to form the structural member, typically called a laminate.

By orienting these continuous fibers in specific directions the designer can adjust the material properties of the laminate to suit the loading to be encountered in use. Some composites having the predominate loading in a given direction, such as landing struts and wing panels, are often constructed of all unidirectional composite laminates. Others, which encounter a more randomly oriented load spectrum, are made by constructing a laminate from a series of properly oriented unidirectional lamina.

In addition to the fiber orientation, advanced composite materials are further grouped into two broad categories based on the type of matrix material used, these being plastic matrix composites and metal matrix composites. Unidirectional composites which have epoxy (plastic) matrices characteristically form large splits in the matrix between fibers near a defect such as a notch. Ductile metal matrix composites, on the other hand, exhibit matrix yielding between fibers near a notch instead of this splitting. It is found to be possible to have stable notch extension and broken fibers in composites which use ductile metals such as aluminum for the matrix material, presumably because of this large scale yielding. This is one question to be considered in the present study.

For both unidirectional and multidirectional composites of the type discussed above, the fundamental component is the unidirectional lamina. It is thus essential that the

behavior of the lamina be clearly understood before the fracture behavior of the multiply laminate can be described. Many of the mathematical models which have been developed consider this fundamental lamina and the present experimental study will attempt to relate the predictions of some of these models to actual laboratory measurements.

Considerable analytical work has been done in modeling the unidirectional lamina with many of the recent mathematical models developed at Clemson University by the authors [1,2]. These models, based on earlier work by Hedgepeth [3] in 1961, assume that the parallel fibers in the lamina carry all of the axial load and the matrix material transmits load to adjacent fibers by shear. An influence function technique was used by Hedgepeth to solve the lamina equilibrium equations. In later work, Hedgepeth and Van Dyke [4] were able to include matrix yielding and splitting in their model, although they were restricted by the solution technique to only one broken fiber in the lamina. Later models, such as the model of Zweben [5], extended Hedgepeth's model to include an arbitrary number of broken fibers while still allowing for matrix damage. Zweben, however, simplified the model considerably by grouping the fibers in three regions, one including all of the broken fibers, one having unbroken fibers which are influenced by the notch, and one group of unbroken fibers which are not influenced by the defect.

A limited amount of experimental results was available at the time of publication of [1], with perhaps the most complete being that of Awerbuch and Hahn [6] using narrow unidirectional boron/aluminum panels. These center-notched panels were loaded to failure so that their notched strengths could be determined. Extensive monitoring of the crack opening displacement (COD) was performed during the tests, along with some observations concerning the stable notch extension and matrix damage. This laminate damage was monitored through the use of radiographs and photomicrographs. The COD, defined as twice the vertical displacement of the center fiber, was monitored through the use of an interferometric displacement gage.

Awerbuch and Hahn were able to predict the load-COD curves using a simplified analytical model which could account for some crack-tip yielding in the matrix. Results for a narrow range of initial notch widths were presented along with some interpretation of the relation between the observed failure modes and deformation characteristics. All of the tests performed by Awerbuch and Hahn, however, were carried out using narrow, 25.4 mm wide specimens. A finite width correction factor was used in the study to allow the predicted stresses for the infinite panel to be compared with the narrow specimens. These investigators assumed that the finite width correction factors available for isotropic plates would be applicable to their fibrous composite

specimens. But even with the finite width correction factors, these investigators were limited to notch widths of 12.7 mm (roughly 71 broken fibers) or less because of the narrow specimen width. All of the specimens used in the experiments were eight-ply; thus nothing was said concerning the effect of laminate thickness on the damage growth and failure mechanisms.

Grandemange and Street [7] performed tests on double edge-notched boron/aluminum panels in an early attempt to investigate fracture mechanisms in fibrous composite materials. Their investigation included unidirectional laminates having a reasonably wide range of thicknesses, but a very narrow range on notch widths. The suggestion was made by these authors that the thickness of a specimen did affect the notched strength of an edge-notched panel. However, the strength of a panel having a given notch width varied only 10 percent over the entire range of thicknesses tested. It is clear that a much wider range of notch widths must be tested before the thickness effect can be thoroughly explained.

A detailed study of fracture of boron/aluminum laminates containing unidirectional and $\pm 45^{\circ}$ fibers is presented by Poe and Sova in [8]. Reedy [9] considered thick (28 ply) unidirectional laminates and suggested in his paper that the thick specimens he used for his experiments should have been more notch sensitive than monolayer panels which he modeled

analytically. Yet in the results published by Reedy, the monolayer model predictions appeared to agree with the experimental results for the thick specimens reasonably well. However, as in the work of Awerbuch and Hahn [6], only one thickness was used in the experiments, and the question of thickness effect on fracture behavior was not addressed.

Reedy also noted the large amounts of longitudinal matrix yielding predicted by the analytical model, and attempted to measure this yielding in the test laminate at various load levels using strain gage rosettes mounted at various points on the panel. The yield region predicted analytically appeared to agree fairly well with the strains measured in the laboratory, but since the strain gages used were 3 mm in width and thus covered nearly 20 fibers, there is some question as to the accuracy of these readings. The gages were clearly connected to some fibers that were broken and some that were not, thus the output of the gages needs a more careful analysis than is available from standard stress-strain relations.

Other attempts have been made to describe the damage growth in fibrous composite panels during fracture. Rollins [10] and Grenis and Levitt [11] attempted to relate the fiber breaks during a loading cycle to the acoustic emissions detected by transducers mounted on the specimens. It was found that the acoustic emission associated with a fiber break could be detected since these emissions were quite

energetic compared to those caused by matrix yielding and splitting. The points at which the various damage modes would occur in the loading sequence and the damage necessary to break a fiber were, however, never adequately explained.

The need for additional experimental results became apparent during the final stages of the analytical modeling by Dharani, Jones, and Goree [12]. It was felt that a clear and logical description of the damage growth and fracture behavior in unidirectional laminates was provided by the micromechanical model. No detailed experimental studies describing this damage growth and fracture behavior were available, however, and much of the motivation for the work to be presented in this study was the need to observe very carefully the damage growth in a unidirectional composite and to compare the results with those predicted by the analysis from [1] and [2].

The analysis given in [1] and [2] is valid for both brittle (plastic) matrix and ductile (metal) matrix composites with the fracture behavior of a brittle matrix laminate such as graphite/epoxy being relatively simple to describe. At very low loads, the brittle matrix splits at the ends of the notch with the splits soon reaching the ends of the specimen for little increase in load. The specimen then fails in net-section tension with essentially no stress concentration effect other than the loss in area due to the notch.

On the other hand the ductile matrix composite such as boron/aluminum exhibits large longitudinal yielding and transverse broken fibers and is thus much more complicated and difficult to model accurately. It was thus proposed that an experimental investigation be conducted using unidirectional boron/aluminum composite panels. It was known from past experience that finished boron/aluminum panels were available that possessed very uniform fiber size and spacing, and that the high quality of these finished specimens would make the tests much more valid. Very detailed records would be kept concerning the amount of matrix yielding or splitting as well as the number of broken fibers present in the laminate at various points in the loading. The results of these tests could then be compared to the damage zones predicted by the mathematical model.

Unlike earlier tests, this proposed investigation would incorporate specimens of various widths and thicknesses (numbers of plies). Through the use of wider specimens, a much broader range of initial notch widths could be investigated than that of Awerbuch and Hahn [6]. These wider notchs could be cut in much wider specimens, reducing the need for the use of the finite width correction factor used in [6]. If the notchs in the proposed tests grew such that a finite width correction factor was needed, a much more accurate solution developed by Dharani [13] for the unidirectional composite laminate could be used. Also, the ques-

tion of thickness effect on damage growth proposed in [7] and [9] could conceivably be answered through the use of specimens having numbers of plies ranging from one to eight.

As in some earlier investigations, the number of broken fibers present in the laminate at various load levels could be determined using X-rays to penetrate the specimens. The X-ray records would be obtained using a portable X-ray source which would allow radiography while the specimen is in the testing machine under load, rather than unloading and placing the specimen in an X-ray cabinet as was done in [6]. It was hoped that photoelastic coatings could be used to monitor the amount of matrix yielding present in the laminates, since this method had been used by others such as Yeow, Morris, and Brinson [14]. But since the thinnest available coatings were thicker than many of the proposed specimens, it was clear after some investigation that the photoelastic coating would not be able to detect the yielding between fibers with the desired accuracy.

It was thus decided that a brittle lacquer surface coating would be the best method by which to measure the yielding present in the matrix between the fibers. It had already been shown by Chaturvedi and Agarwal [15] that a brittle coating would crack at a given threshold strain in a direction perpendicular to the maximum principal strain even on a unidirectional composite material. Because the brittle coating can be applied in a very thin layer it is sensitive

to local effects which occur over dimensions on the order of the fiber spacing. Thus the location and orientation of the cracks on the specimens in the proposed tests should enable the investigators to determine the extent of yielding present at selected load levels.

One aspect of damage growth in composites that has not been investigated thoroughly is the effect of different matrix properties on the damage growth and fracture behavior. Only some very recent work by Reedy [16,17] has attempted to determine the result of using a stronger or weaker aluminum matrix material to hold the fibers. This work was again limited in scope, using only one notch width and narrow, 25.4 mm wide specimens. It was thus suggested that some of the proposed specimens have an aluminum matrix that had been heat-treated to a T6 condition instead of the fully annealed 6061 aluminum matrix in the remainder of the panels. This stronger matrix should alter the fracture behavior, since it is through the matrix that the load is transferred from the broken fibers to the remaining unbroken ones. Furthermore, unlike the work in [16] and [17], a wide range of notch widths and panel thicknesses could be tested to provide much more information about the effect of matrix properties.

A series of tests using a wide range of specimens having different notch widths, overall widths, numbers of plies, and matrix properties was thus proposed. A complete

description of the materials and test procedure used in the tests is described in the next section.

Certain commercial materials are identified in this paper in order to specify adequately which materials were investigated in the research effort. In no case does such identification imply recommendation or endorsement of the product by NASA, nor does it imply that the materials are necessarily the only ones or the best ones available for the purpose.

CHAPTER II

EXPERIMENTAL PROCEDURE

Materials

The specimens used in this investigation were all unidirectional boron/aluminum composite panels of various widths and thicknesses. The panels, manufactured by Amercom, Inc. in Chatsworth, California, consisted of 0.142 mm (5.6 mil) diameter boron fibers in a 6061 aluminum matrix. Some of the panels were heat-treated after the initial manufacture such that the aluminum matrix would possess the properties of standard 6061-T6 aluminum instead of an annealed 6061-0 aluminum matrix. Equal numbers of one-, two-, four-, and eight-ply specimens were fabricated, with a thickness of approximately 0.178 mm per ply. A complete listing of the test specimens used in this study can be found in Table (I). It should be noted that a set of specimens is defined as one single-ply specimen, one two-ply specimen, one four-ply specimen, and one eight-ply specimen, all having the same notch size and laminate width. Slightly thicker aluminum foil was used on the single-ply panels in order to increase out-of-plane stiffness. Thus the fiber volume fraction for the single-ply panels was around 35 percent, while the volume fraction for all other specimens was very close to 50 percent.

Table I. List of specimens used in experimental investigation.

Panel Width (W)	Notch Width (2a)	Matrix Temper*
25.4 mm	1.59 mm	1 set 6061-0
25.4 mm	3.18 mm	1 set 6061-0, 1 set 6061-T6
25.4 mm	4.76 mm	1 set 6061-0, 1 set 6061-T6
25.4 mm	6.35 mm	1 set 6061-0
50.8 mm	1.59 mm	1 set 6061-0
50.8 mm	6.35 mm	1 set 6061-0, 1 set 6061-T6
50.8 mm	9.52 mm	1 set 6061-0, 1 set 6061-T6
50.8 mm	15.9 mm	1 set 6061-0
73.1 mm	3.18 mm	1 set 6061-0
73.1 mm	12.7 mm	1 set 6061-0, 1 set 6061-T6
73.1 mm	15.9 mm	1 set 6061-0, 1 set 6061-T6
73.1 mm	19.1 mm	1 set 6061-0
101.6 mm	15.9 mm	1 set 6061-0
101.6 mm	19.1 mm	1 set 6061-0, 1 set 6061-T6
101.6 mm	22.2 mm	1 set 6061-0
101.6 mm	25.4 mm	1 set 6061-0, 1 set 6061-T6

*One set equals one single-ply panel, one two-ply panel, one four-ply panel, and one eight-ply panel.

Specimens having widths of 25.4, 50.8, 73.1, and 100.6 mm were cut from large panels obtained from the manufacturer. These cuts were parallel to the fibers and were made with a diamond saw. The edges were later ground to ensure minimum surface damage due to cutting. All of these experimental specimens were approximately 30 cm in length. Center notches of various widths were then introduced by E.D.M. (Electrostatic Discharge Machining). Normally the width of the notch did not exceed one-quarter of the overall width of the panel.

Finally, the specimens were carefully cleaned and polished to eliminate further the possibility of surface flaws that might affect the testing. Two strain gages were mounted on each specimen at points well below the notch so that the remote strain could be measured and recorded. The strain gages also enabled the experimenters to determine if the panel was indeed being subjected to a uniform remote stress. The last step in the preparation was to epoxy aluminum doublers to each end of each panel so that the testing machine grips would not damage the ends of the specimens. A representation of a typical test specimen is shown in Figure (1).

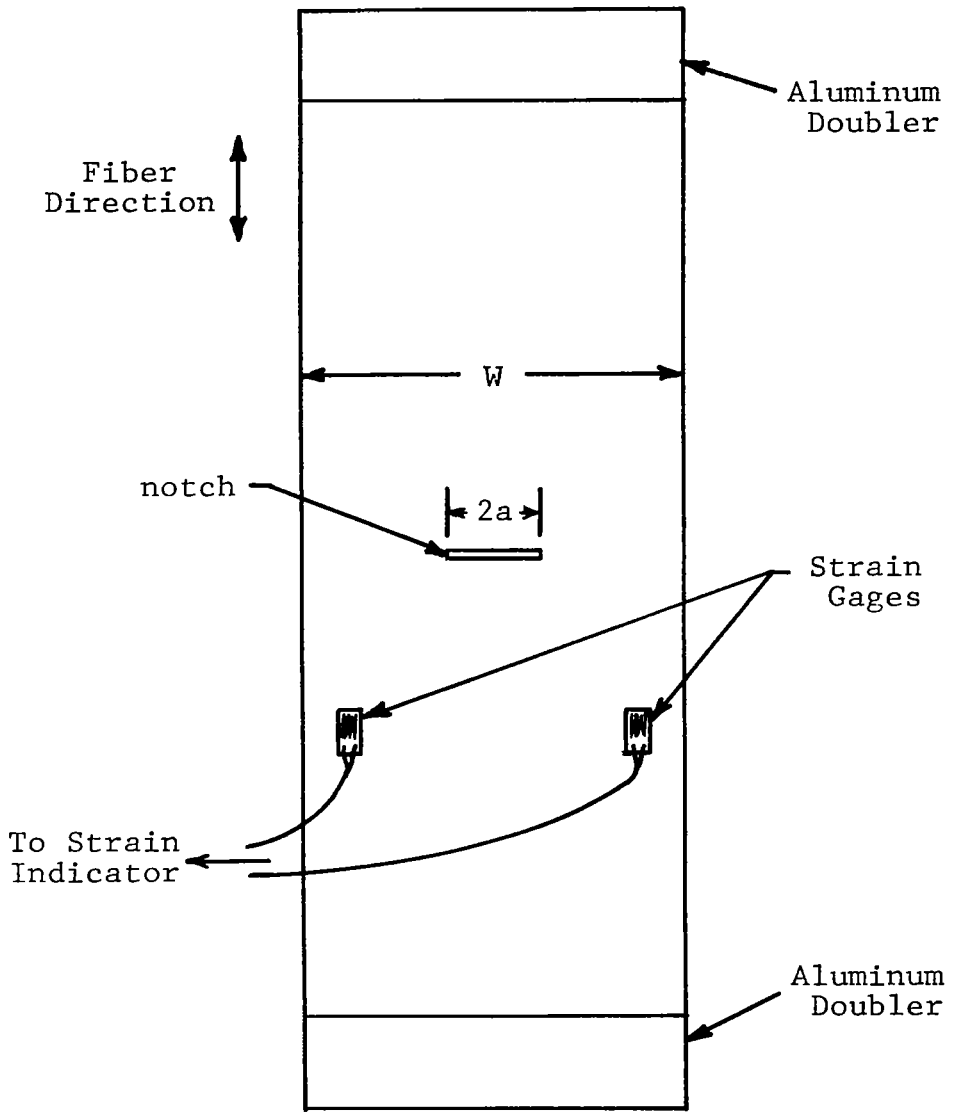

Figure 1. Typical Test Specimen.

Radiographic Technique

The radiographs used in these experiments were taken by exposing the specimens to low level X-rays for a specified amount of time. The source of these X-rays was a Model MTK 140Be X-ray machine manufactured by the Philips Company of West Germany. This is a portable unit and has the significant advantage that the radiographs can be taken while the specimens are in the testing machine and under load.

Much time and experimentation was involved in determining the best exposure time and film to focus distance (FFD) for each specimen thickness. The X-ray source used was capable of varying both the voltage and the current which produce the X-rays. It was quickly discovered that each of the variable parameters must be chosen correctly if an acceptable degree of resolution was to be realized. Many test shots were taken of a given laminate at various currents, voltages, distances, and exposure times. The negatives from these tests were then used to make radiographic prints to determine the correct exposure parameters.

It was found that the single-ply and the two-ply specimens could be x-rayed at an FFD of 50 cm with a current of 5 mA. On the thicker four-ply and eight-ply specimens, the best radiographs were taken at an FFD of 80 cm with a current of 5 mA. The higher FFD serves to place the X-ray focal point further away from the object, thus making the X-ray seem more like a point source; that is, the rays are

almost parallel when they strike the specimen. The voltages and exposure times used varied depending on the thickness of the panel. A graph of current-exposure time product versus the specimen thickness for various voltages is shown in Figure (2). Any X-ray exposure taken with data from this graph was found to give excellent resolution on the radiographic print. As an example, the four-ply panels, with a thickness of 0.712 mm, were x-rayed for three minutes at 30 kV with a tube current of 5 mA, giving the required product of fifteen mA-min as determined from the graph.

The image produced from the X-ray is captured by simply securing a sheet of Type 55 Polaroid film to the back of the specimen at various load levels during the test. It must be emphasized that the film is not placed in a film holder, such as a Polaroid Model 455, which has an intensifying screen. The intensifying screen is not needed for this type of exposure; in fact, use of the film holder actually made the resolution worse on the radiograph. Thus the sheet of film is taped to the specimen encased only in the light paper provided by the manufacturer.

The number of X-rays absorbed or transmitted by a material is dependent on its atomic number. For example, an X-ray of a graphite/epoxy panel will produce no distinct fiber pattern on a radiograph since both the fibers and the matrix are composed of essentially carbon. In fact, boron (atomic number = 5) and aluminum (atomic number = 13)

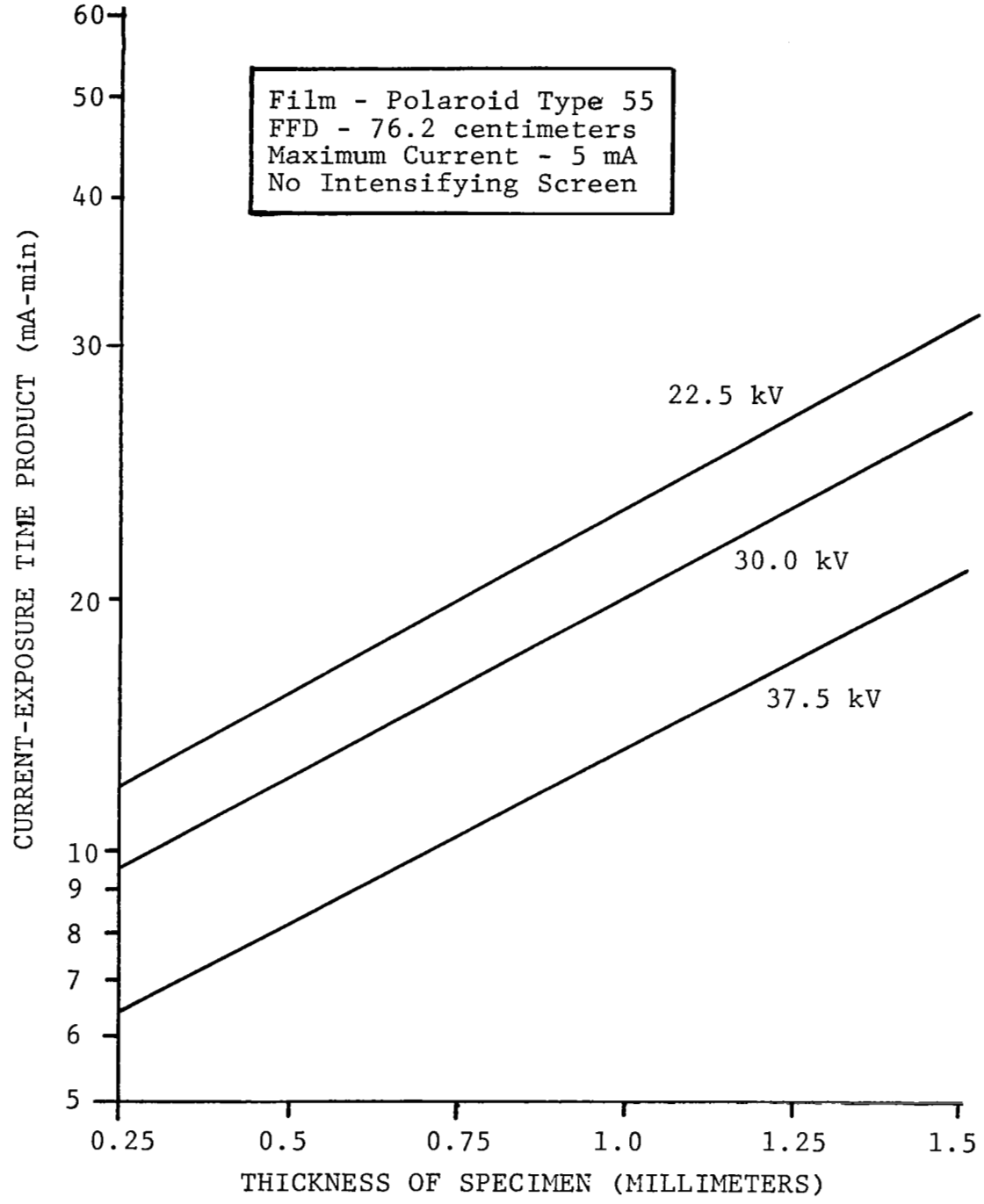

Figure 2. X-ray Exposure Chart.

transmit amounts of X-rays that are so close that it is difficult to distinguish between the two of them on a radiograph. The boron fibers commonly available, however, are manufactured by depositing the boron on a thin tungsten filament, and this tungsten (atomic number = 74) core will appear as a very dark black line on a radiograph. Thus the tungsten core of each fiber can be easily identified on the radiographic print.

A typical radiograph of a single-ply boron/aluminum panel is shown in Figure (3). The dark lines are the tungsten cores of the boron fibers, while the light area around these cores is the boron itself. The medium gray area between the fibers is the aluminum matrix. Thus as the specimen is loaded and fibers begin to break, it is a simple matter to count the number of broken fibers ahead of the notch at various load levels. It is also possible to obtain a very accurate measure of the crack opening displacement (COD) by merely scaling the appropriate fiber displacements directly from the radiographic print made in the darkroom. COD measurements were also taken with a clip gage which is specifically designed to measure crack opening displacement for notched specimens. The output of this gage can be carefully calibrated such that the strain output from the gage can be converted to a displacement in millimeters.

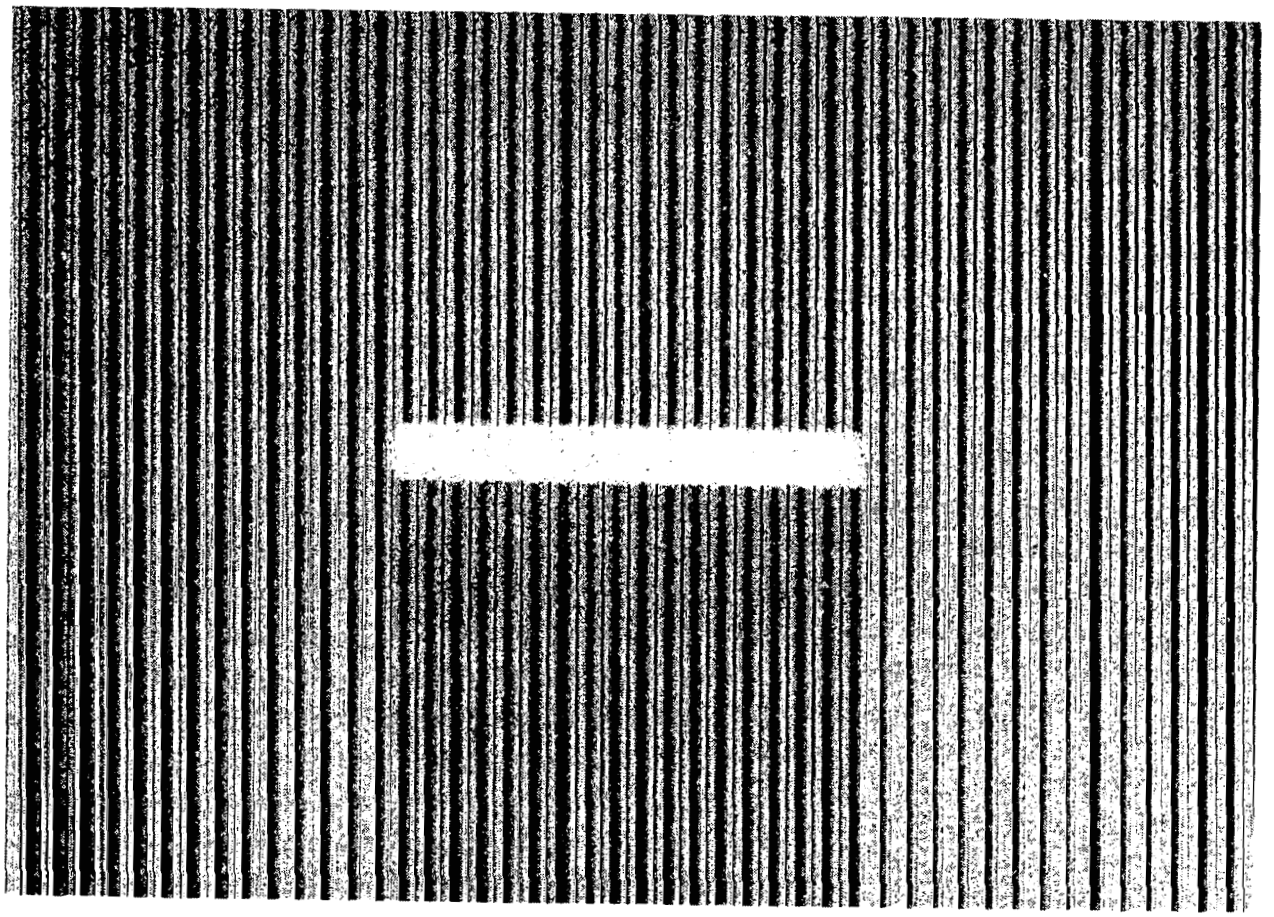

Figure 3. Radiograph of single-ply boron/aluminum composite panel.

Brittle Coating Technique

A brittle lacquer was applied to each specimen to measure the amount of longitudinal yielding between the last broken fiber and the first unbroken fiber at the end of the notch. The brittle lacquer used in these tests was the commercially available Tenslac, manufactured by the Measurements Group in Raleigh, North Carolina. This lacquer will crack when a certain threshold strain is reached in the boron/aluminum panel. This threshold strain can be affected by the coating thickness as well as the temperature and humidity of the test environment.

As previously mentioned, each specimen was carefully cleaned and polished to provide a specimen surface that was free from surface flaws. The polished surface also provided a highly reflective surface below the brittle lacquer. This made the cracks reflect the light much more clearly so that the extent of cracks could be observed and photographed. It was noted that the ability to see a given crack in the coating was strongly affected by the angle at which the light approached the surface of the specimen. The cracks could not be seen if the light approached the surface along a line normal to that surface. Rather, the best results were obtained when the approaching light made an angle of approximately 30 degrees with the surface normal.

The brittle lacquer was applied to each specimen in up to twenty very thin coats to minimize bubbling and provide

the desired "orange-peel" finish. The final thickness of the lacquer coating was approximately 0.075 millimeters which gave a threshold strain of 1200 to 1800 microstrain depending on test conditions. The threshold strain for each specimen tested was measured by using strain gages that were mounted on each panel on the opposite side from the coating. The remote strain at which the cracks appeared directly opposite the gages was taken as the threshold strain for that specimen. This procedure eliminated the need of preparing calibration bars or even assuming a nominal threshold strain. Rather, the exact threshold strain at the time of the test for each specimen could be accurately measured and recorded. The brittle lacquer coating also gave a very clear picture of the stress state at the remote sections of the specimens. If the remote stress was truly uniform, the cracks in the coating would be straight and perpendicular to the fibers outside the region affected by the defect. The output from the strain gages was measured through the use of a Vishay VE-20 Strain Indicator and a Vishay VE-21 Switching and Balancing Unit.

General Testing Procedure

After allowing the brittle coating to dry for 18 to 24 hours, the specimens were loaded statically with a Baldwin tensile testing machine. A photograph of the test set-up is shown in Figure (4). A baseline X-ray was taken of each panel before the loading cycle was begun so that any damage caused by machining or polishing could be noted. Then as the loading sequence began, photographs were taken of the cracks in the coating at various load intervals with a Nikon FM camera equipped with a close-up lens. A bright light was used to illuminate the crack pattern so that a small lens aperture could be set to increase depth-of-field.

X-rays were taken in the manner described earlier at selected load levels so that the number of broken fibers in the specimen could be determined. The majority of the X-ray exposures were taken in the last half of the load cycle since the first fiber breaks occurred at approximately 50 percent of the failure load. The crack opening displacement was measured both from the radiographs and with a clip gage specifically designed to measure COD.

A total of ten to twelve X-rays and twelve to fifteen brittle coating photographs were made during each test. The strain output from each gage was recorded at numerous load levels as were the load readings from the Baldwin machine. This testing procedure was repeated for boron/aluminum panels of many different widths, thicknesses, and initial notch widths.

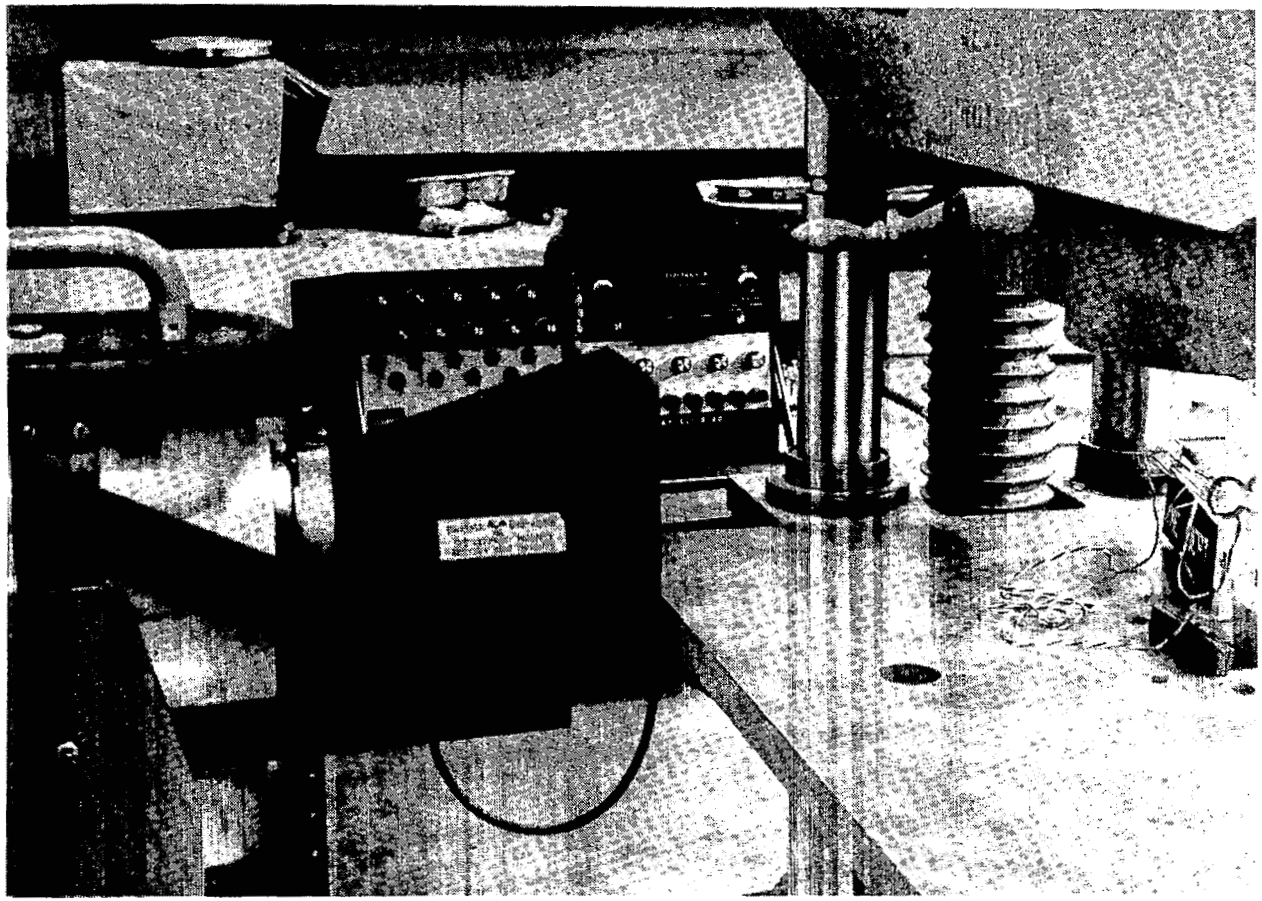

Figure 4. Experimental Test Set-up.

CHAPTER III

ANALYSIS

Mathematical Model Description

Though the main emphasis of this paper is the experimental investigation, it is important that the mathematical model which motivated the present study and the assumptions made therein are clearly understood. Thus at this point, a brief description of the equations involved in the derivation of the shear-lag model will be presented. Following Goree and Gross [1], the laminate is modeled as a two-dimensional region, having a single row of parallel, identical, equally spaced fibers, separated by matrix as shown in Figure (5). The initial damage is taken to consist of an arbitrary number of broken fibers such that all breaks lie along the x-axis. The longitudinal matrix damage is introduced at the end of the initial notch as in [1]. The additional notch tip transverse damage consists of an arbitrary number of broken fibers which are constrained by the adjoining matrix and/or the unbroken fibers through the thickness. These fibers in the transverse damage zone will be referred to as constrained fibers. It is mathematically untractable to account precisely for the distribution of fiber damage occurring in the region ahead of the notch. The model assumes that all the breaks occur on the x-axis and accounts

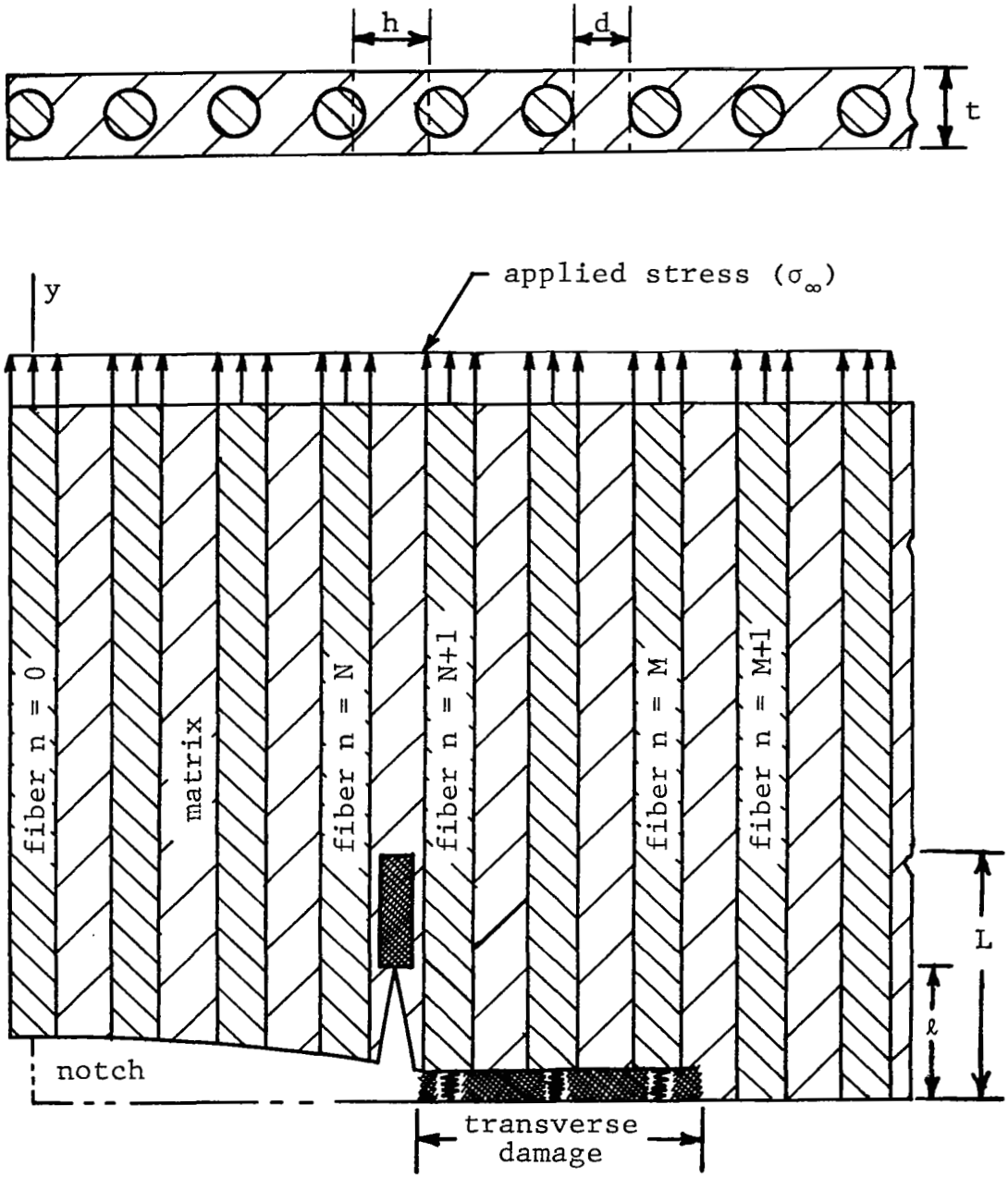

Figure 5. Two-dimensional unidirectional lamina with broken fibers, longitudinal matrix splitting and yielding, and transverse fiber and matrix damage (first quadrant).

for the reduction in stiffness of the transverse damage zone by defining a stiffness coefficient, γ, such that

$$\gamma = \frac{\text{stress in the constrained fiber}}{\text{stress in the first unbroken fiber}} .$$

The free-body diagram shown in Figure (6) is considered with additional conditions for the last broken fiber, denoted by n = N, and y $\leq$ L, to account for the longitudinal damage taken as

$$\tau|_{N+1} = - \tau_o \langle y - \ell \rangle, \qquad (1)$$

where

$$\langle y - \ell \rangle = 1, \quad y \geq \ell, \text{ and}$$
$$\langle y - \ell \rangle = 0, \quad y < \ell. \qquad (2)$$

L is defined as the total damaged length (see Figure 5), ℓ as the split length, and τ_o as the matrix yield stress. Yielding is assumed to occur when the matrix reaches the yield strain, γ_o. Splitting occurs at a multiple of γ_o as given by the particular matrix material.

The equilibrium equations in the longitudinal and transverse directions for all fibers n, with the exception of N and N + 1 when y $\leq$ L, are then

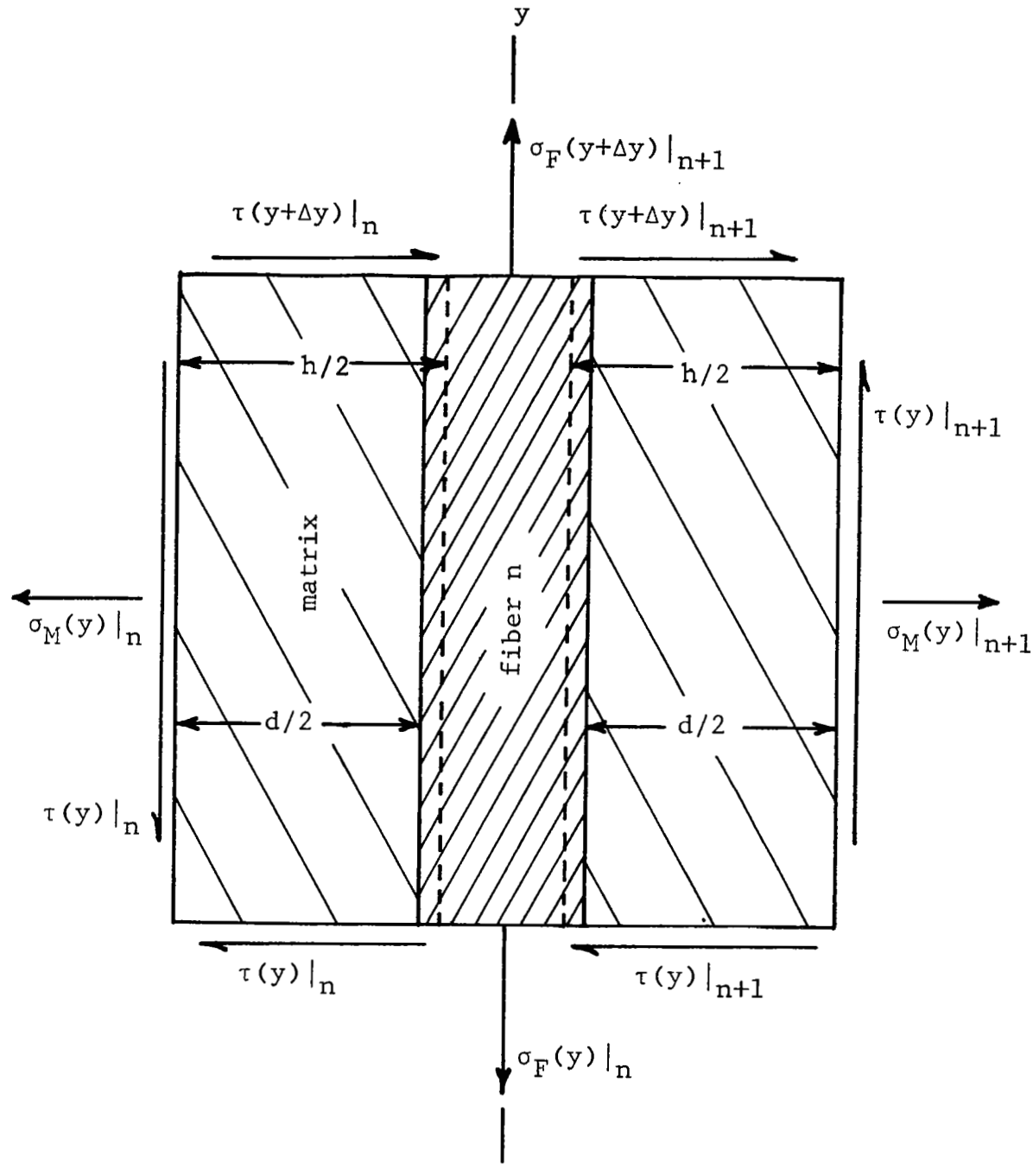

Figure 6. Free-body diagram of a typical element.

$$\frac{A_F}{t}\frac{d\sigma_F|_n}{dy} - \tau|_{n+1} - \tau|_n = 0, \qquad (3)$$

and

$$\sigma_M|_{n+1} - \sigma_M|_n + \frac{h}{2}\frac{d}{dy}\{\tau|_{n+1} + \tau|_n\} = 0. \qquad (4)$$

For fiber N, when $y \le L$, $\tau|_{N+1} = -\tau_o \langle y - \ell \rangle$, and the equilibrium equations are

$$\frac{A_F}{t}\frac{d\sigma_F|_N}{dy} - \tau_o\langle y - \ell\rangle - \tau|_N = 0, \qquad (5)$$

and

$$\sigma_M|_{N+1} - \sigma_M|_N + \frac{h}{2}\frac{d}{dy}\{-\tau_o\langle y - \ell\rangle + \tau|_N\} = 0. \qquad (6)$$

For fiber N + 1, when $y \le L$, $\tau|_{N+1} = -\tau_o \langle y - \ell \rangle$, and the equilibrium equations are

$$\frac{A_F}{t}\frac{d\sigma_F|_{N+1}}{dy} + \tau|_{N+1} + \tau_o\langle y - \ell\rangle = 0, \qquad (7)$$

and

$$\sigma_M|_{N+2} - \sigma_M|_{N+1} + \frac{h}{2}\frac{d}{dy}\{\tau|_{N+2} - \tau_o\langle y - \ell\rangle\} = 0. \qquad (8)$$

The stress-displacement relations common to the shear-lag assumption,

$$\sigma_F|_n = E_F \frac{dv_n}{dy}, \tag{9}$$

$$\tau|_{n+1} = G_M (v_{n+1} - v_n)/h \text{ , and} \tag{10}$$

$$\sigma_M|_{n+1} = E_M (u_{n+1} - u_n)/h \text{ ,} \tag{11}$$

are introduced into the equilibrium equations, leading to the replacement of the three stress quantities by the axial and transverse displacements. These assumptions, however, simplify the equilibrium equations by removing the transverse displacement dependence from the longitudinal equilibrium equation. The fiber stress and the matrix shear stress can then be determined without solving the transverse equilibrium equation. Only the longitudinal equilibrium equation will now be considered. For all fibers, except N and N+1 where $y \leq L$, the longitudinal equilibrium equation becomes

$$\frac{E_F A_F h}{G_M t} \frac{d^2 v_n}{dy^2} + v_{n+1} - 2v_n + v_{n-1} = 0. \tag{12}$$

For fiber N where $y \leq L$,

$$\frac{E_F A_F h}{G_M t} \frac{d^2 v_N}{dy^2} + v_{N-1} - v_N - \frac{h}{G_M} \tau_o \langle y - \ell \rangle = 0. \tag{13}$$

For fiber N+1 where $y \leq L$,

$$\frac{E_F A_F h}{G_M t} \frac{d^2 v_{N+1}}{dy^2} + v_{N+2} - v_{N+1} + \frac{h}{G_M} \tau_o \langle y - \ell \rangle = 0. \tag{14}$$

It is convenient to use the non-dimensional forms of Equations (12), (13), and (14). Noting the coefficient of the second derivative term in the above equations, define

$$y = \left[\frac{E_F A_F h}{G_M t}\right]^{\frac{1}{2}} \eta \quad \text{and} \quad \sigma_F|_n = \sigma_\infty \bar{\sigma}_n \ .$$

The other required quantities, such as the axial displacement (v_n) and the matrix yield stress (τ_o), can also be written in their non-dimensional forms. From the definitions of y and $\sigma_F|_n$ it follows that

$$\left.\begin{aligned}
&v_n = \sigma_\infty \left[\frac{A_F h}{E_F G_M t}\right]^{\frac{1}{2}} V_n = \frac{\tau_o h}{\bar{\tau} G_M} V_n, \text{ where} \\
&\tau_o = \sigma_\infty \left[\frac{G_M A_F}{E_F h t}\right]^{\frac{1}{2}} \bar{\tau} \text{ or } \sigma_\infty = \frac{\tau_o}{\bar{\tau}} \left[\frac{E_F h t}{G_M A_F}\right]^{\frac{1}{2}} = \frac{T_o}{\bar{\tau}}, \\
&\sigma_F|_n = \sigma_\infty \frac{dV_n}{d\eta} = \frac{\tau_o}{\bar{\tau}} \left[\frac{E_F h t}{G_M A_F}\right]^{\frac{1}{2}} \frac{dV_n}{d\eta}, \\
&\tau_n = \sigma_\infty \left[\frac{G_M A_F}{E_F h t}\right]^{\frac{1}{2}} \{V_n - V_{n-1}\} = \frac{\tau_o}{\bar{\tau}} \{V_n - V_{n-1}\}, \\
&L = \left[\frac{E_F A_F h}{G_M t}\right]^{\frac{1}{2}} \alpha, \text{ and } \ell = \left[\frac{E_F A_F h}{G_M t}\right]^{\frac{1}{2}} \beta.
\end{aligned}\right\} \quad (15)$$

The quantities n, $\bar{\tau}$, $\bar{\sigma}_n$, V_n, α, and β are non-dimensional, whereas E_F, A_F, t, L, and ℓ represent the actual fiber modulus, fiber area, lamina thickness, and damage zone dimensions, respectively.

The resulting equilibrium equations in non-dimensional form are given by

$$\frac{d^2V_n}{d\eta^2} + V_{n+1} - 2V_n + V_{n-1} = 0, \tag{16}$$

$$\frac{d^2V_N}{d\eta^2} + V_{N+1} - 2V_N + V_{N-1} = - f(\eta), \text{ and} \tag{17}$$

$$\frac{d^2V_{N+1}}{d\eta^2} + V_{N+2} - 2V_{N+1} + V_N = f(\eta). \tag{18}$$

where $f(\eta)$ is a new unknown function such that

$$f(\eta) = V_N - V_{N+1} - \bar{\tau}_o \langle \eta - \beta \rangle, \quad \eta < \alpha, \text{ and}$$
$$f(\eta) = 0, \qquad \eta \geq \alpha. \tag{19}$$

These differential-difference equations may be reduced to differential equations by introducing the even valued transform as

$$\bar{V}(\eta,\theta) = V_0(\eta)/2 + \sum_{n=1}^{\infty} V_n(\eta) \cos(n\theta), \tag{20}$$

from which

$$V_n(\eta) = \frac{2}{\pi} \int_0^{\pi} \bar{V}(\eta,\theta) \cos(n\theta) d\theta. \tag{21}$$

Making use of the above transformation and the orthogonality property of the circular functions, the three

equilibrium equations may be written as one equation valid for all values of n and η as

$$\frac{2}{\pi}\int_0^{\pi}\{\frac{d^2\overline{V}}{d\eta^2} - 2[1 - \cos(\theta)]\overline{V}\}\cos(n\theta)d\theta = \frac{2}{\pi}X$$

$$<\alpha-\eta>\int_0^{\pi} f(\eta)\{\cos[(N+1)\theta] - \cos(N\theta)\}\cos(n\theta)d\theta. \qquad (22)$$

This equation is of the form

$$\frac{2}{\pi}\int_0^{\pi} F(\eta,\theta)\cos(n\theta)d\theta = 0 \qquad \text{for all } \eta \text{ and } n.$$

Noting the definition of $\overline{V}(\eta,\theta)$ in Equations (20) and (21) it is seen that the function $F(\eta,\theta)$ is even valued in θ and therefore, if the integrand is to vanish for all η, the function $F(\eta,\theta)$ must be zero. The single equation specifying $\overline{V}(\eta,\theta)$ is then

$$\frac{d^2\overline{V}}{d\eta^2} - \delta^2\overline{V} = - <\alpha-\eta> D^2 f(\eta), \qquad (23)$$

where

$$\delta^2 = 2[1 - \cos(\theta)] = 4\sin^2(\theta/2), \text{ and}$$
$$D^2 = \cos(N\theta) - \cos[(N+1)\theta].$$

The solution to the problem of vanishing stresses and displacements at infinity and uniform compression on the ends of the broken fibers will now be sought. The complete solution is obtained by adding the results corresponding to uniform axial stress and no broken fibers to the following solution. The appropriate boundary conditions are thus

$$V_n = 0 \qquad \text{as} \qquad \eta \to \infty, \tag{24}$$

$$\frac{dV_n}{d\eta} = 0 \qquad \text{as} \qquad \eta \to \infty, \text{ and} \tag{25}$$

$$V_n = 0 \qquad \text{for } \eta = 0, \text{ for unbroken fibers,} \tag{26}$$

$$\frac{dV_n}{d\eta} = \overline{\sigma}_n = -1, \text{ for broken fibers (n=0 to n=N),} \tag{27}$$

$$\frac{dV_n}{d\eta} = -1 + \gamma \frac{dV_{M+1}}{d\eta}, \text{ for constrained fibers (n=N+1 to n=M).} \tag{28}$$

The complete solution to Equation (23) satisfying vanishing stresses and displacements at infinity is given by

$$\overline{V}(\eta,\theta) = A(\theta)\, e^{-\delta\eta} + \frac{D^2}{\delta} \int_{\eta}^{\alpha} \{\sinh[\delta(\eta-t)]\langle\alpha-t\rangle\, f(t)dt, \tag{29}$$

where the unknown functions are $A(\theta)$ and $f(t)$. The remaining boundary conditions give

$$\frac{dV_n(0)}{d\eta} = \frac{2}{\pi}\int_0^{\pi}\{-\delta A(\theta) + D^2\int_0^{\alpha}\cosh(\delta t)f(t)dt\}\cos(n\theta)d\theta = -1,$$

$$n = 1, 2, \ldots, N, \qquad (30)$$

$$\frac{dV_n(0)}{d\eta} = \frac{2}{\pi}\int_0^{\pi}\{-\delta A(\theta) + D^2\int_0^{\alpha}\cosh(\delta t)f(t)dt\}\ X$$

$$\cos(n\theta)d\theta = -1 + \overline{\delta\sigma_F}|_{M+1},\ n = N+1, \ldots, M, \qquad (31)$$

$$V_n(0) = \frac{2}{\pi}\int_0^{\pi}\{A(\theta) - \frac{D^2}{\delta}\int_0^{\alpha}\sinh(\delta t)f(t)dt\}\cos(n\theta)d\theta = 0,$$

$$n = M+1, \ldots, \infty. \qquad (32)$$

Equation (32) is solved exactly by taking

$$A(\theta) - \frac{D^2}{\delta}\int_0^{\alpha}\sinh(\delta t)f(t)dt = \sum_{m=0}^{\infty} B_m\cos(m\theta) \qquad (33)$$

where m is a broken fiber index and the B_m are constants. The stress in the first unbroken fiber, $\overline{\sigma_F}|_{M+1}$ is given by

$$\frac{dV_{M+1}}{d\eta} = \frac{2}{\pi}\int_0^{\pi}\{-\delta A(\theta) + D^2\int_0^{\alpha}\cosh(\delta t)f(t)dt\}\ X$$

$$\cos[(M+1)\theta]d\theta = -1 + \overline{\sigma_F}|_{M+1}. \qquad (34)$$

Using Equations (33) and (34) in Equations (30) and (31), $A(\theta)$ and $\overline{\sigma_F}|_{M+1}$ may be eliminated, resulting in M+1 algebraic equations for M+1 constants B_m in terms of $f(\eta)$ which is, as yet, unknown. For longitudinal matrix damage,

Equations (30) and (31) must be supplemented by the conditions that

$$f(\eta) = g(\eta) - \overline{\tau} \langle \eta - \beta \rangle, \qquad \eta < \alpha, \text{ and} \tag{35}$$

$$g(\alpha) = \overline{\tau}\ , \tag{36}$$

where

$$g(\eta) = V_N - V_{N+1}.$$

From Equations (28) and (33), $A(\theta)$ may be eliminated to obtain $\overline{V}(\eta,\theta)$ in terms of constants B_m and the unknown function $f(t)$. Recalling the relation between $\overline{V}(\eta,\theta)$ and $V_n(\eta)$, an expression can be obtained for the axial fiber displacement $V_n(\eta)$ as

$$V_n(\eta) = \frac{2}{\pi} \int_0^{\pi} e^{-\delta\eta} \sum_{m=0}^{M} B_m \cos(m\theta)\cos(n\theta)\,d\theta$$

$$+ \frac{1}{2} \int_0^{\alpha} f(t) \{C_n(|t-\eta|) - C_n(t+\eta)\}\,dt, \tag{37}$$

where

$$C_n(\xi) = \frac{2}{\pi} \int_0^{\pi} \frac{D^2}{\delta} e^{-\delta\xi} \cos(n\theta)\,d\theta.$$

Equations (30) and (31) then become

$$\frac{2}{\pi}\int_0^{\pi}\{-\delta\sum_{m=0}^{M}B_m\cos(m\theta) + D^2\int_0^{\alpha}e^{-\delta t}g(t)dt$$

$$- D^2\frac{\tau}{\tau}\int_{\beta}^{\alpha}e^{-\delta t}dt\}\cos(n\theta)d\theta = -1,$$

$$n = 0, 1, \ldots, N, \qquad (38)$$

and

$$\frac{2}{\pi}\int_0^{\pi}\{-\delta\sum_{m=0}^{M}B_m\cos(m\theta) + D^2\int_0^{\alpha}e^{-\delta t}g(t)dt$$

$$- D^2\frac{\tau}{\tau}\int_{\beta}^{\alpha}e^{-\delta t}dt]\{\cos(n\theta) - \gamma\cos[(M+1)\theta]\}d\theta = -1 + \gamma,$$

$$n = N+1, N+2, \ldots, M. \qquad (39)$$

Equations (36) and (37) give

$$g(\eta) = \frac{2}{\pi}\int_0^{\pi}e^{-\delta\eta}\sum_{m=0}^{M}B_m\cos(m\theta)\{\cos(n\theta)$$

$$- \cos[(N+1)\theta]\}\,d\theta +$$

$$+\frac{1}{2}\int_0^{\alpha}g(t)\{C_N(|t-\eta|) - C_N(t+\eta) - C_{N+1}(|t-\eta|)$$

$$+ C_{N+1}(t+\eta)\}\,dt -$$

$$-\frac{\tau}{2}\int_{\beta}^{\alpha}\{C_N(|t-\eta|) - C_N(t+\eta) - C_{N+1}(|t-\eta|)$$

$$+ C_{N+1}(t+\eta)\}\,dt. \qquad (40)$$

which is a Fredholm integral equation of the second kind. The last condition that must be satisfied is that

$$g(\alpha) = \overline{\tau}. \tag{41}$$

The series equation and the integral equation are coupled by the Fourier coefficients and the function $g(\eta)$ and may be solved on a digital computer using a Gauss-Legendre quadrature scheme. Recent improvements in the solution scheme have reduced the computation time to less than two minutes, even for a very large number of broken fibers and large matrix damage.

Brittle Coating Interpretation

The mathematical model described in the previous section gives the fiber displacements and stresses throughout the laminate as well as the longitudinal yield region between the last broken fiber and the first unbroken fiber. An important step in relating the behavior predicted by the model to the measured laboratory values is thus to compare the measured longitudinal yield zone with the predicted value of the yield length from the model. The difficulty in this comparison is the interpretation of the crack pattern found in the brittle coating photographs.

Using the fiber stresses and displacements from the mathematical model it is possible to approximate the surface stress state in the aluminum matrix between the fibers.

Since the thin coating of brittle lacquer is sensitive to strains in this small region, the angle of the cracks in the coating should correspond to the principal strain (or stress) angles calculated from a simple Mohr's circle analysis for the aluminum. It should be noted that the matrix normal stress in the vertical direction was omitted in the shear-lag analysis for the fiber stresses since this stress is small compared to the fiber stress. However, it is appropriate to now consider this matrix stress since it is part of the stress state in the matrix which influences the crack pattern in the coating.

A good approximation for the average matrix normal strain in the vertical direction can be calculated by averaging the strains in the two adjacent fibers.

$$\varepsilon_y|_n = \frac{\sigma_\infty}{2E_F} \left(\frac{dV_n}{d\eta} + \frac{dV_{n+1}}{d\eta} \right) . \qquad (42)$$

The horizontal matrix strain is assumed due to a Poisson contraction alone, and is thus derived by multiplying Equation (42) by the Poisson ratio for aluminum, 0.3. The stresses in the matrix are then $\sigma_y = E_M \varepsilon_y$ and $\sigma_x = 0$. Finally, the matrix shear stress is calculated from Equation (15) as

$$\tau_n = \frac{\tau_o}{\bar{\tau}} (V_n - V_{n+1}) . \qquad (43)$$

Thus a typical element as shown in Figure (7) below has a known state of stress and the angle through which the element must rotate to reach the angle of principal stress can be calculated from

$$\tan(2\theta) = \frac{2\tau_{xy}}{\sigma_x - \sigma_y} \tag{44}$$

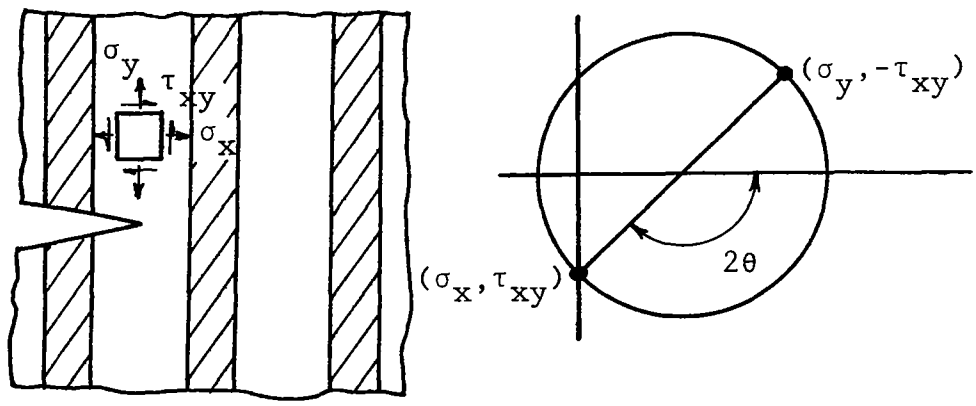

Figure 7. Mohr's Circle Analysis.

The growth of longitudinal damage predicted from the above analysis can now be compared to the growth from actual specimen photographs. The longitudinal crack pattern for a specimen having an overall width of 73.2 mm and an initial notch width of 12.7 mm will be examined at various load levels and compared to predicted strain data from the model.

The first load step examined is very early in the cycle before any longitudinal yielding has begun. At an axial

load of 800 N the model predicted that very few cracks should form, since the strain falls below the threshold strain of 1500 με at a y-value of approximately 1 mm. The model further predicts that these first cracks that form in the coating will form at an angle of 37 degrees from the horizontal. Table (II) shows the predicted data from the model at the load levels to be examined in this analysis. Figure (8) shows the appearance of the coating at a load of 800 N. It is clear that these first cracks, forming an angle measured to be 32 degrees, appear directly above the end of the notch between the last broken fiber and the first unbroken fiber. Moreover, the uppermost crack forms at a y-value on the order of that predicted by the strain values computed from the analysis.

At a load of 3000 N the model predicts that approximately 2.5 mm of longitudinal matrix will yield and that the principal strain in the matrix will exceed the brittle lacquer threshold strain value for y-values less than 5 mm, with the last predicted crack forming at an angle of 30 degrees. Examination of Figure (9) reveals that the uppermost crack, at a y-value of 6 mm, forms an angle of 29 degrees with the horizontal. In this figure it can also be seen that a region of very intense cracking has formed, consisting of short, closely spaced cracks and lacquer crazing. The length of the region containing these short cracks corresponds very closely to the yield length of 2.5 mm predicted by the model.

The length of the longitudinal matrix yield region at 4500 N is predicted by the model to be approximately 5 mm, and the uppermost crack in the coating at this load should form 8 mm above the notch at an angle of 29 degrees. Figure (10) shows that the uppermost crack is present 12 mm above the notch at an angle of 27 degrees and that the region of severe cracking and crazing has grown to approximately 5 mm.

Finally, in Figure (11) the uppermost crack forms 14 mm above the notch at an angle of 20 degrees with the horizontal, and the region of severe cracking has grown to 10 mm at this load level of 6500 N. The predicted location and orientation of the last crack at this load level are 15 mm above the notch at an angle of 22 degrees with the horizontal. The yield length predicted by the mathematical model at this load level is 10 mm. Thus the stresses and strains in the matrix actually measured in the laboratory appear to agree reasonably well with those predicted by the mathematical model. The growth of the crack region as well as the severely cracked region is shown in graphical form in Figure (12). It is clear that the brittle coating provides a very good qualitative picture as well as some quantitative data concerning the yield region at the end of the notch and its growth as the load is increased.

It should be noted that the cracking discussed above occurs relatively early in the load cycle before the first fiber break has occurred. As fibers begin to break in the

laminate, the loading is stopped and restarted each time an X-ray exposure is made. As is the case with all brittle lacquers, the load must be removed completely each time the loading is stopped if the threshold is to remain valid. Of course, this would greatly alter the stiffness of the previously yielded aluminum matrix and thus change the behavior of the laminate. The loading cycle was thus continued after each X-ray exposure without first removing the load.

The brittle coating, while providing actual numerical approximations in the early part of the load cycle before the first fiber has broken, can provide only qualitative results later in the cycle. It is felt, however, that the severely cracked region is closely associated with yielding in the matrix. Several tests were performed using pure aluminum notched panels and in each case the region(s) in which yielding was known to occur exhibited this same intense cracking. The region of intense cracking and flaking is thus used as indicator of matrix yielding and will be referred to as the severe damage length in the remainder of this paper.

Table II. Brittle Coating Interpretation Data.

	Uppermost Crack Location		Uppermost Crack Angle		Severe Damage Region	
Load	Predicted	Observed	Predicted	Observed	Predicted	Observed
800 N	1 mm	1 mm	37°	32°	0	0
3000 N	4 mm	5 mm	30°	29°	2.5 mm	2.5 mm
4500 N	8 mm	11 mm	29°	27°	5 mm	5 mm
6500 N	14 mm	18 mm	22°	20°	10 mm	10 mm

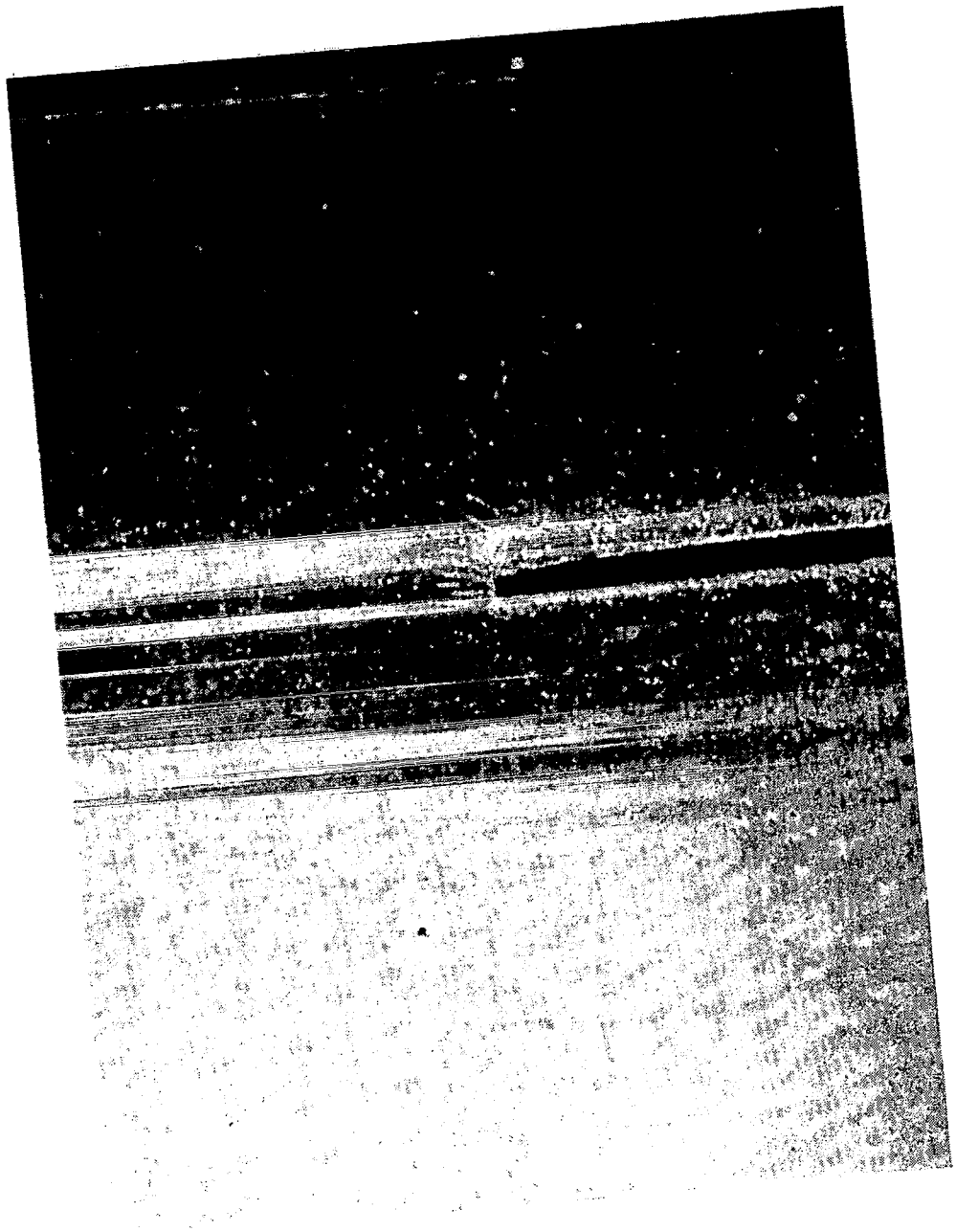

Figure 8. Brittle coating crack pattern for an axial load of 800 N.

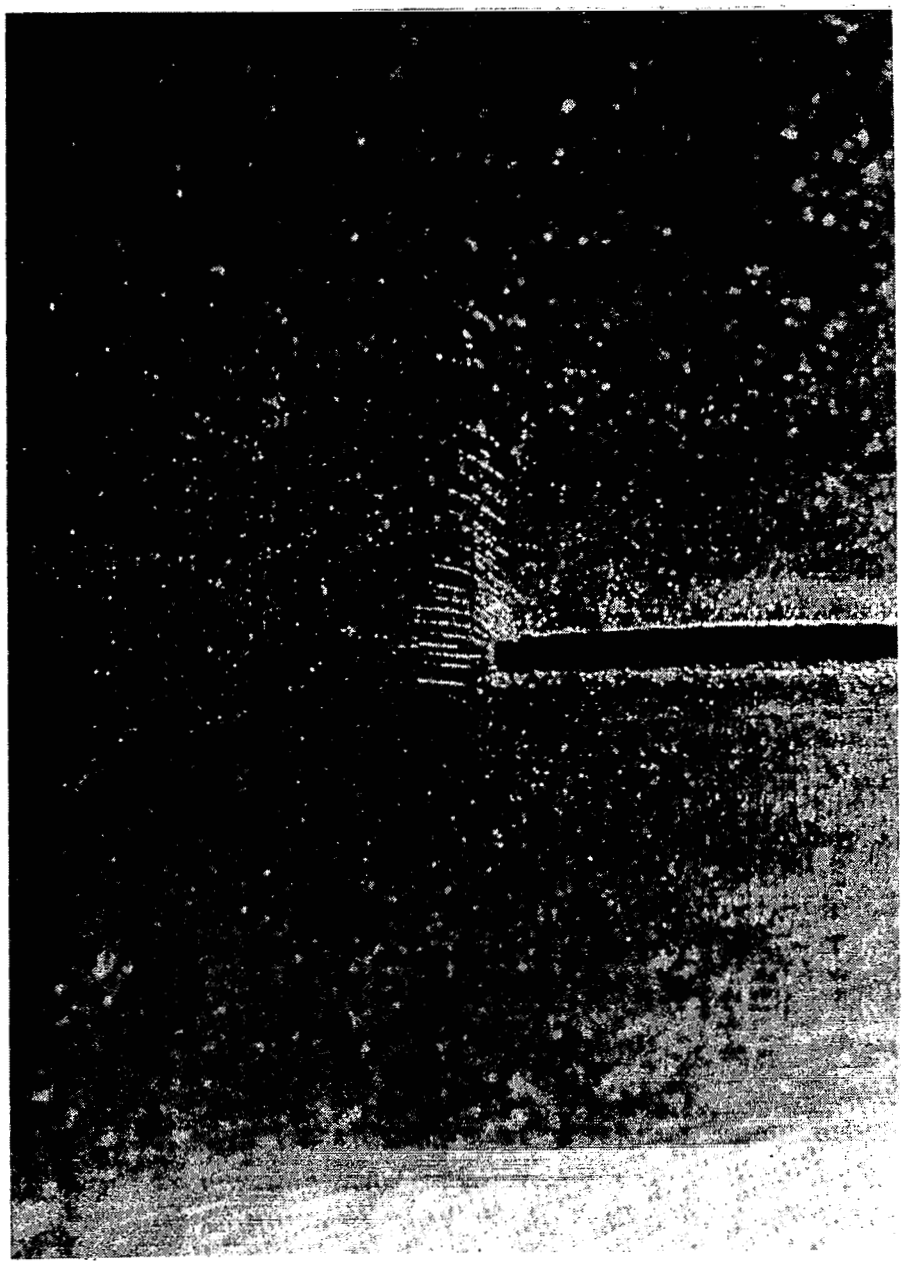

Figure 9. Brittle coating crack pattern for an axial load of 3000 N.

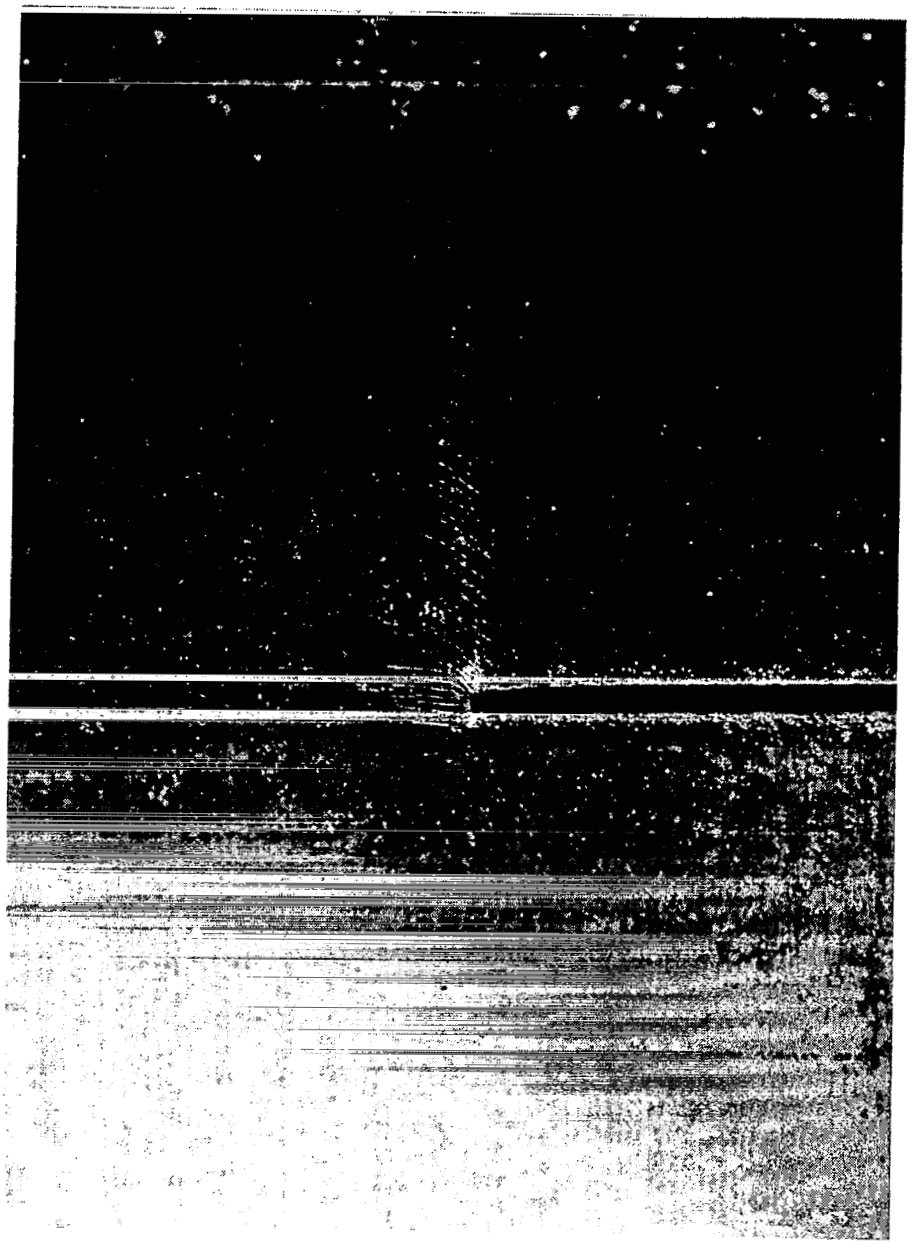

Figure 10. Brittle coating crack pattern for an axial load of 4500 N.

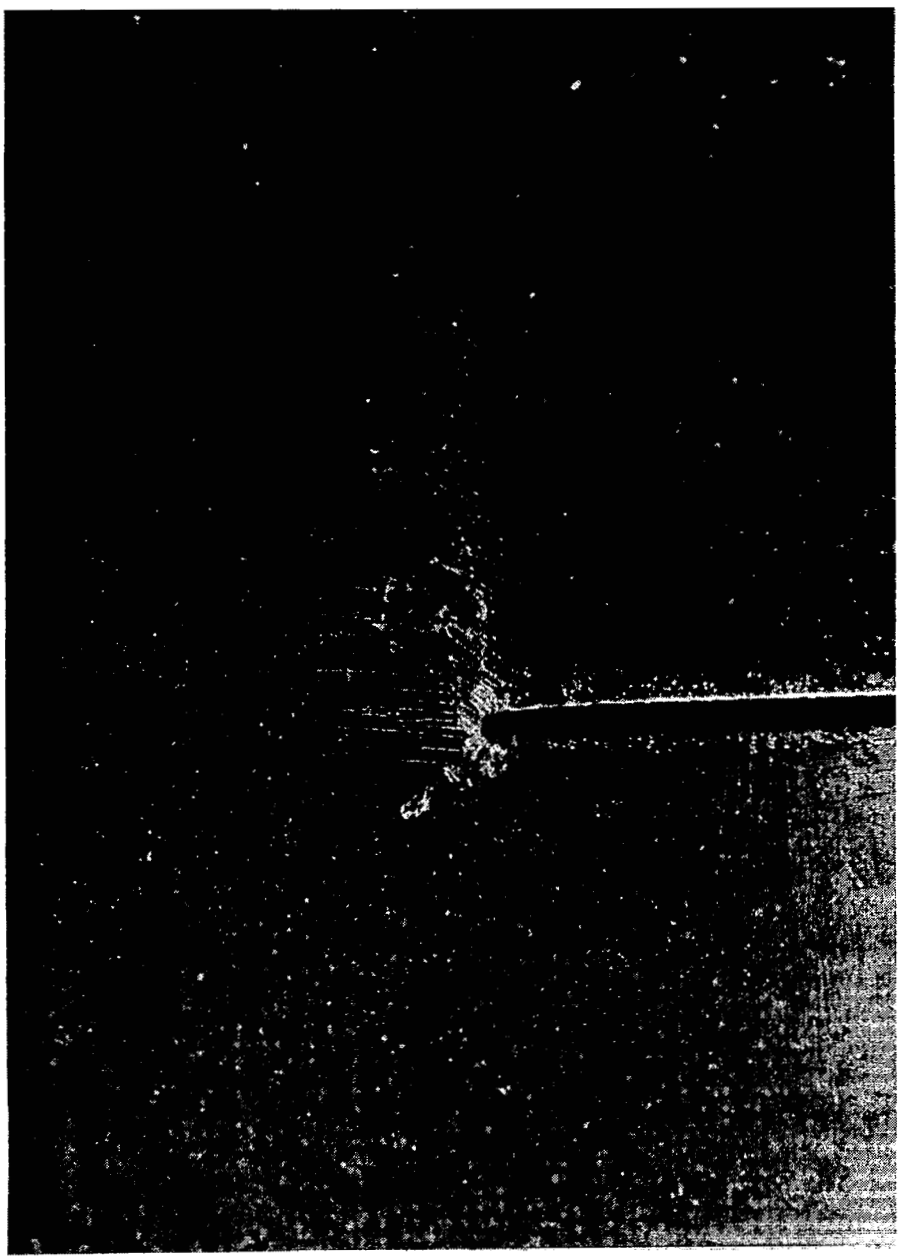

Figure 11. Brittle coating crack pattern for an axial load of 6500 N.

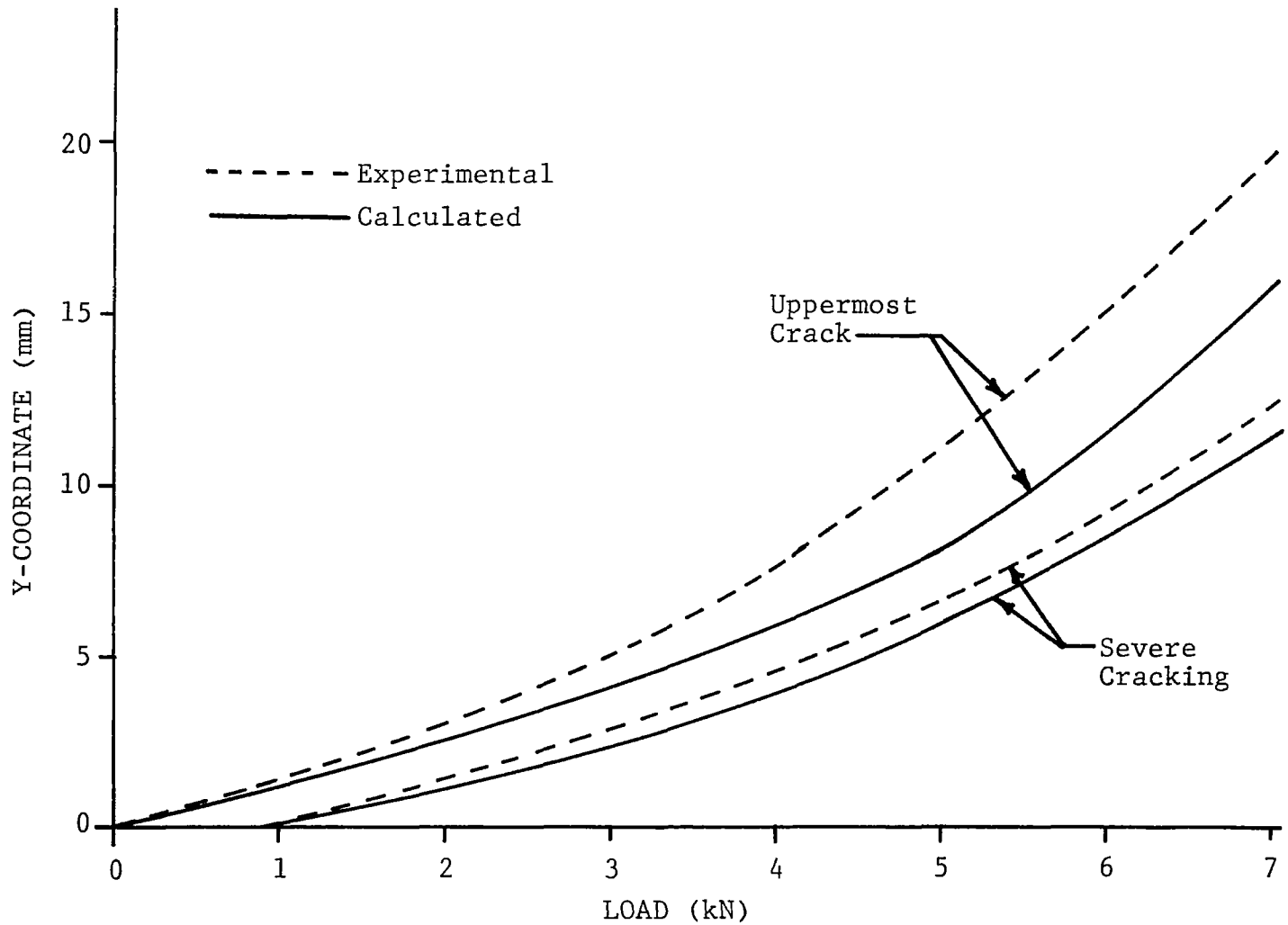

Figure 12. Brittle coating interpretation data in graphical form.

CHAPTER IV

RESULTS

Damage Growth Sequence

The main objective of this paper is to determine accurately the properties of boron/aluminum laminates and then compare the predicted values to those measured in the laboratory using actual specimens. The experimental tests should provide values for the matrix yield length, all fiber displacements, fiber stresses, and stable notch extension. Material properties and laminate dimensions from handbooks and manufacturer's specifications should allow the experimenters to convert the non-dimensional predicted values from the model to real values suitable for comparison with experimental results.

As previously discussed, the use of radiographs and brittle coating photographs will present a very detailed picture of the growth of damage during a loading cycle of any unidirectional boron/aluminum laminate. It is therefore appropriate to begin the examination of the results of this study with a step-by-step presentation of a typical set of photographs of one of the experimental specimens. The specimen chosen for this analysis is typical of all of the test panels, exhibiting both matrix yielding and stable notch extension in the form of broken fibers ahead of the notch.

The set of photographs and radiographs show the progression of damage in a two-ply boron/aluminum laminate which is 73.1 mm wide. A 19.05 mm wide notch (109 broken fibers per ply) was cut perpendicular to the fiber direction in the center of the panel before the testing procedure was begun. Brittle coating photographs and X-ray exposures were made at selected intervals in the loading sequence. The series of radiographs and photographs is presented in Figures (13) through (28) beginning at the end of this section.

As previously mentioned, a baseline X-ray was taken of each specimen before the loading cycle was begun to detect any damage which may have been caused by machining or polishing. The baseline X-ray for the two-ply specimen is shown in Figure (13). The right end of the notch can be seen in this radiograph, along with the fiber cores which run perpendicular to the notch. The initial notch opening was 0.381 mm; thus crack opening displacement at each load level could be measured from the radiographs once the scale factor had been determined. It is clear that there are more fibers visible in this radiograph than in the earlier single-ply radiograph. This indicates that the fibers in each ply, as expected, are not perfectly aligned with the fibers in adjacent plies. It can be seen, however, that there are usually two fiber cores very close together on the radiograph, indicating the two fibers in adjacent plies.

In the first few photographs, the cracks in the brittle coating grow in the longitudinal direction, even though no fiber breaks have occurred. In Figure (17) it can be seen that the first fiber breaks have occurred, indicated by the breaks in the fiber cores near the end of the notch. It should be noted that from this point there will be no longitudinal growth of the severe damage region, since the first previously unbroken fiber is now free to displace. The progression of damage, indicated by severe cracking and flaking of the brittle lacquer, will now be in the transverse direction as more fibers continue to break.

First fiber failure typically occurred at 55-60 percent of the ultimate failure load for all laminates tested, independent of the laminate width, thickness, initial notch width, or the matrix temper (6061-0 or 6061-T6). Subsequent fiber failure normally occurs at 75 to 80 percent ultimate, with visible notch extension occurring at roughly 95 percent ultimate. This behavior is described in Table (III). The present specimen shown in Figures (13) through (28) were chosen primarily because of the quality of the brittle coating photographs and the radiographs, even though in this sequence the second fiber failure does not occur until 93 percent of the ultimate laminate failure load.

In Figure (24) the severe damage region in the coating has grown transversely from the notch, clearly indicating the existence of more than one longitudinal damage region in

Table III. Loads* at which subsequent fiber breakage occurs for 73.1 mm B/Al panels with 15.9 mm notches (89 broken fibers per ply).

Matrix		1-ply	2-ply	4-ply	8-ply
6061-O	First fiber break	55 %	50 %	60 %	55 %
	Second fiber break	85 %	80 %	83 %	72 %
	Beginning of visible notch extension	98 %	97 %	94 %	95 %
6061-T6	First fiber break	56 %	60 %	59 %	55 %
	Second fiber break	83 %	81 %	79 %	78 %
	Beginning of visible notch extension	98 %	94 %	97 %	93 %

*These loads are given as a percentage of the ultimate notched failure load for each particular specimen.

the matrix. It is this phenomenon that allows the COD to grow at a faster rate than predicted by the model, since the model at the present time can include only one yield region. The last figures in the damage sequence indicate that the transverse damage region continues to grow until the failure load of the laminate is reached. It should be noted that the extension of the notch in the form of broken fibers does not occur in a straight line parallel to the notch. Rather, the crack grows in a jagged fashion with the fiber breaks occurring at different vertical locations as the crack grows and more fiber breaks are observed. The fibers in this region are thus broken but still able to carry some reduced amount of load since the matrix around them is still intact. This phenomenon exactly parallels the assumptions made for the constrained fibers in the previous section, indicating the physical basis for the constrained fiber approximation.

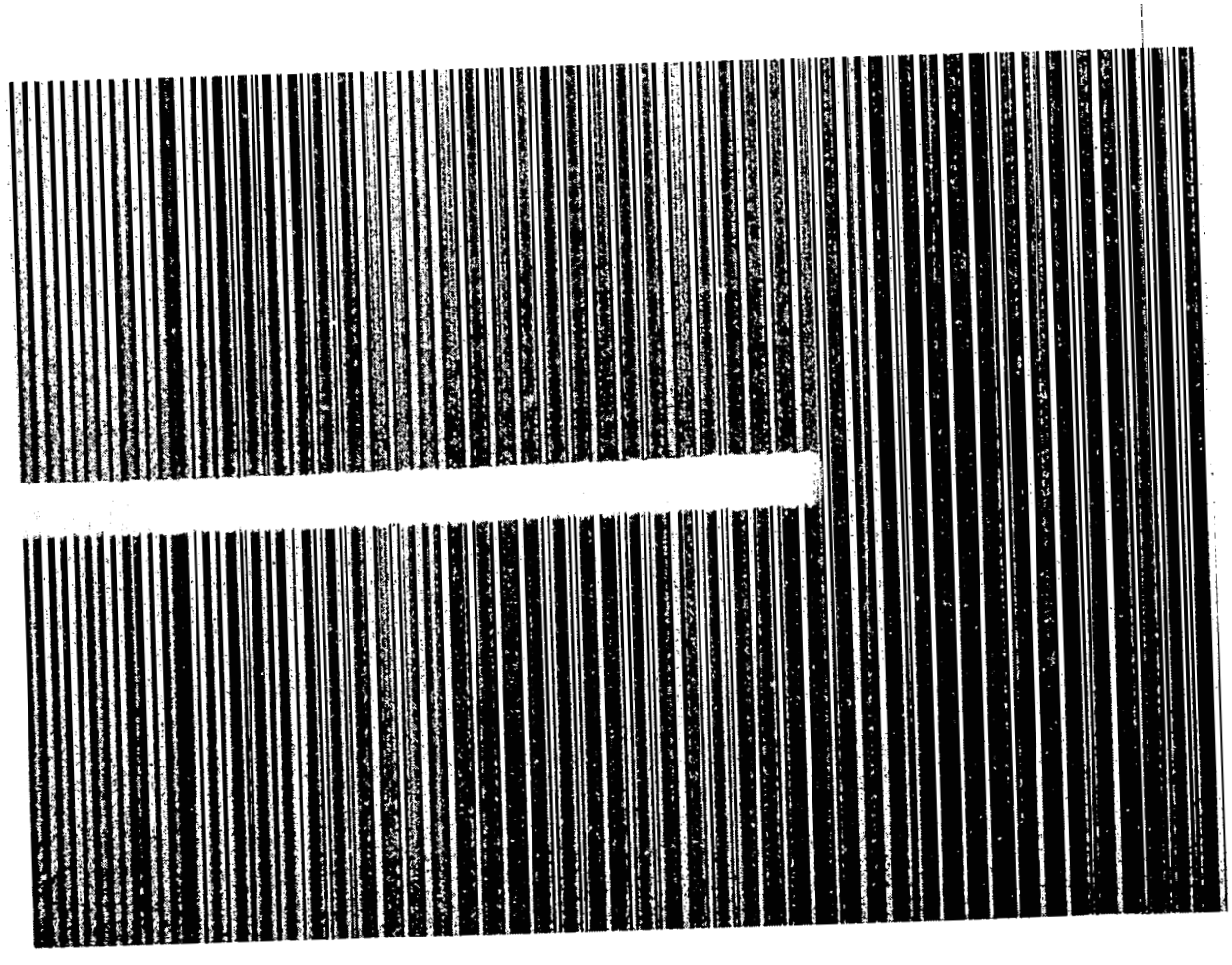

Figure 13. Baseline radiograph of a notched, two-ply boron/aluminum composite panel.

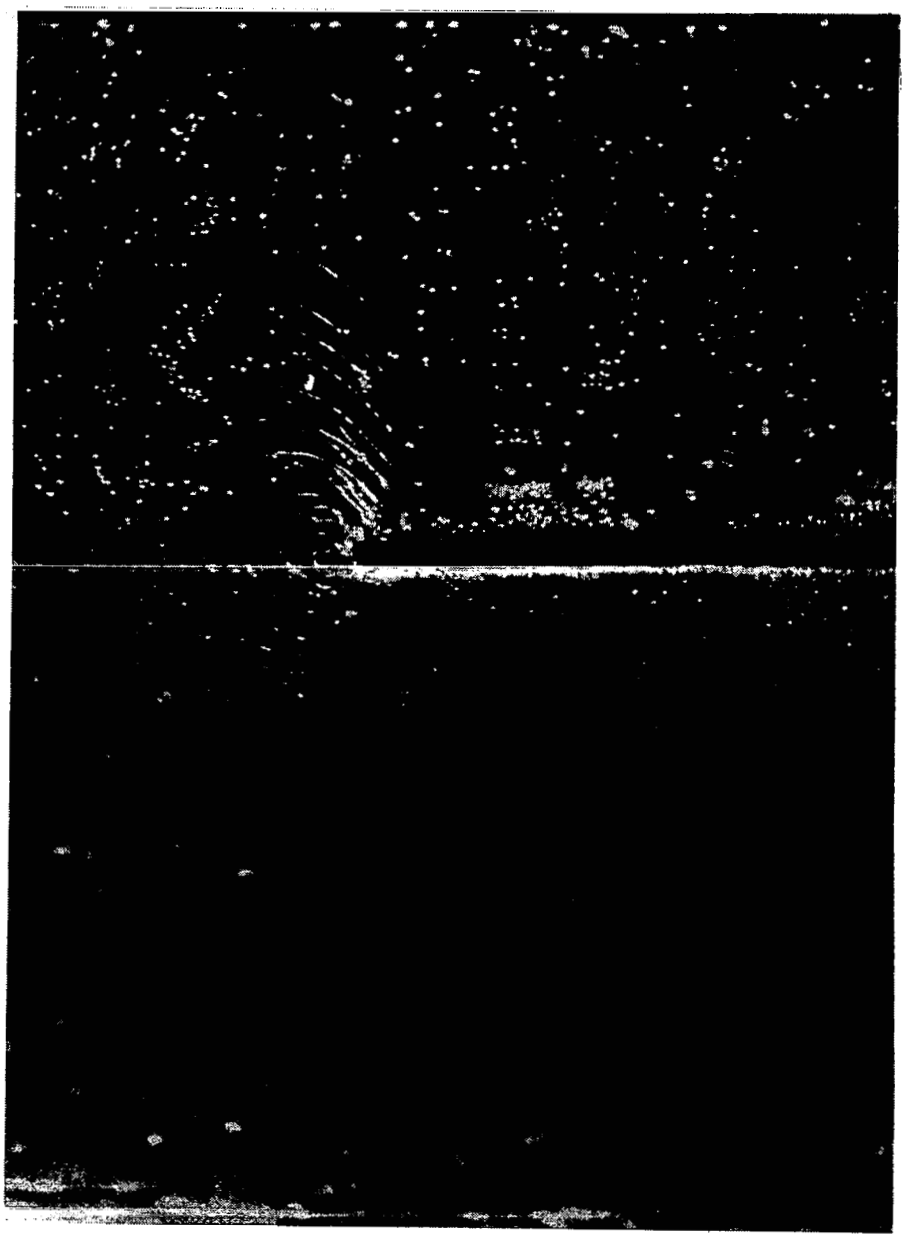

Figure 14. Brittle lacquer crack pattern at 2670 N showing formation of first cracks in the coating.

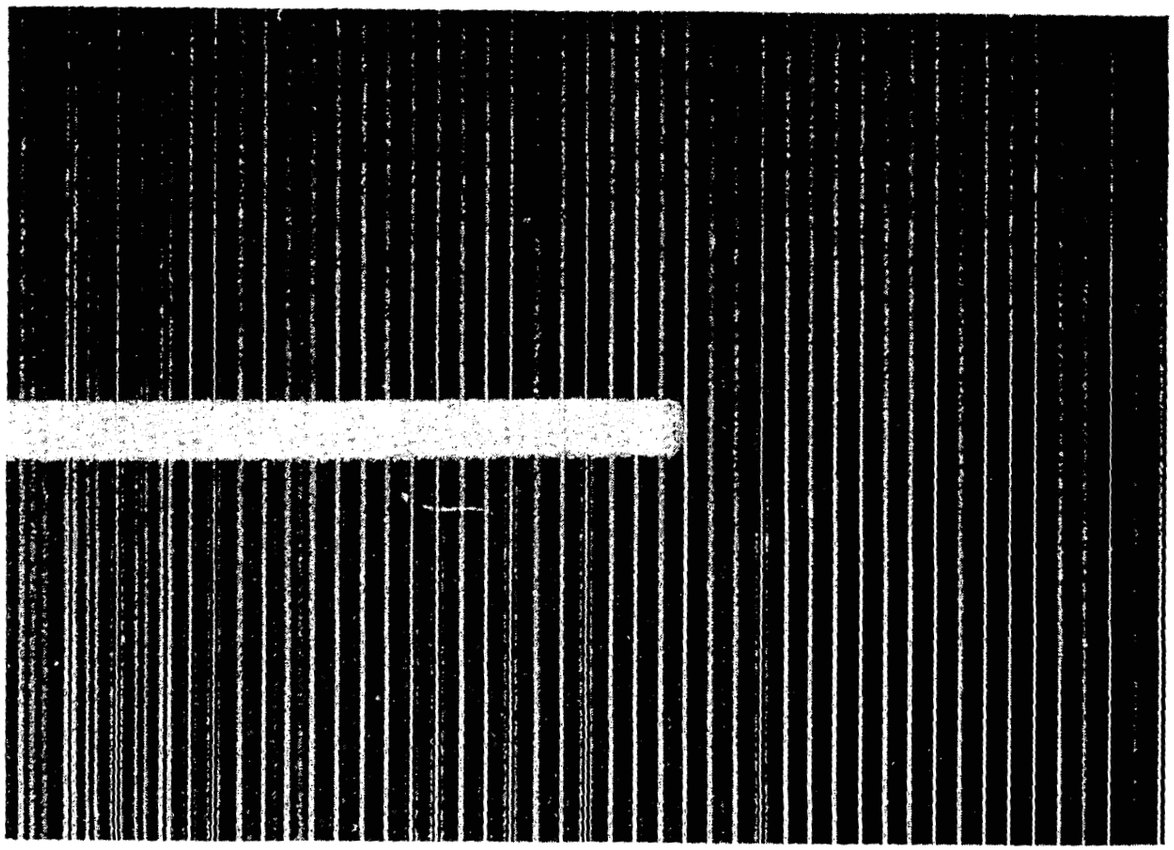

Figure 15. Radiograph of two-ply panel at 5340 N (35% failure load).

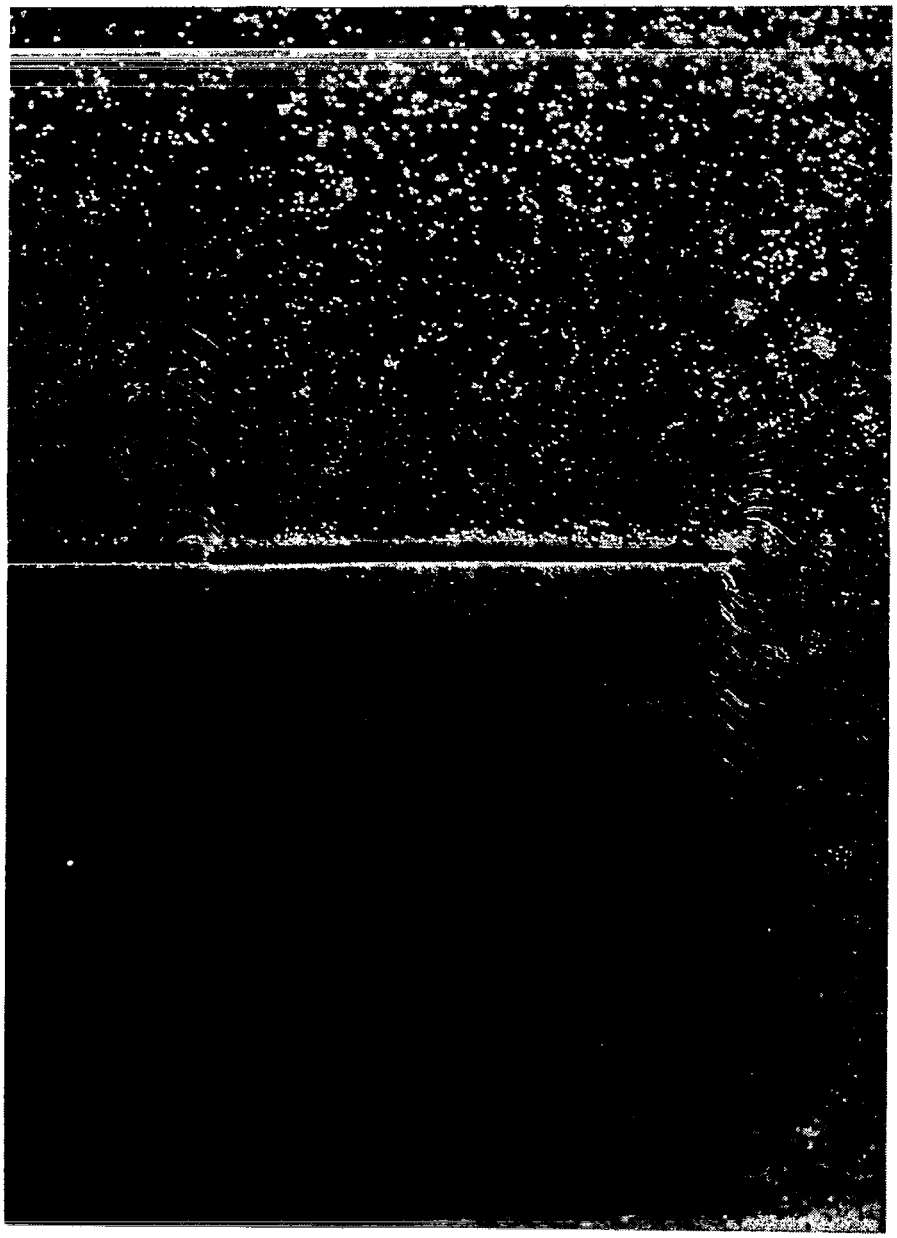

Figure 16. Brittle lacquer crack pattern at 5340 N.

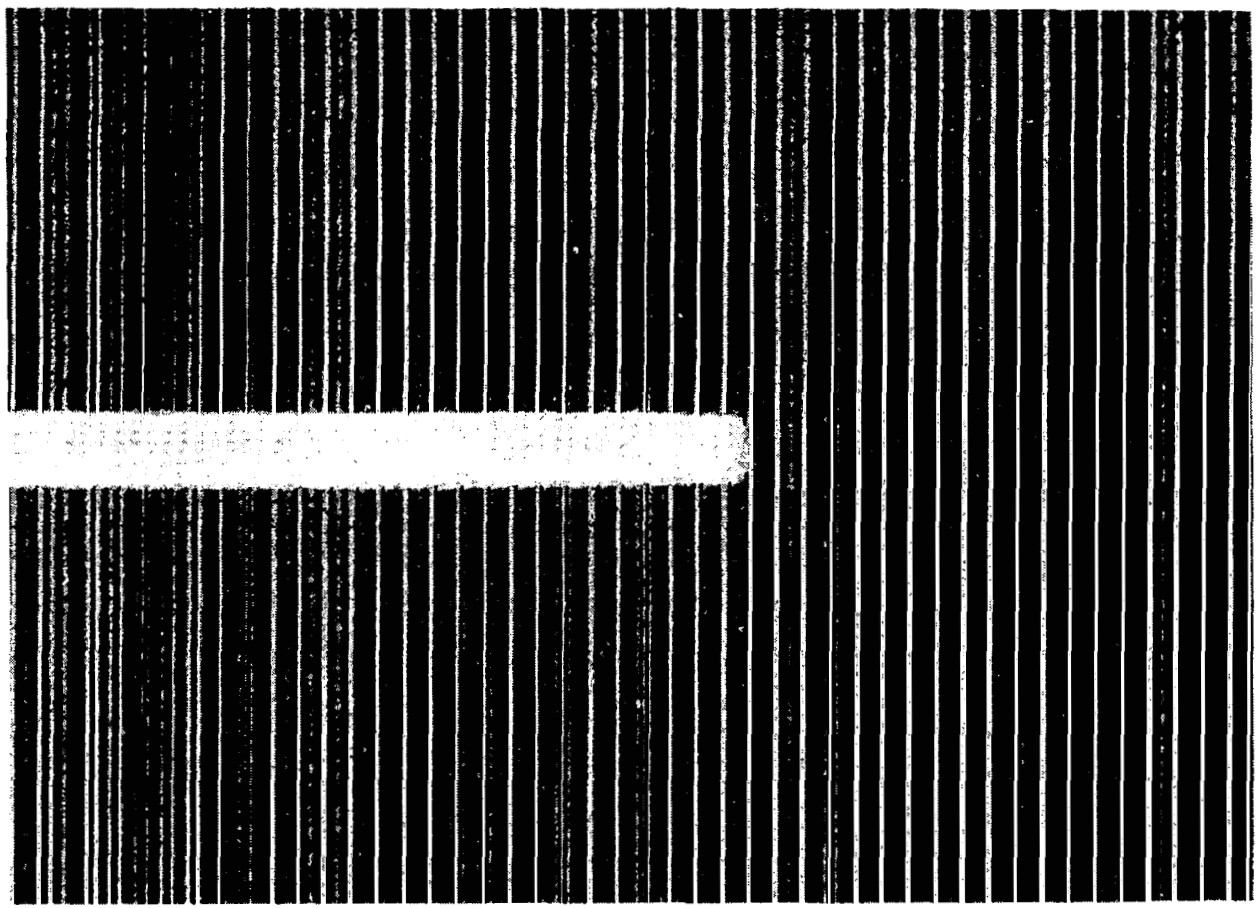

Figure 17. Radiograph of two-ply panel at 8010 N (53% failure load) showing first fiber break occurring at the upper, right-hand portion of the notch.

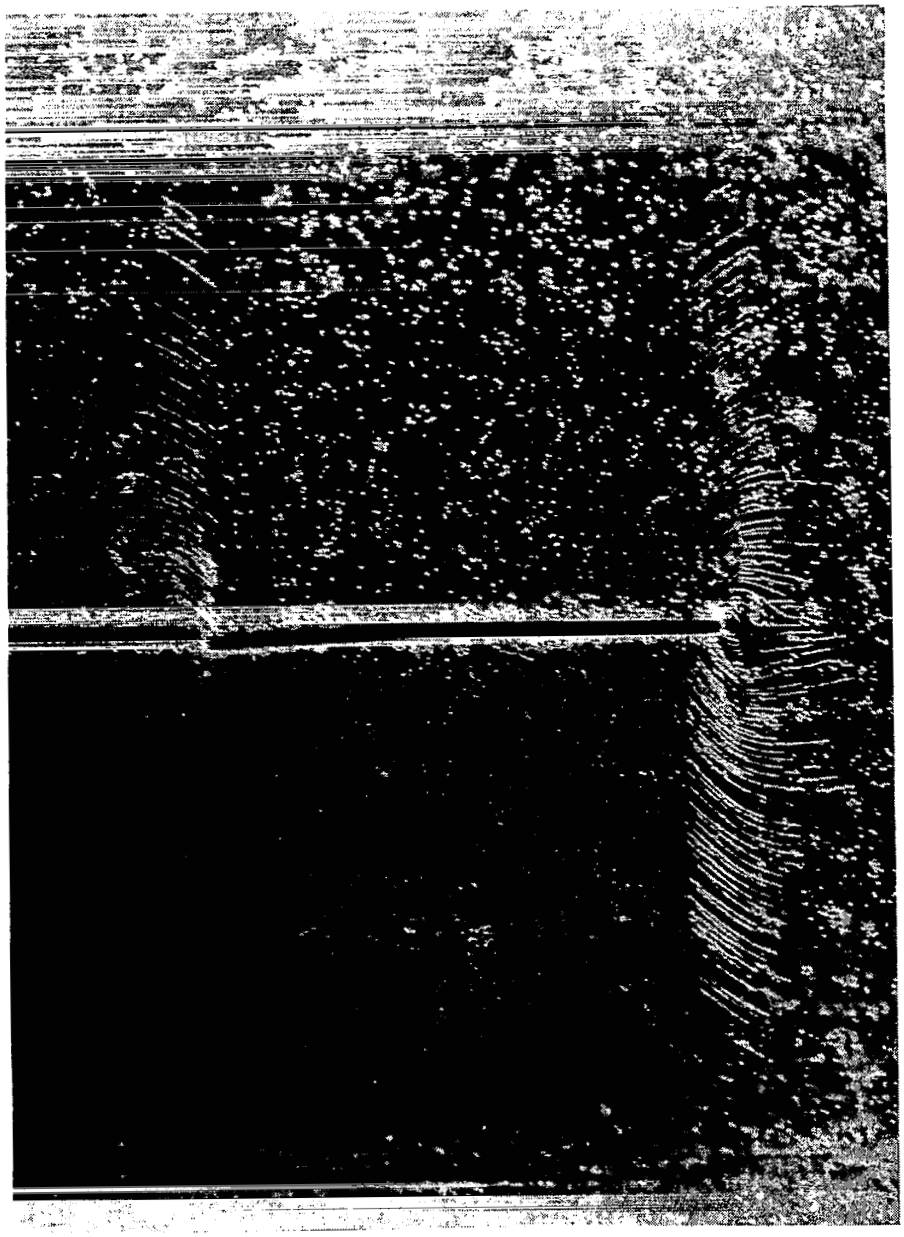

Figure 18. Brittle lacquer crack pattern at 8010 N.

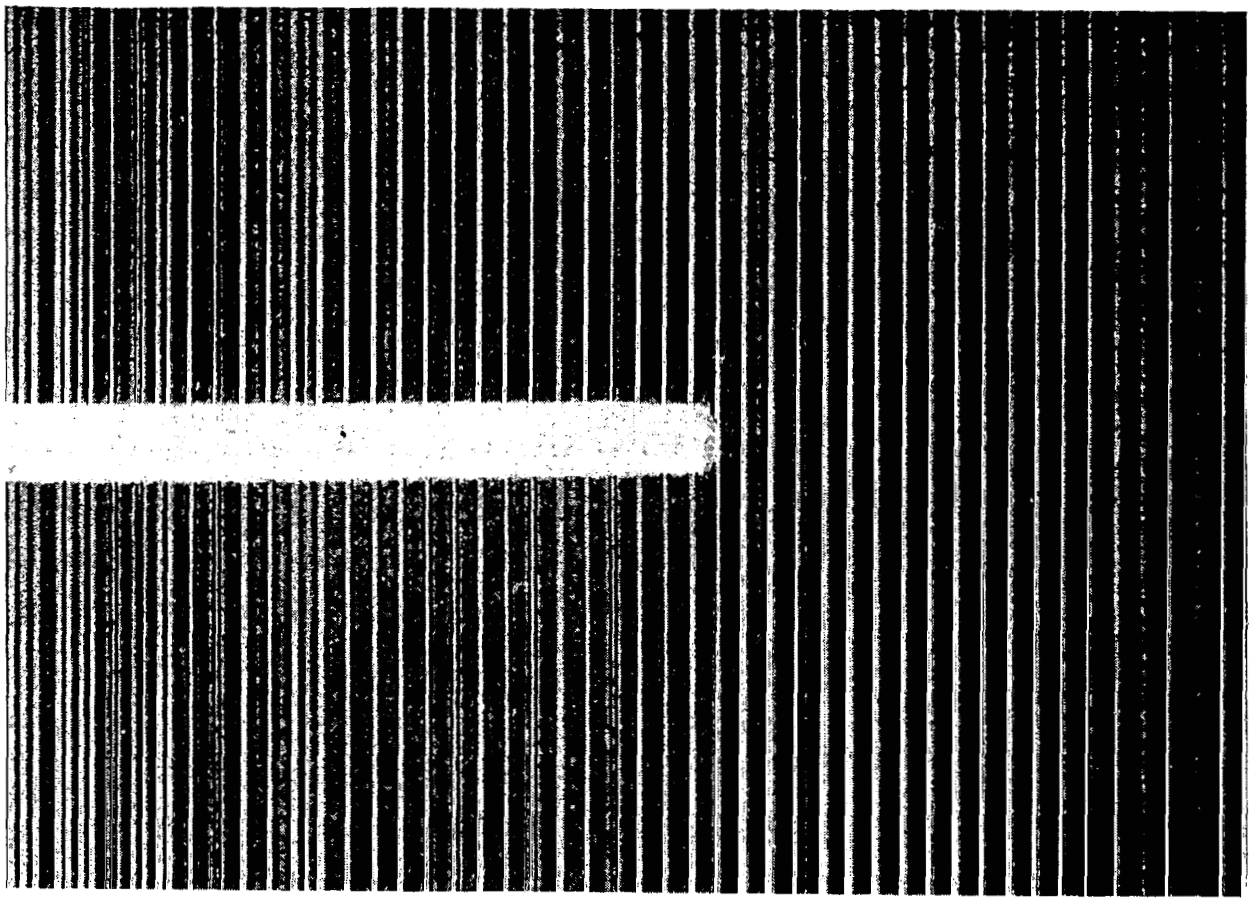

Figure 19. Radiograph of two-ply panel at 9350 N (63% failure load).

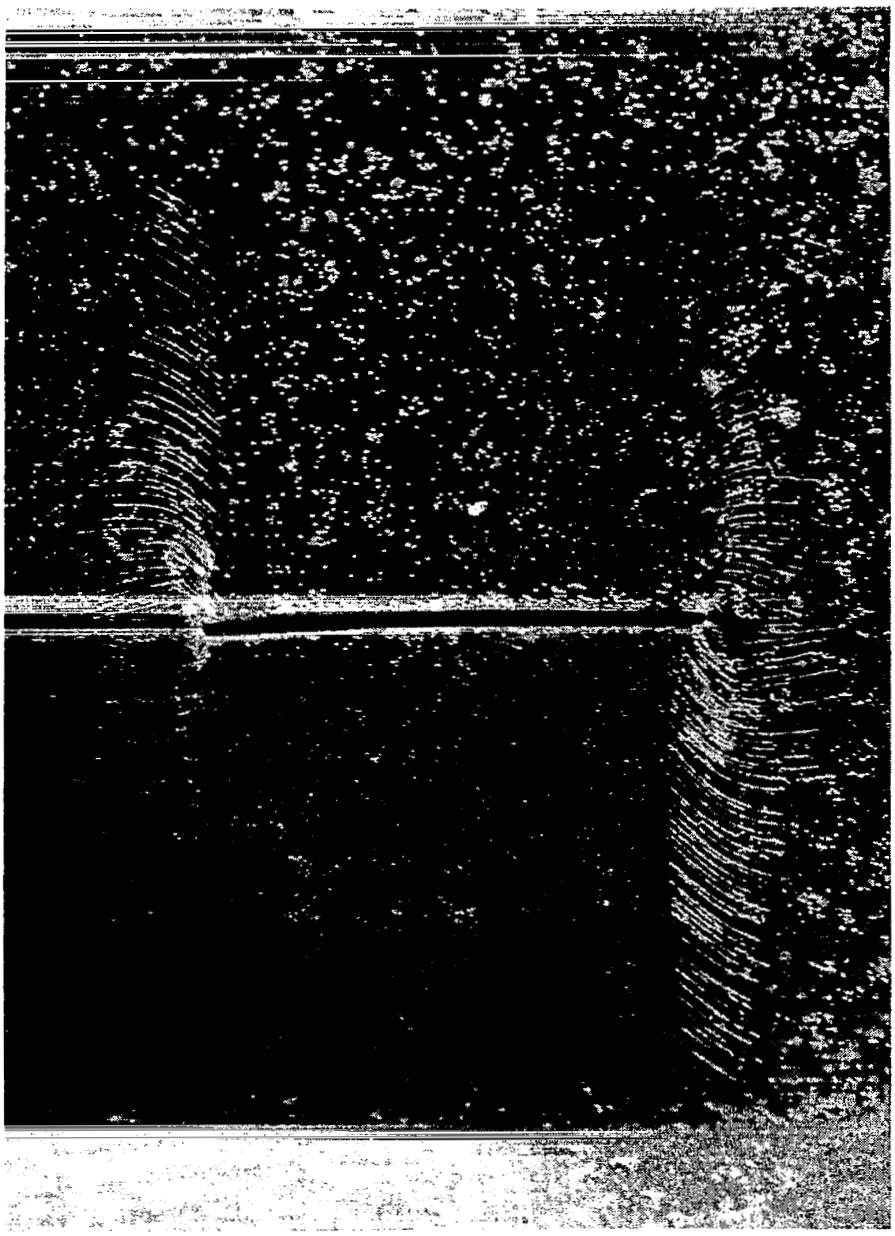

Figure 20. Brittle lacquer crack pattern at 9350 N showing transverse growth of severe damage region.

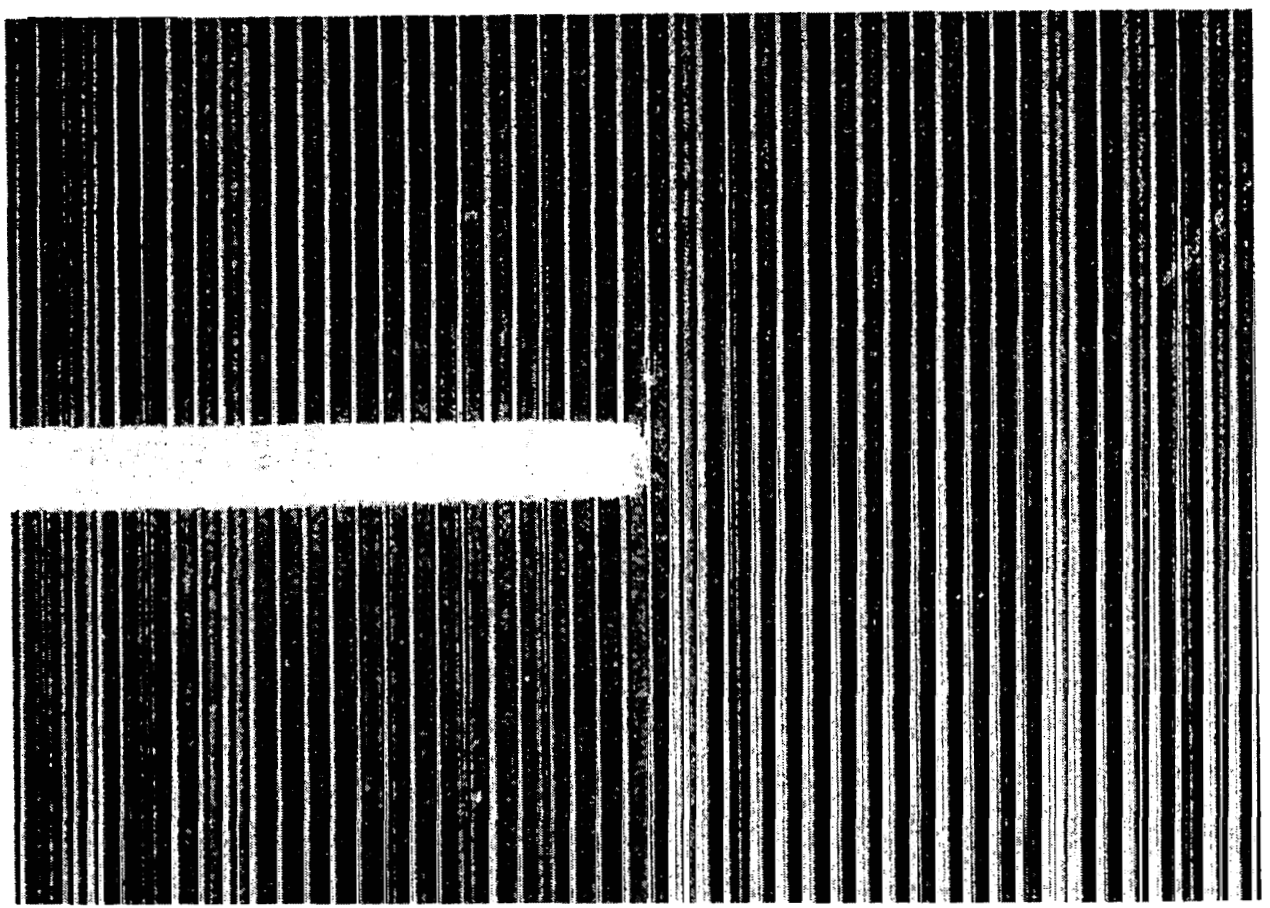

Figure 21. Radiograph of two-ply panel at 11,100 N (79% failure load).

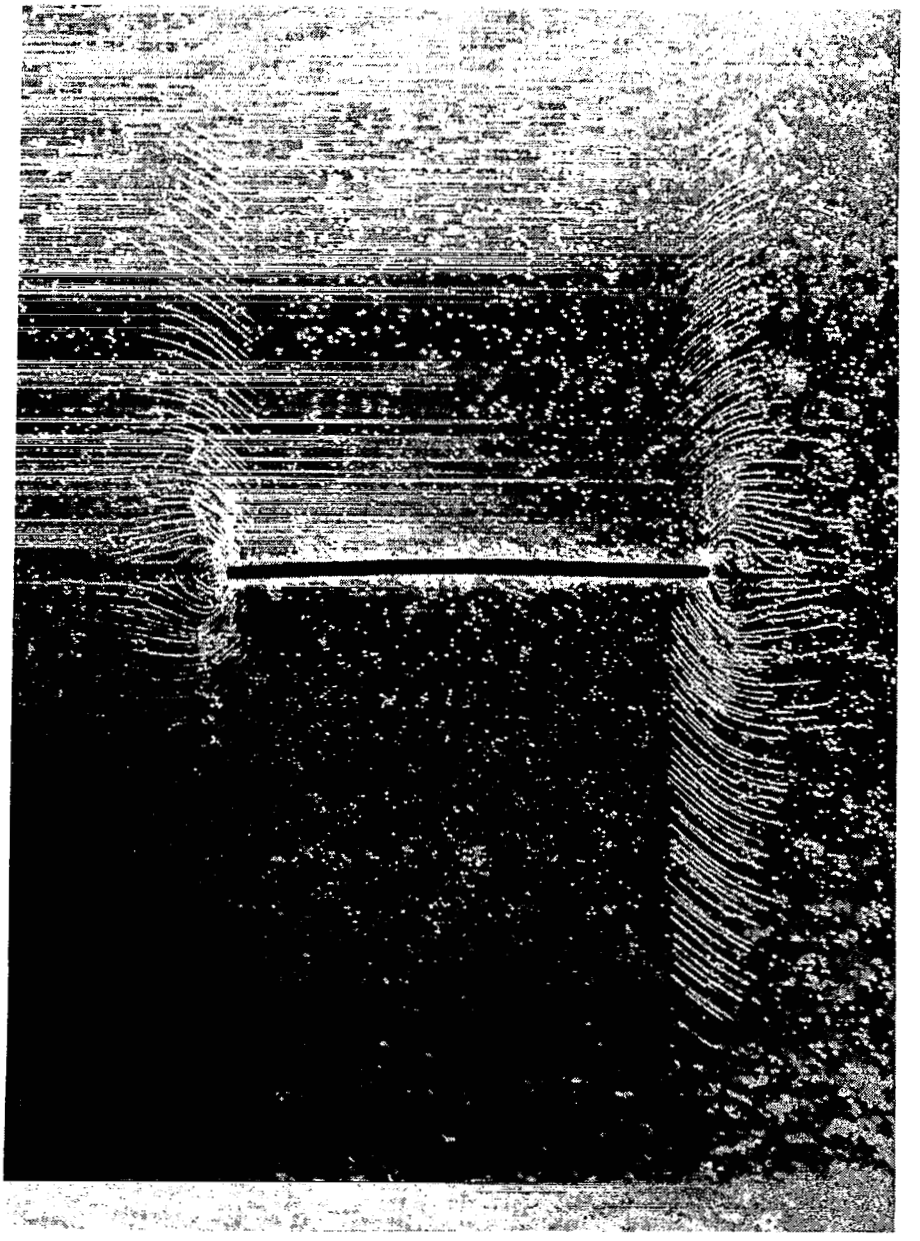

Figure 22. Brittle lacquer crack pattern at 11,100 N.

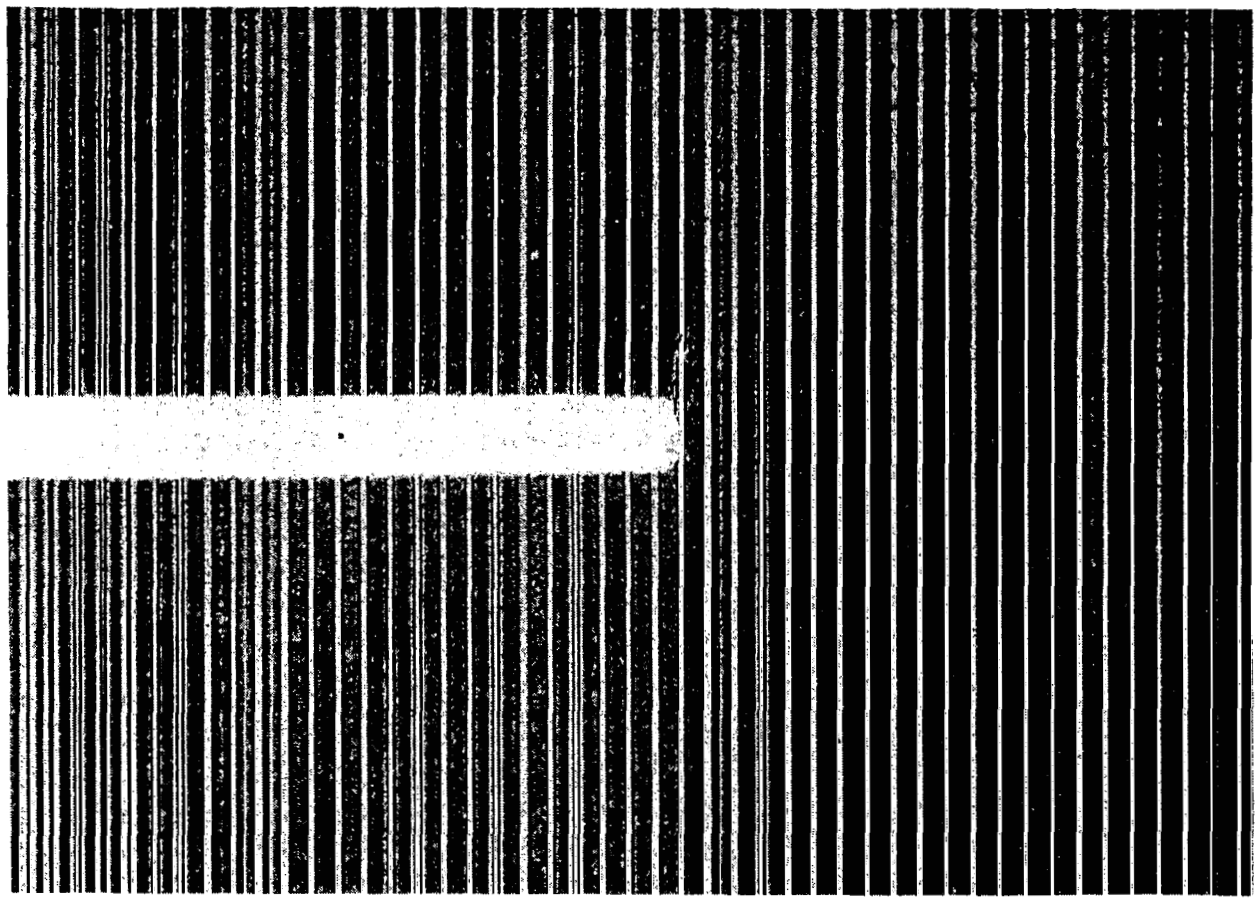

Figure 23. Radiograph of two-ply panel at 12,500 N (90% failure load).

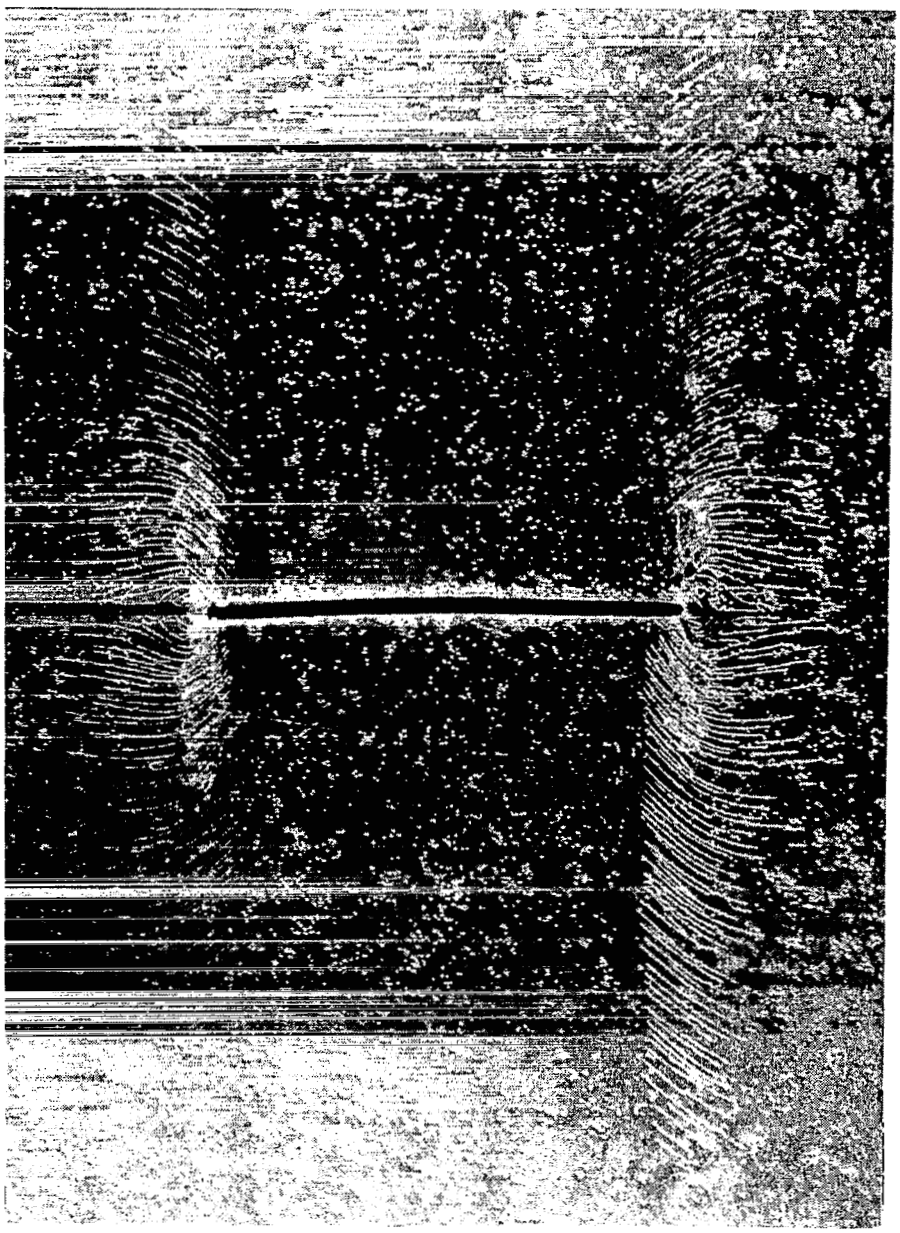

Figure 24. Brittle lacquer crack pattern at 12,500 N.

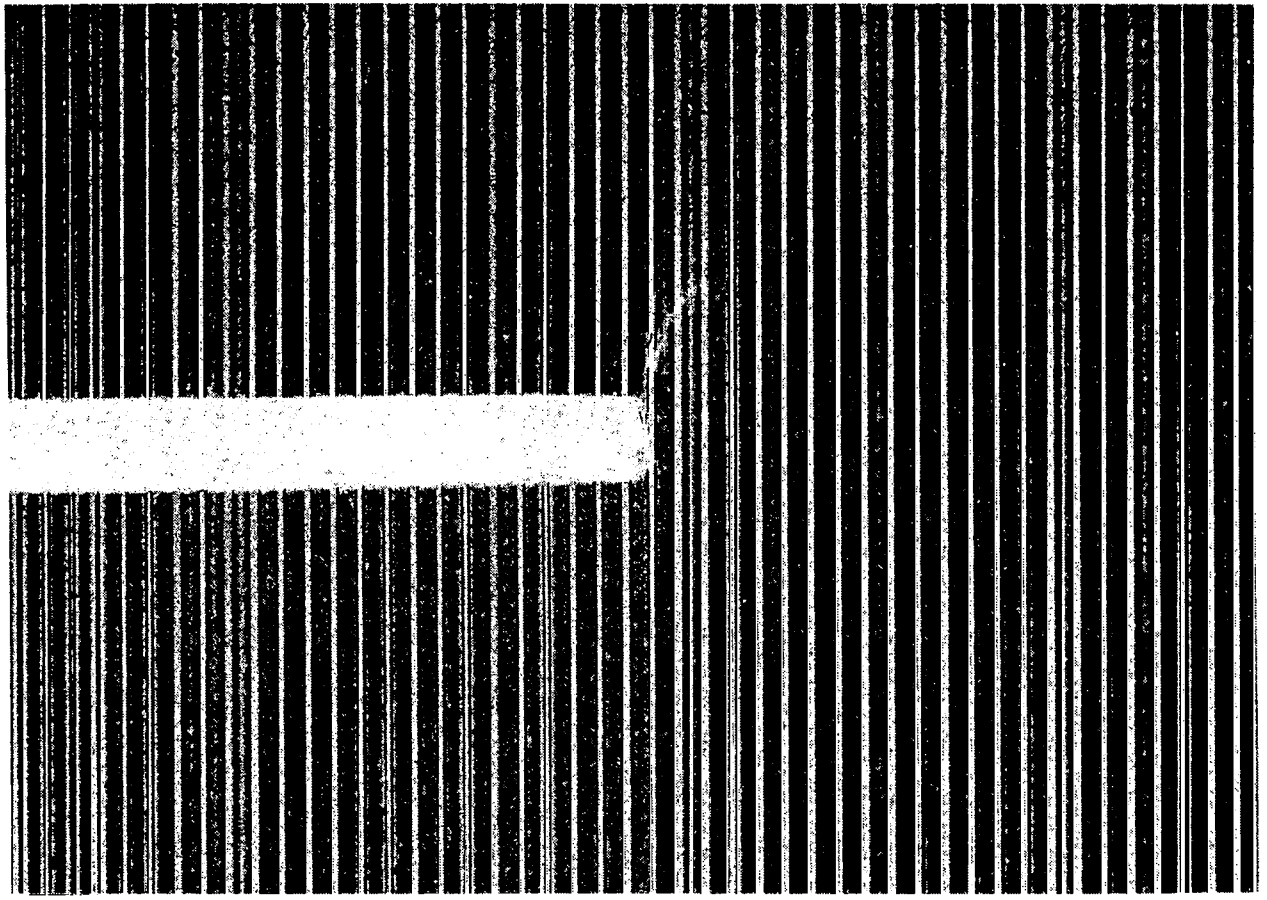

Figure 25. Radiograph of two-ply panel at 12,800 N (93% failure load) showing additional fiber breaks at the right end of the notch.

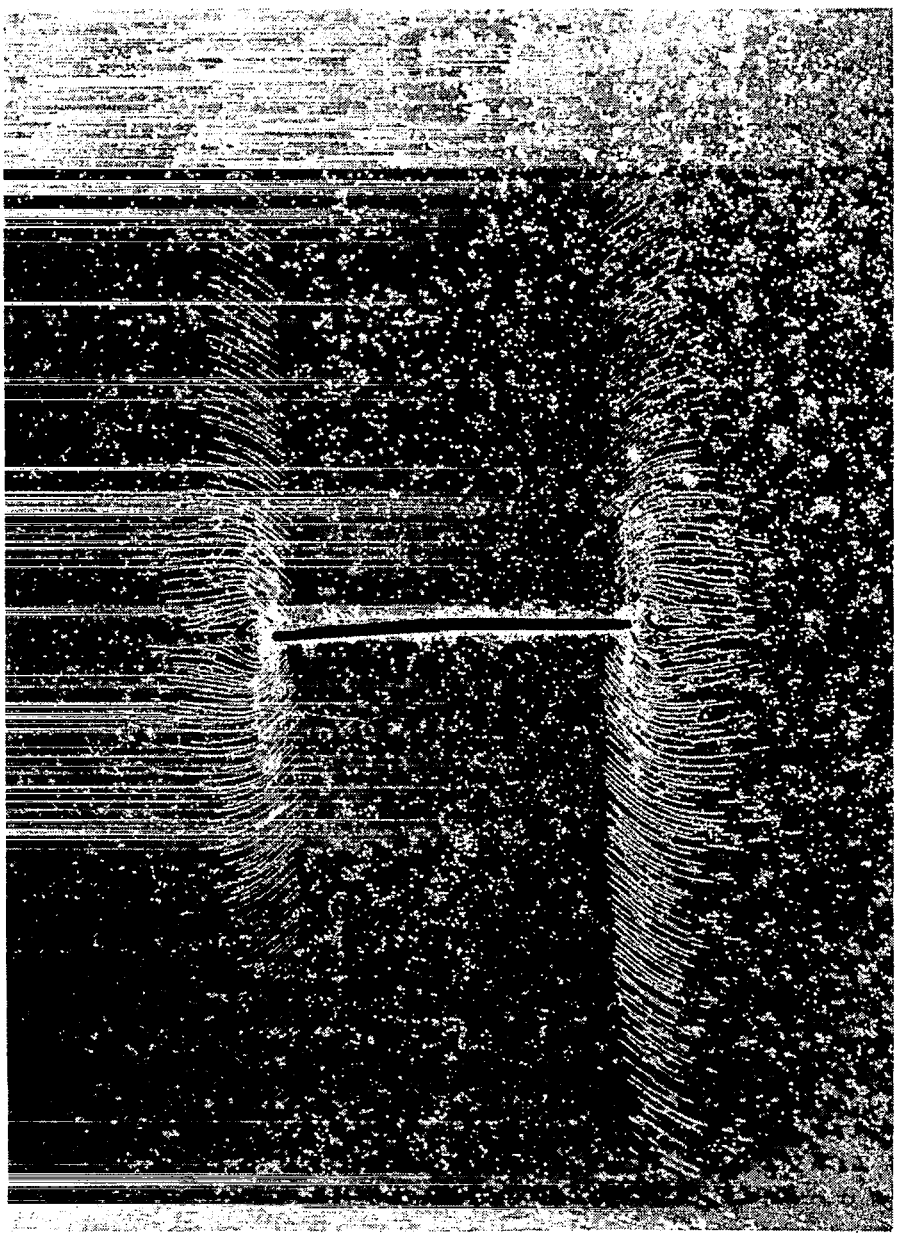

Figure 26. Brittle lacquer crack pattern at 12,800 N.

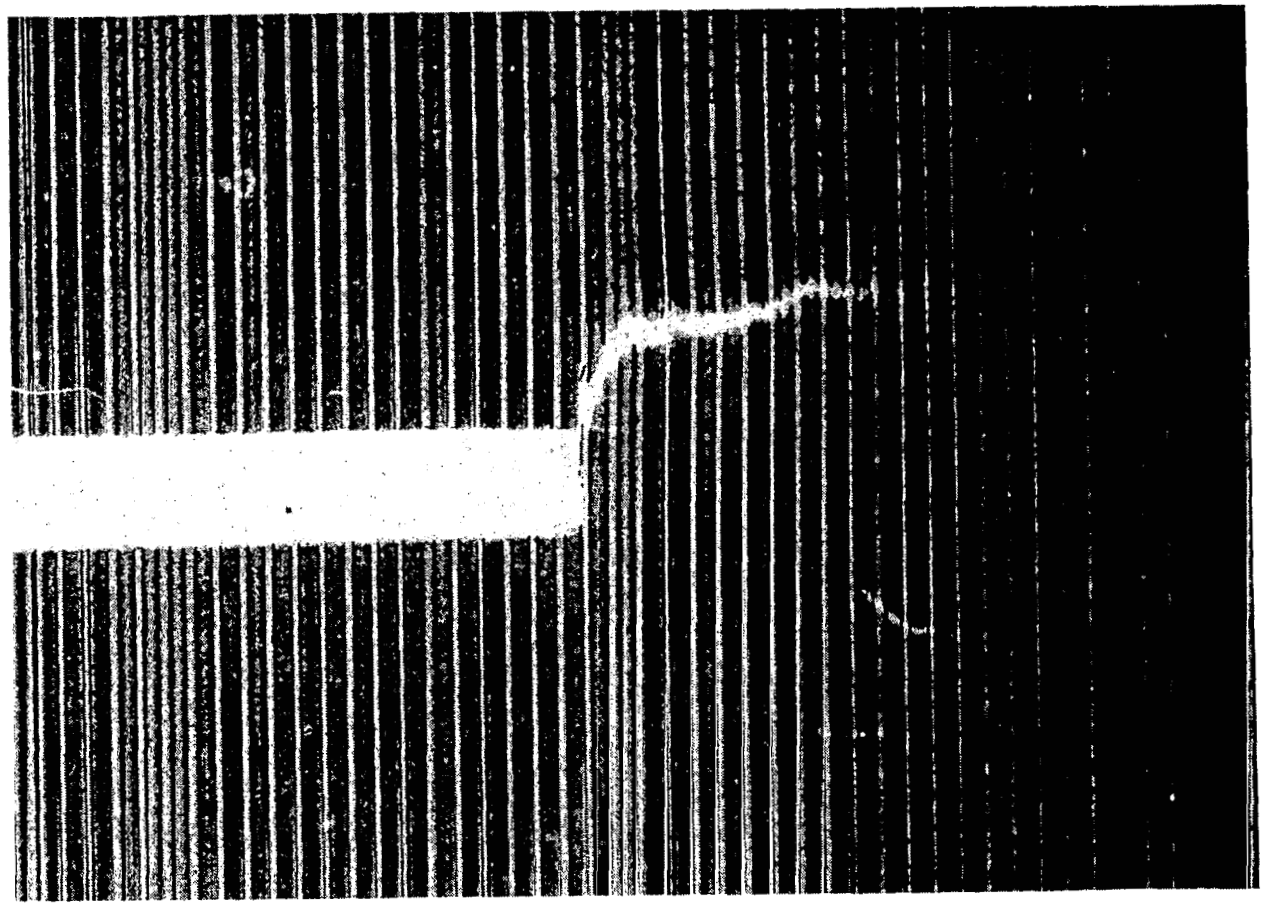

Figure 27. Radiograph of two-ply panel at 13,200 N (96% failure load) showing additional fiber breaks and large crack extension.

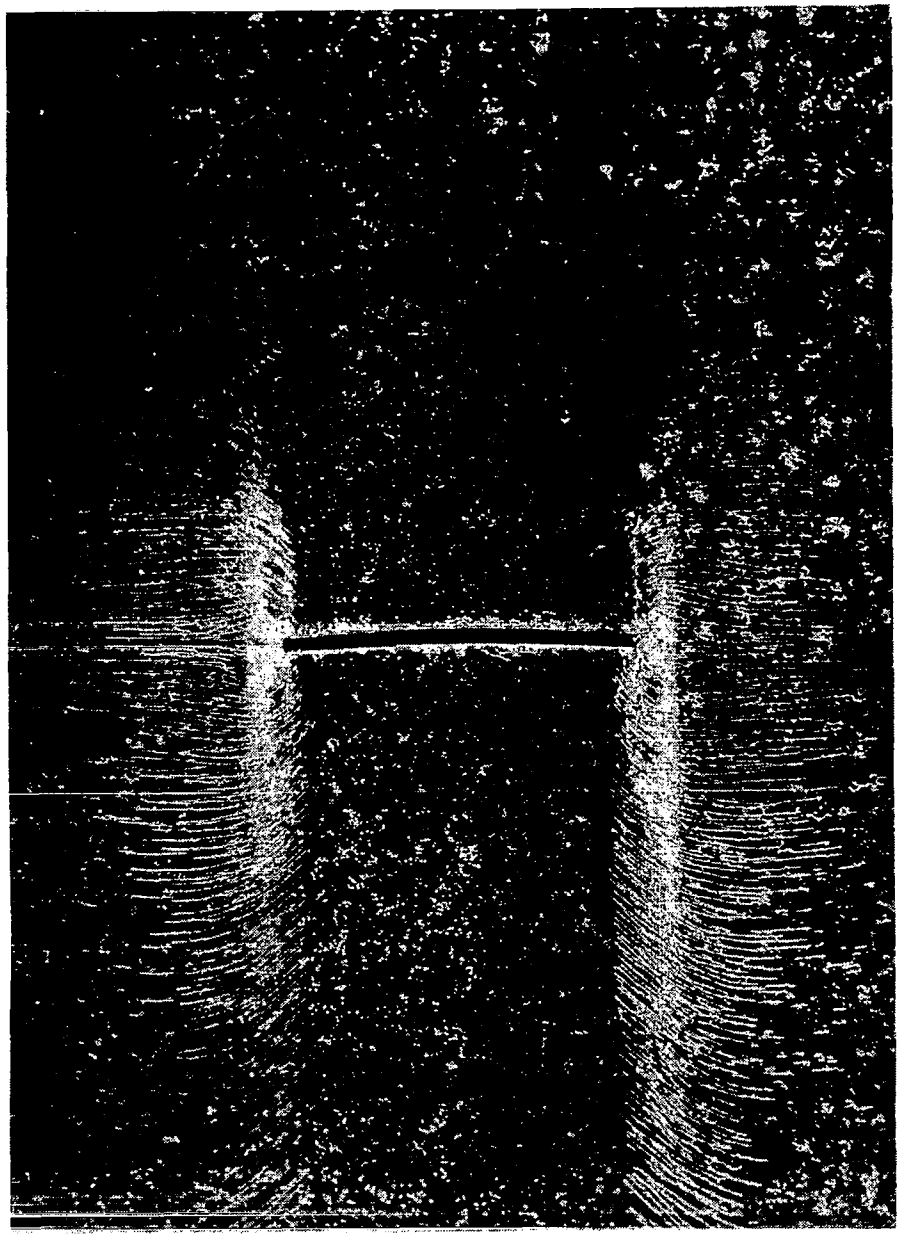

Figure 28. Brittle lacquer crack pattern at 13,200 N showing large transverse progression of the severe damage region.

General Results and Discussion

By examining the sequence of photographs and radiographs previously discussed, one can form a very clear picture of the manner in which damage accumulates in a unidirectional laminate as the failure load is approached. Similar sequences could be presented for the entire range of specimens since the same testing procedure was followed for every specimen used in the study. The two-ply sequence presented, however, was quite typical of all of the tests and it was thus felt that the remainder of the results could be presented more effectively in the form of graphs which show results of all of the tests. Each of the questions raised in the introduction will be answered and discussed thoroughly in the remainder of this section.

The question of thickness effect on the behavior of a unidirectional laminate can now be answered by examining the results of each set of tests. A full range of specimen thicknesses was tested for each panel width and initial notch width. It was observed that the severe matrix damage region as well as the overall appearance of the brittle coating at any given remote strain was very similar for the single-ply, the two-ply, the four-ply, and the eight-ply. The maximum length of this severe longitudinal matrix damage region (at failure) versus the number of plies is plotted for various numbers of crack lengths in Figure (29). Excellent agreement between the length of the observed damage

region and that predicted by the model exists as discussed in the previous section. This behavior is also discussed later in this section when a comparison is made between laminates having different matrix properties.

It was also noted that the dimensions of the transverse damage region were very similar for a given initial notch width. The total number of broken fibers (per ply) ahead of the notch was approximately the same for the one-, two-, four-, and eight-ply laminates, as one can see in Figure (30). Thus, from these two graphs, is it clear that the longitudinal yielding and transverse damage regions depend very little on the number of plys in the unidirectional laminate for relatively thin laminates.

Figure (31) shows the crack opening displacement (COD) for the set of specimens with an initial notch of nineteen broken fibers (or 3.17 mm). It is clear that the COD for each thickness is almost the same for a given percentage of the failure load and therefore the same remote strain. It can also be noted that the first fiber break occurs between 50 and 55 percent of the ultimate failure load for each thickness tested. This phenomenon was observed in all of the tests regardless of notch width or specimen thickness. Figure (31) also indicates that the maximum COD at failure was almost identical for the four thicknesses tested.

Figures (32) and (33) show the COD behavior for specimens with 53 and 89 initially broken fibers, respectively.

It is again clear that the specimen thickness has little effect on the COD for a given percentage of the failure load. The first fiber breaks occur at roughly the same remote strain level for a given notch width, as shown in the earlier graph. The appearance of the brittle lacquer coating was observed to be the same for each thickness as in earlier tests. Also, the stress necessary to break the first fiber, the length of the severe damage region, and the notched strength of each laminate all are in close agreement with the quantities predicted by the mathematical model. This agreement will be discussed in detail later in this section. The similarity in behavior regardless of the specimen thickness (for up to eight plies) was observed for all initial notch widths, thus clearly indicating that a thick panel with unidirectional fibers in each ply can indeed be modeled as an equivalent monolayer.

Another important objective of the present study was to determine the effect of different matrix properties on the fracture behavior of unidirectional laminates. Toward this end, certain sets of panels (as detailed in Table I) were heat-treated to bring their matrix properties close to the 6061-T6 condition instead of the fully annealed 6061-O condition as in the other panels. It was felt that a matrix with a different effective stiffness and yield strength would alter the fracture behavior since it is the matrix alone that transfers load to adjacent fibers in the laminate.

Figure (34) clearly shows that again the COD at a given percentage of the ultimate failure load is not strongly dependent on the number of plys in the laminate for the 6061-T6 panels. As in the 6061-0 tests, the first fiber break occurs at 50 to 55 percent of the failure load. The COD at failure for the four thicknesses is almost the same, though it should be noted that this COD is much less than the COD for a similar panel with an annealed aluminum matrix. This change will be discussed fully, as it will help to determine the effect of matrix properties on the damage growth.

Figure (35) is a remote stress-COD curve for various notch widths in a four-ply, 6061-0 matrix panel. As expected, specimens with short notches are stiffer than specimens with longer notches. Figure (36) shows the COD behavior for the same notch widths in a four-ply, 6061-T6 matrix panel. It is clear that there is a drastic difference in the notch opening under load when the properties of the matrix are changed. The stronger 6061-T6 matrix does not allow the fibers to displace nearly as much as the fully annealed 6061-0 matrix.

It was suggested in [2] that the mathematical model employing the shear-lag assumption could predict accurately the load-COD curves for specimens of various notch widths if certain laminate material properties were known. Specifically, these are the normalized matrix yield stress and the

effective shear stiffness of the fiber-matrix region which are calculated from an experimental load-COD curve. By using these properties, the load-COD behavior for any number of broken fibers could then be predicted accurately. Agreement was demonstrated in [2] for the narrow specimens and short notch lengths presented by Awerbuch and Hahn [6]. Using the much more extensive results of the present study it can be shown that, until large transverse damage is present, the load-COD curves for longer notch widths can also be matched.

In Figure (37) a typical load-COD curve for a 4-ply unidirectional boron/aluminum composite panel is given for specimens having an overall width of 73.1 mm and 89 initially broken fibers. Both a specimen having a 6061-0 annealed matrix and a 6061-T6 matrix are shown, along with the load-COD curves predicted by the model. Using the values for the yield stress, τ_o, and the effective shear stiffness, G_M/h, given in [2], the load-COD curve for the 6061-0 specimen can be closely matched at lower load levels even for longer notches than in [6]. The agreement is not as good for large notch extension as discussed later in this section. It must now be determined if appropriate changes in the two properties mentioned above will allow the model to predict accurately the load-COD curve for the 6061-T6 specimen.

The load-COD curve for the 6061-T6 panel can be matched by increasing the value of the matrix yield stress 3.5 times to 308 X 10^6 N/m^2 and the value of the effective shear stiffness 1.5 times to 172.5 X 10^{12} N/m^3. These changes not only seem quite reasonable but the yield stress change agrees well with standard aluminum properties. The change in the value for G_M/h is attributed more to a change in the shear transfer length, h, than to a change in G_M which should remain relatively constant with any heat-treatment. The yield stress for 6061-T6 aluminum, on the other hand, is roughly 3-4 times the yield stress of 6061-0 aluminum.

The results given in Figures (35), (36), and (37) for a given number of broken fibers are seen to be the same for lower loads, (i. e., below that required for matrix yielding at the crack tip). In this low load range the experimental COD results are also predicted accurately by the orthotropic elasticity solution for a crack as given by Lekhnitskii [18]. For the elasticity solution the results are linear and the shear modulus, G_M, was taken to be the same for both matrix materials. The 6061-0 matrix follows this linear representation for only the first few percent of the total load while the 6061-T6 matrix remains linear over about ten to fifteen percent of the total load. As the material model used in the analysis [2] for the matrix was taken to be elastic-perfectly plastic it is reasonable to expect that the model would fit the experimental results better for the

6061-T6 than for the 6061-0. This is indeed indicated by figure (37). The fact that the 6061-0 calculated results have a different initial slope than the experimental results also follows from this bi-linear fit to the highly non-linear behavior of the annealed matrix.

The major deviation from the predicted curves occurs after several fibers have broken and the notch has begun to extend a significant amount. The extent of transverse notch extension for various notch widths and matrix tempers is shown in Table (IV) below.

Table IV. Extent of stable notch extension at failure for selected initial notch widths in B/Al panels.

Matrix		2a=3.18 mm W=25.4 mm	2a=9.52 mm W=50.8 mm	2a=15.9 mm W=73.1 mm
6061-0	Constrained Fibers	3	4	5
	Total Number of Broken Fibers	3	8	14
6061-T6	Constrained Fibers	2	3	3
	Total Number of Broken Fibers	2	5	7

It was observed in all cases that the notches in the specimens having annealed matrices ran much further before fracture than the 6061-T6. Matrix yielding and broken fibers

accentuate or increase the notch opening. Thus, the COD for the annealed matrix specimens will be considerably greater than the COD for the T6 matrix at a load level corresponding to significant damage. It should be noted that the number of constrained fibers around which the aluminum matrix is still intact is almost constant for all initial notch widths for a given matrix temper. This number of constrained fibers also agrees with the number required by the mathematical model to fit the strength results.

It was mentioned in the previous section that the appearance of the brittle coating indicated that there may be more than one yield region near the end of the notch. As each successive fiber break occurs, the newly broken fiber can move with respect to the unbroken adjacent fiber. Thus a new region of significant displacement and matrix yielding will form, allowing the COD to increase more than if the matrix remains elastic. At the present time the models of [2] can incorporate only one yield region between the last broken fiber and the first unbroken fiber. Thus, if more than one yield region forms, the model cannot predict accurately the displacements of fibers after the notch extension has begun.

Future plans include the modification of the mathematical model to include a new yield region as each successive fiber is broken during a loading cycle. However, substantial information can be obtained by summarizing the present

experimental data. Figure (38) shows the crack opening displacement at failure as a function of the number of initially broken fibers. Clearly the crack opening displacement for the 6061-T6 panels is substantially less than that of the fully annealed 6061-0 panels. In fact, the difference becomes larger as the number of initially broken fibers is increased. This phenomenon is caused by the relatively large notch extension of the fully annealed specimens. The stronger T6 matrix cannot absorb as much energy through yielding as the annealed matrix, thus the load is transferred to the next unbroken fiber sooner and the notch extension becomes unstable, leading to earlier failure.

The longitudinal damage length as described in an earlier section is plotted as a function of the number of broken fibers in Figure (39). The predicted value for this damage length is obtained by calculating the yield length necessary to reach the breaking stress in the next unbroken fiber through the use of the mathematical model. This value should correspond to the severe damage region on the experimental specimens since there should be no further yielding in the region between fibers once the next fiber has broken and is free to displace. It is clear that the predicted trend of damage growth from the model is a very good indicator of the actual damage present in a unidirectional laminate. The stronger T6 matrix substantially reduces the yielding in the matrix and thus reduces the amount of damage

tolerance possessed by a boron/aluminum laminate. The result of increasing the yield strength of the matrix material used in a unidirectional laminate is thus to make the laminate more notch sensitive and actually weaker than a laminate having a more ductile, energy-absorbing matrix.

The notched strengths of the test panels and the reduction in strength for the 6061-T6 matrix can be studied in Table (V) and in Figure (40). It should again be noted that the effect of the change in matrix properties becomes much more evident as the notch becomes larger; that is, the number of initially broken fibers is increased. As in [2], the strength curve for the fully-annealed 6061-0 matrix specimens can be predicted by the mathematical model using 6 constrained fibers ahead of the notch. It should be remembered that in the damage photograph sequence shown earlier there were approximately 6 constrained fibers ahead of the notch tip even for large notch extension. The strength curve for the 6061-T6 panels can be approximated by using 3 constrained fibers ahead of the notch. This change has physical significance; the stable notch extension is larger for the fully annealed specimens than for the heat-treated specimens. Thus as discussed earlier, the heat-treating of the matrix actually reduces the damage tolerance capabilities of the laminate and makes the unidirectional laminate weaker than one with a fully annealed matrix. It is noted that the notched strengths found in this study for the 6061-T6 matrix

agree well with notched strengths found by Awerbuch and Hahn in [19].

One should be careful in extending this reasoning to even stronger matrix materials in which the transition is made from longitudinal yielding to longitudinal splitting. For example, an epoxy matrix is one in which little yielding is exhibited but longitudinal splits occur at the notch tips under low load. This phenomenon is discussed in [2] and has been observed by many investigators. It is important to realize that once this small split forms, it will quickly grow to the machine grips in an experimental test (or to infinity as predicted by the model). The stress concentrations are then removed and the notched laminate will fail at the net section failure load. Thus the conclusion that a stiffer or stronger matrix will weaken the notched laminate is valid only for matrices that are not brittle enough to form longitudinal splits between fibers at the end of the notch. Some small splitting was observed in the present study in 6061-T6 laminates with very long notches, possibly indicating that the T6 matrix is close to the transition from matrix yielding to splitting.

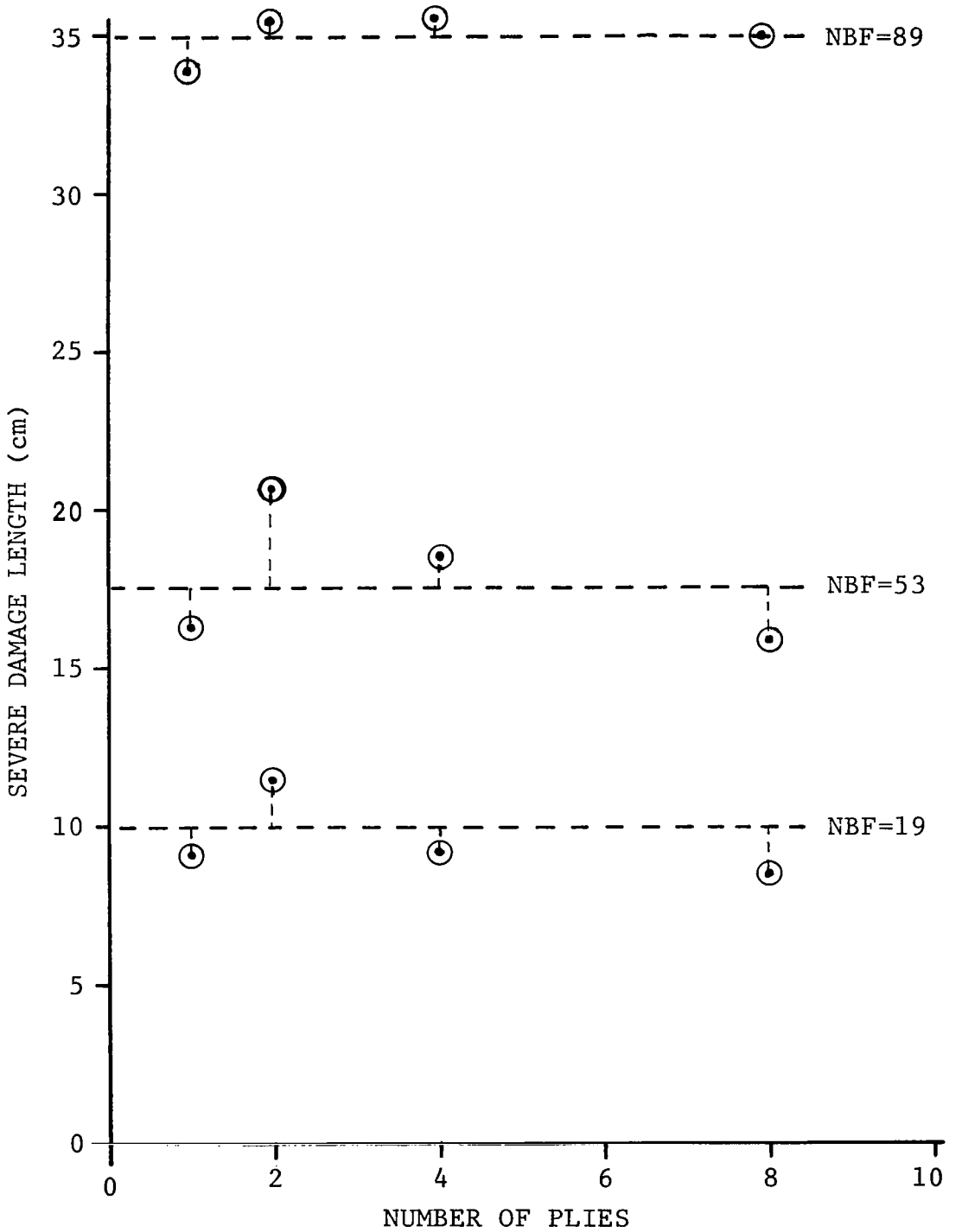

Figure 29. Variation of the severe damage length with the number of plies for selected numbers of broken fibers.

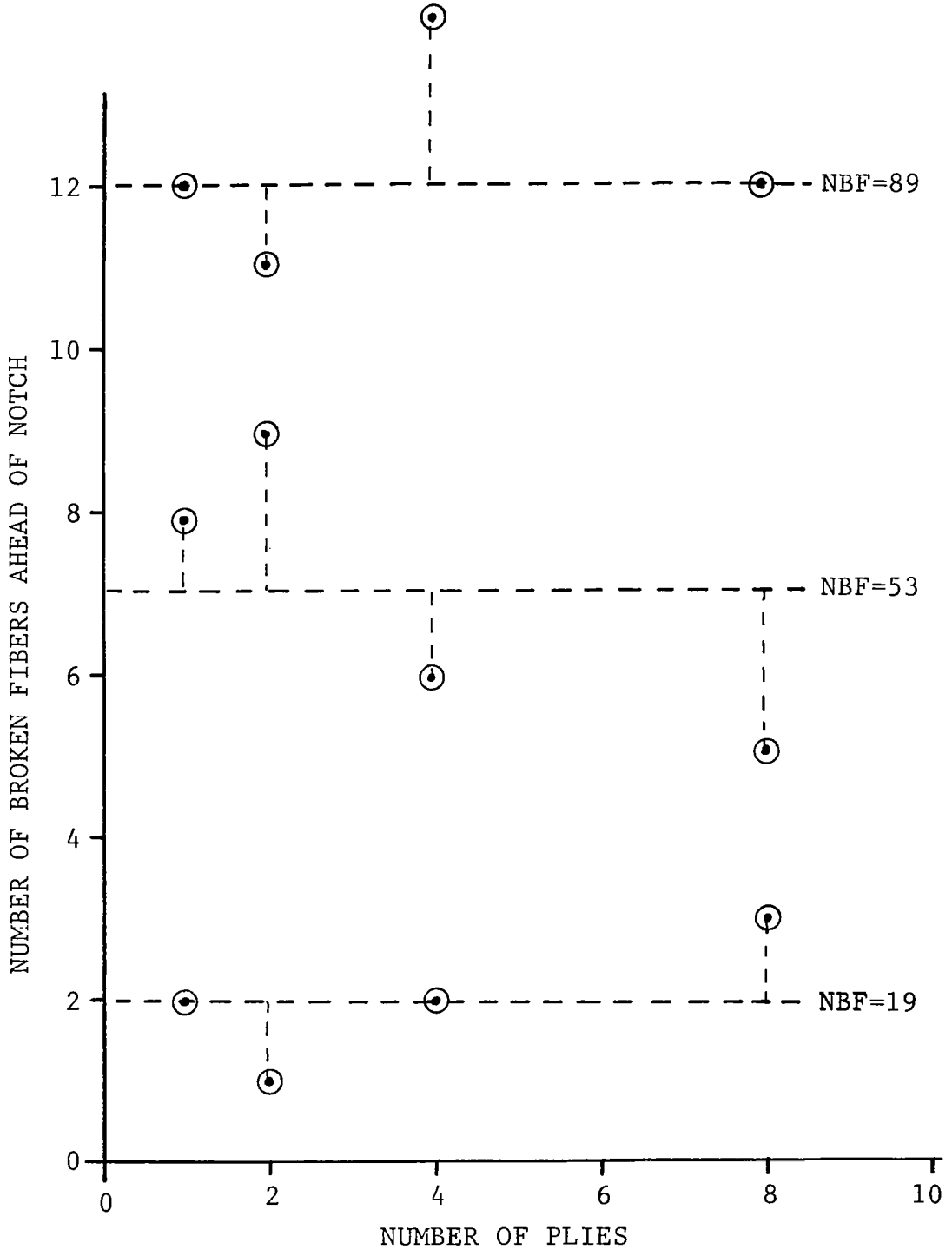

Figure 30. Variation of the transverse notch extension with the number of plies for selected numbers of broken fibers.

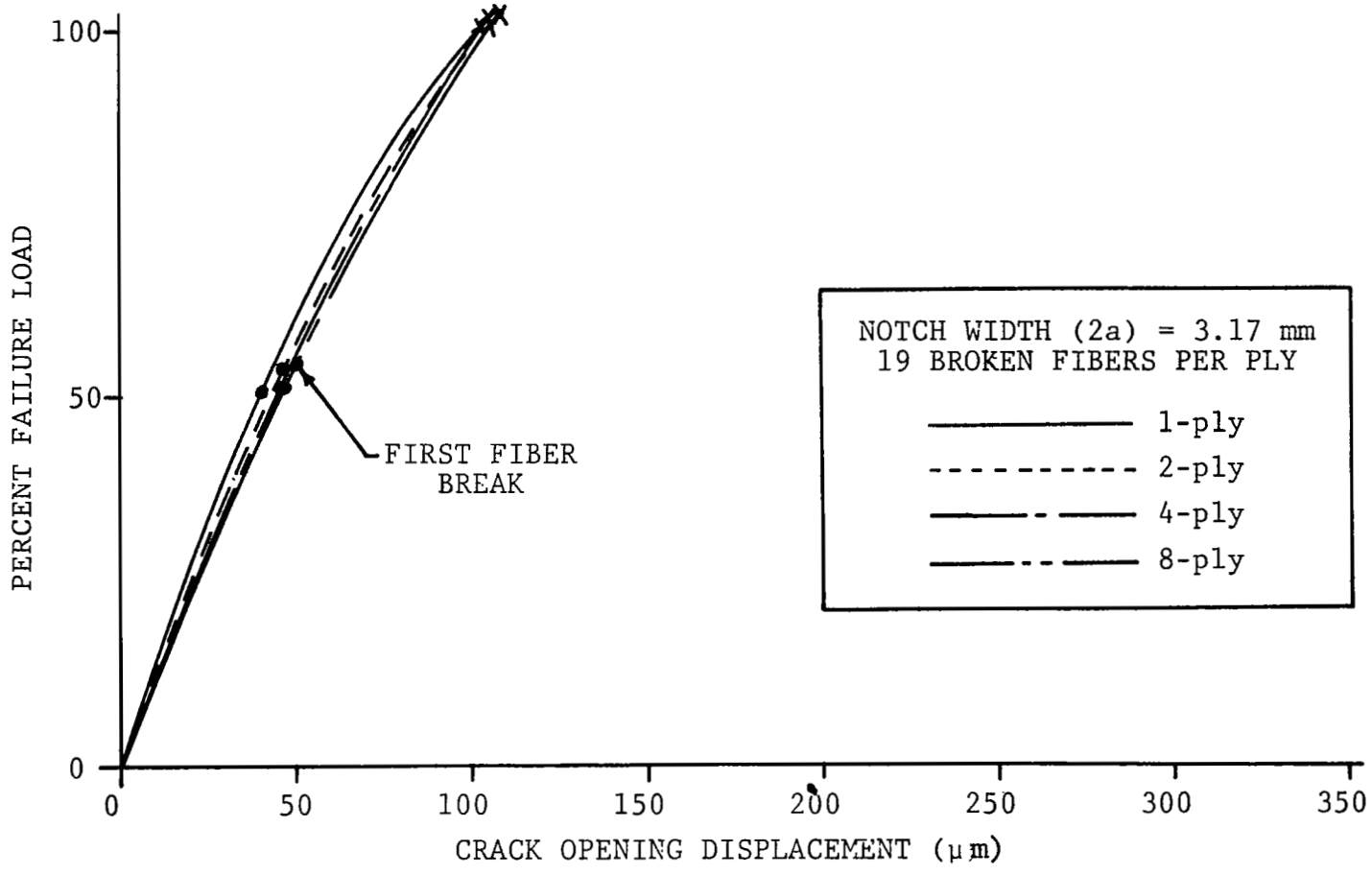

Figure 31. Percent failure load versus crack opening displacement for 19 broken fibers per ply; comparison of various numbers of plies for a 6061-0 Al matrix.

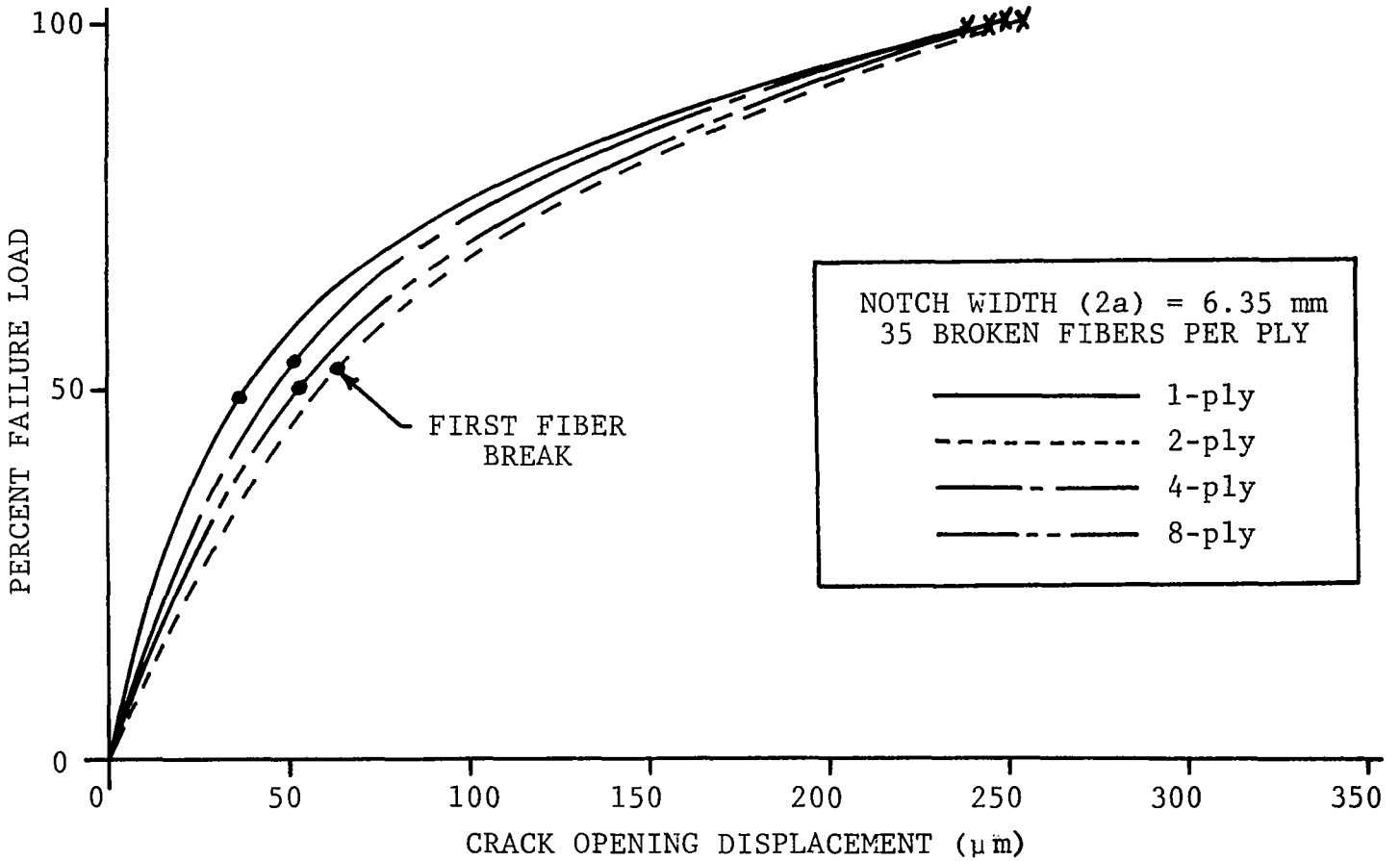

Figure 32. Percent failure load versus crack opening displacement for 35 broken fibers per ply; comparison of various numbers of plies for a 6061-0 Al matrix.

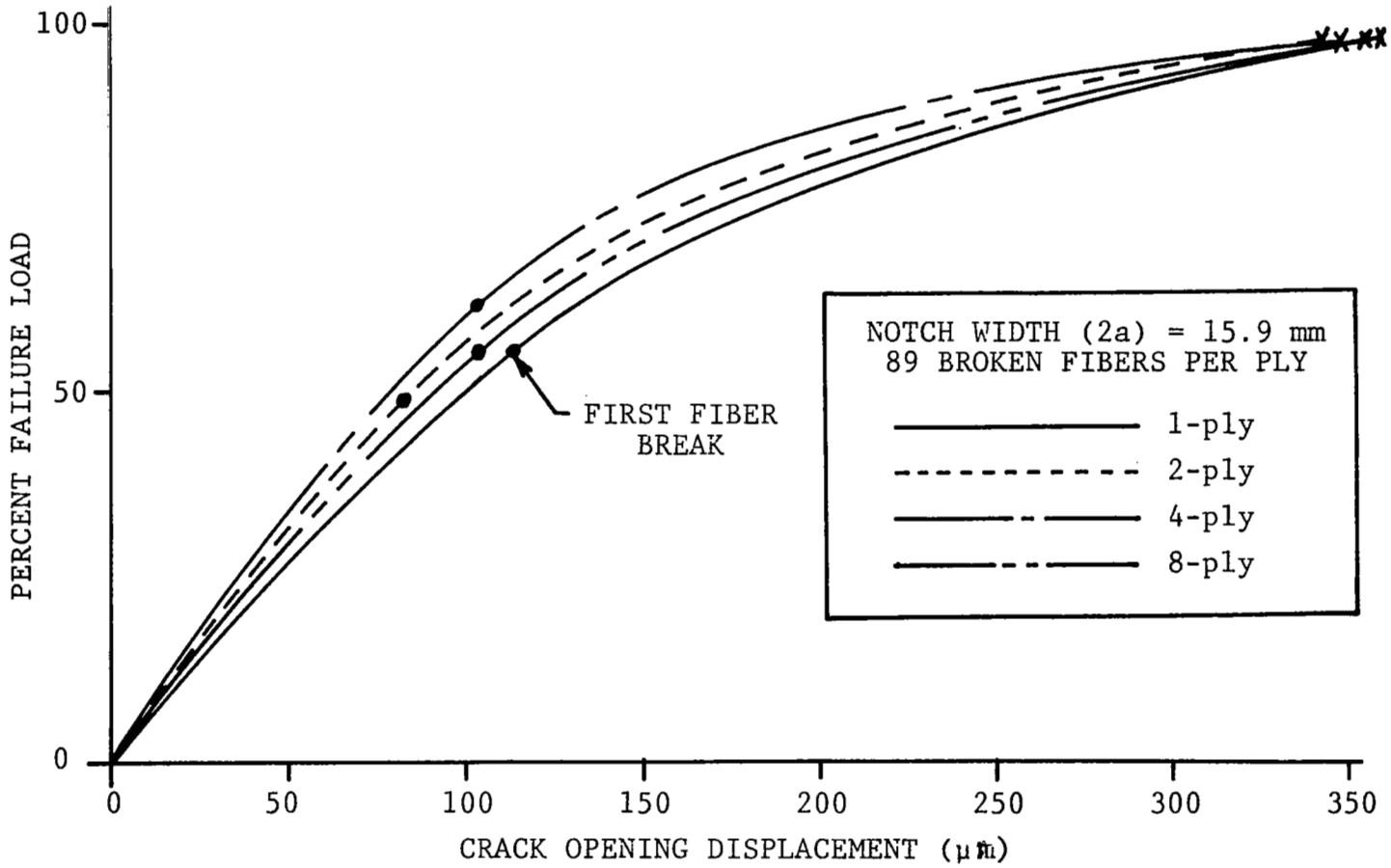

Figure 33. Percent failure load versus crack opening displacement for 89 broken fibers per ply; comparison of various numbers of plies for a 6061-0 Al matrix.

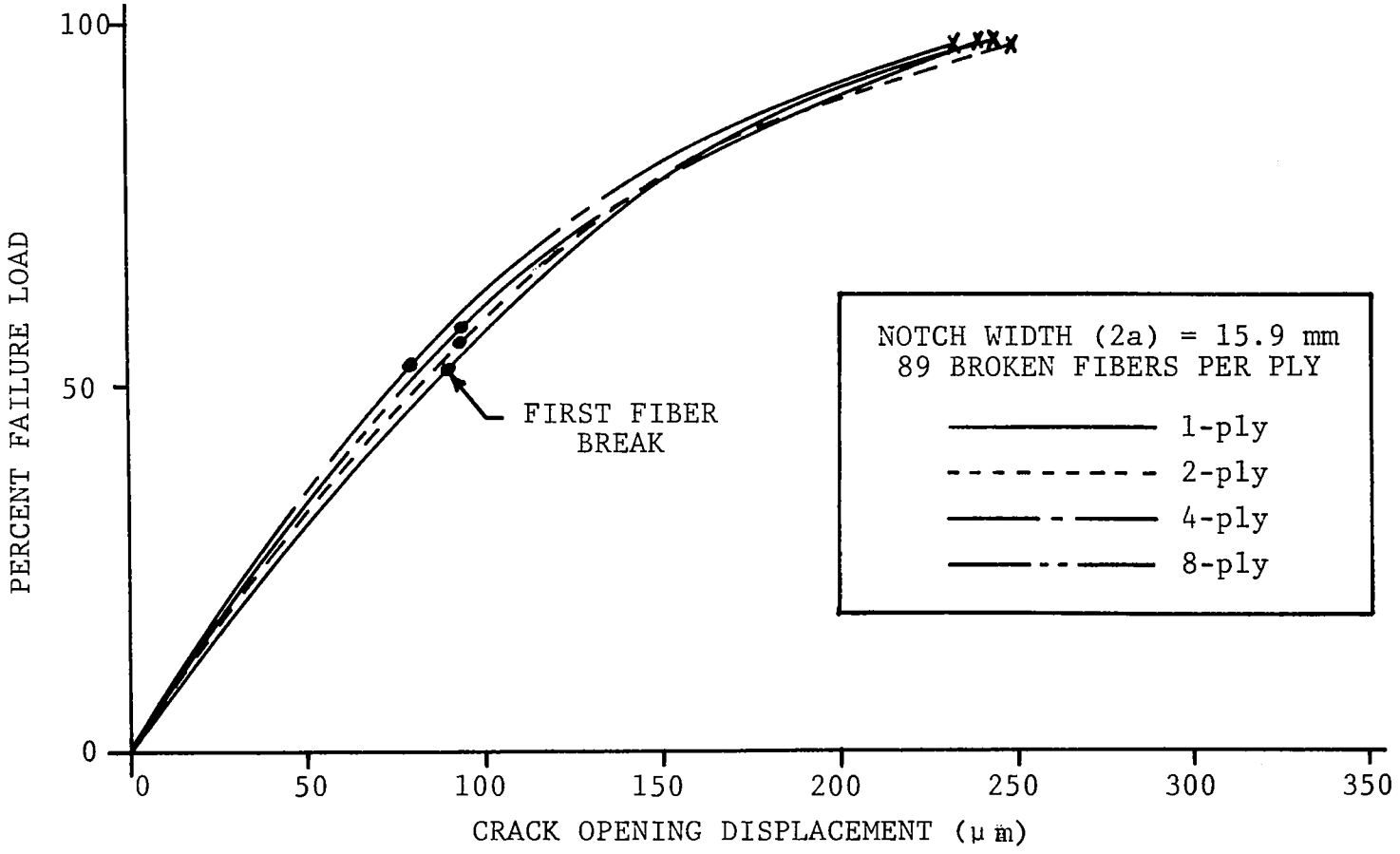

Figure 34. Percent failure load versus crack opening displacement for 89 broken fibers per ply; comparison of various numbers of plies for a 6061-T6 Al matrix.

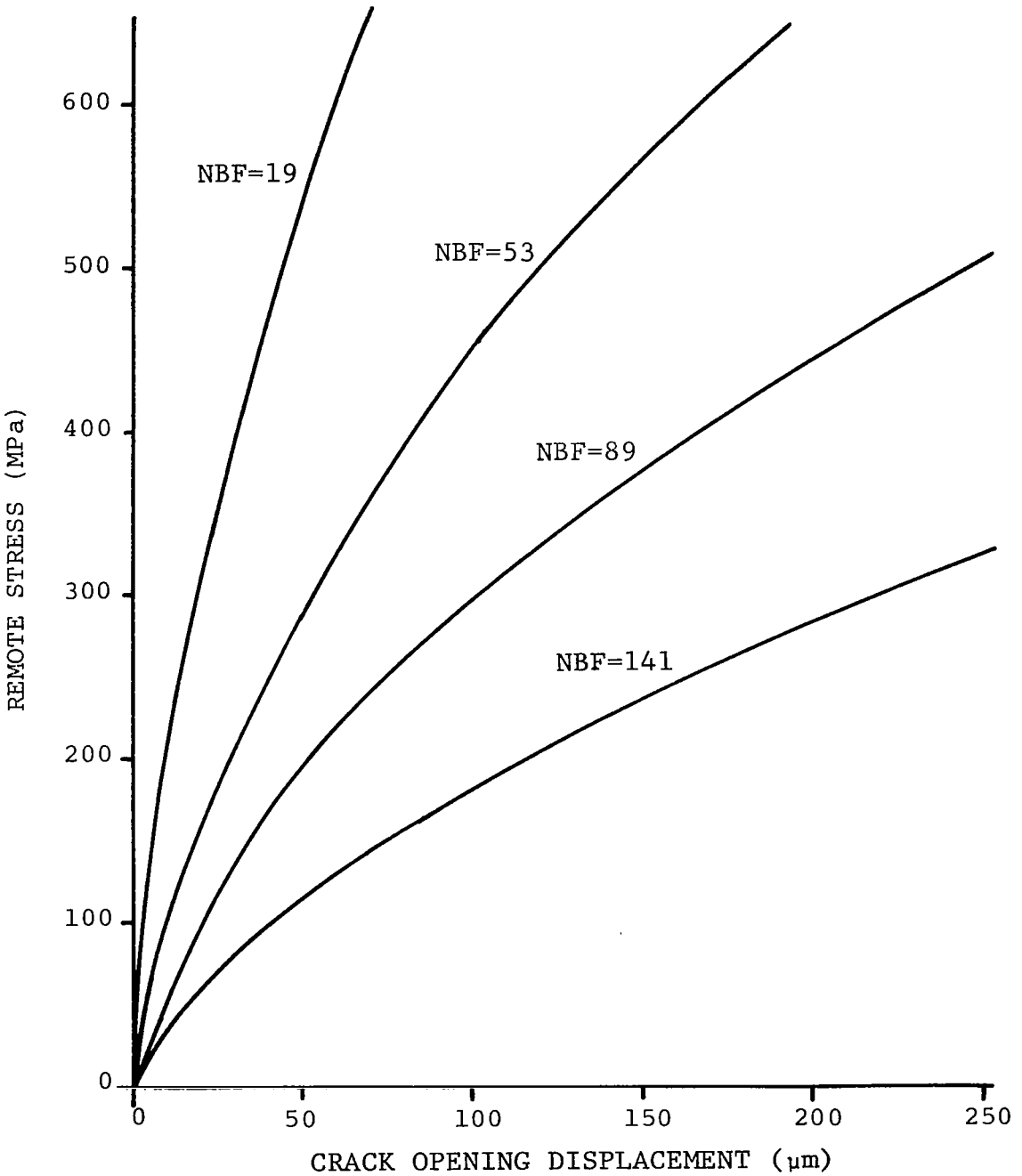

Figure 35. Remote stress versus crack opening displacement for selected numbers of broken fibers in panels having a 6061-0 aluminum matrix.

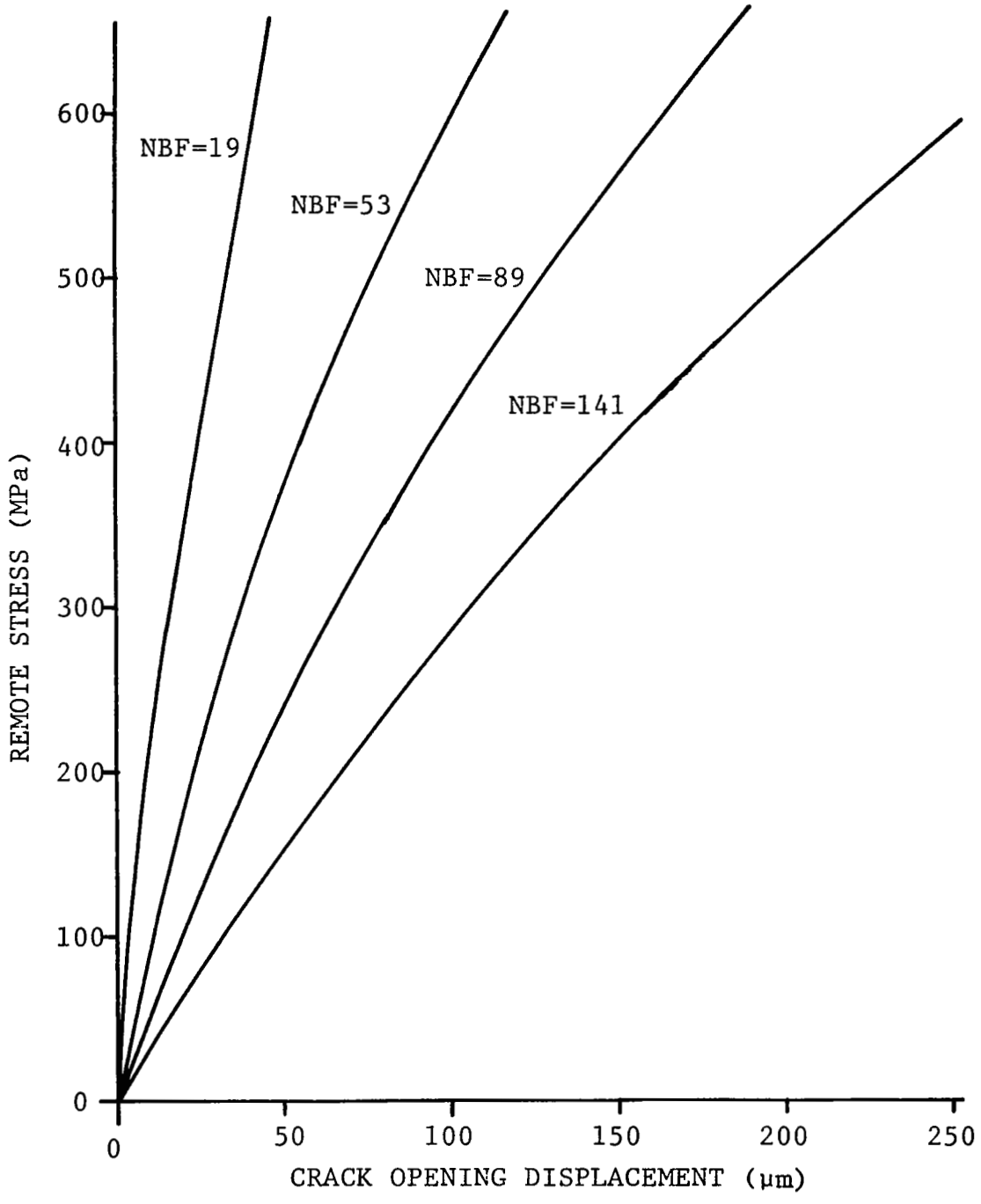

Figure 36. Remote stress versus crack opening displacement for selected numbers of broken fibers in panels having a 6061-T6 aluminum matrix.

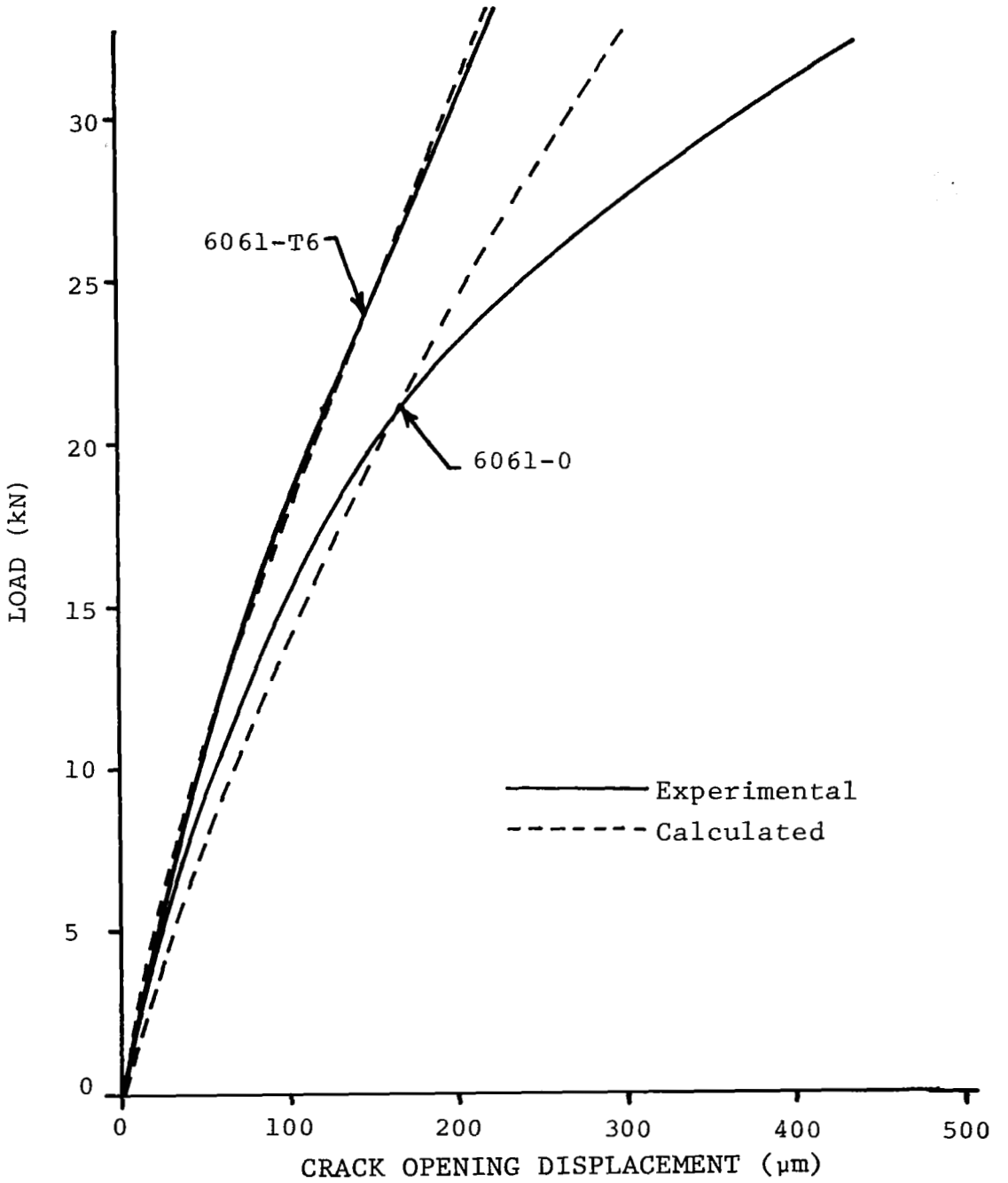

Figure 37. Load versus crack opening displacement for 89 broken fibers in a 4-ply panel; comparison of the analytical and experimental curves.

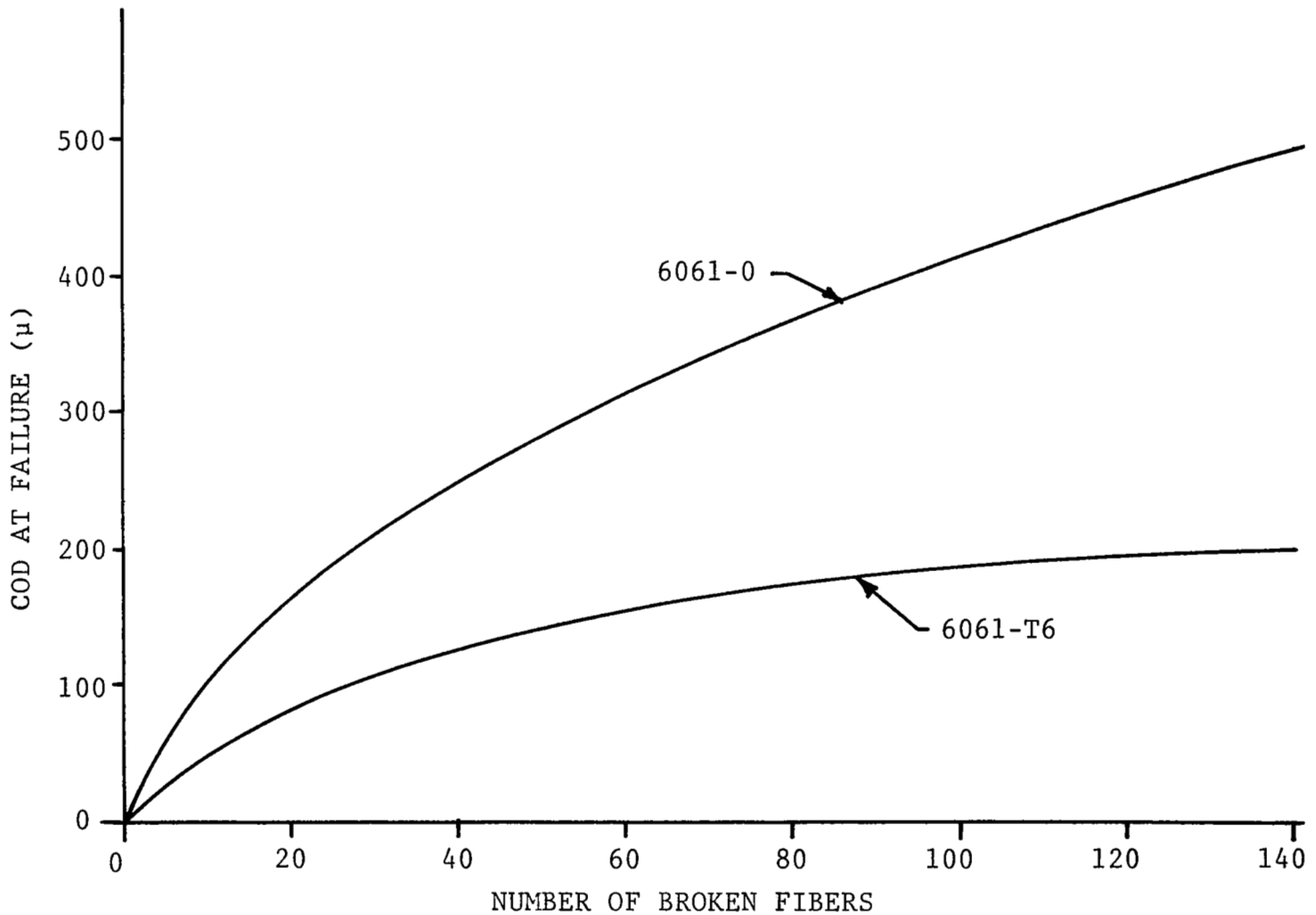

Figure 38. Crack opening displacement at failure as a function of the number of broken fibers; comparison of the different matrix tempers.

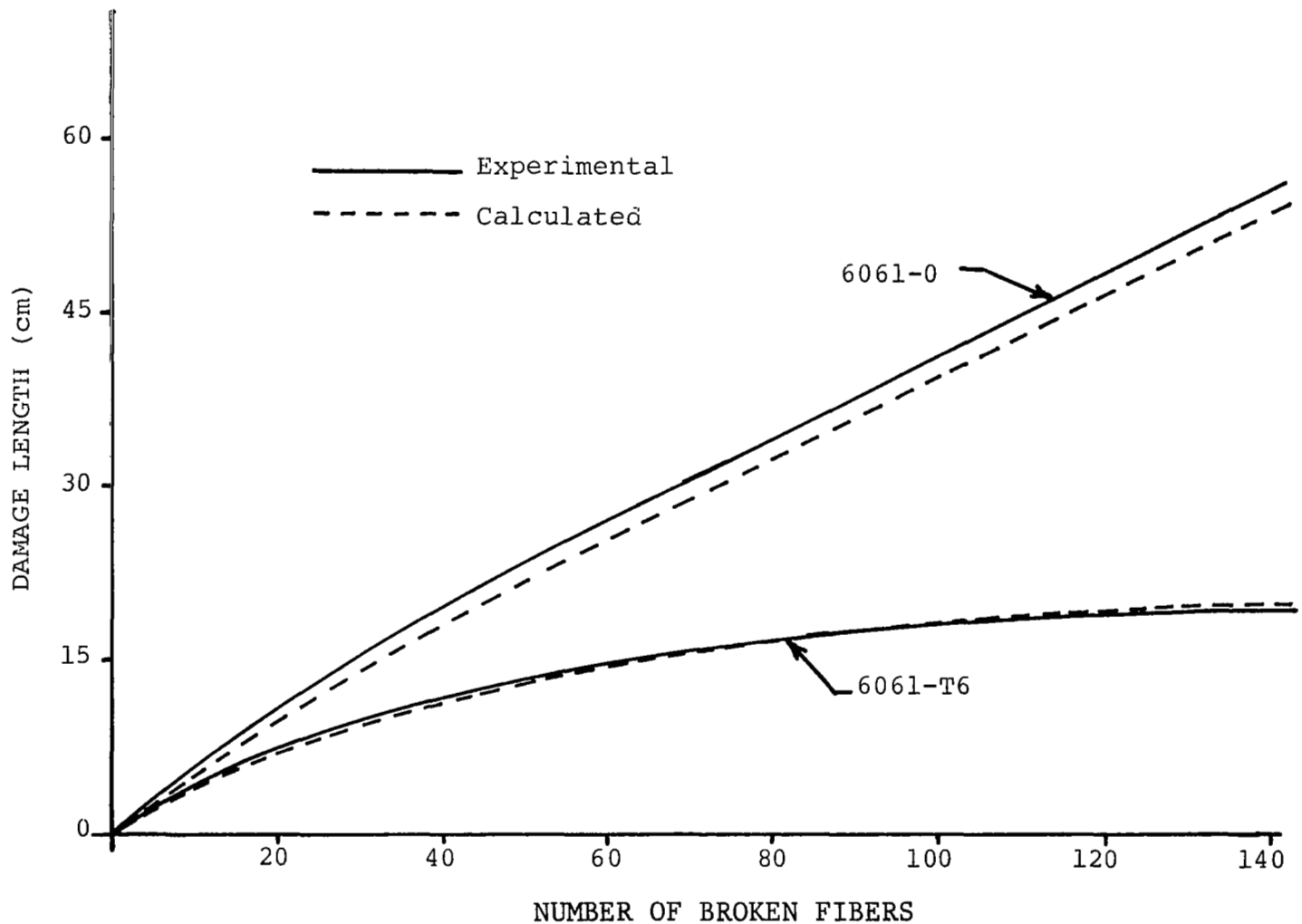

Figure 39. Severe damage length at first fiber break as a function of the number of broken fibers; comparison of the different matrix tempers.

Table V. Strengths of Selected Boron/Aluminum Panels (GPa).

Thickness	Matrix	Unnotched Strengths	Notched Strengths		
			2a=3.18 mm W=25.4 mm	2a=9.52 mm W=50.8 mm	2a=15.9 mm W=73.1 mm
1-ply	6061-0	1.60	1.15	0.95	0.83
	6061-T6	1.59	1.02	0.59	0.53
2-ply	6061-0	1.62	1.00	0.85	0.72
	6061-T6	1.64	0.88	0.64	0.62
4-ply	6061-0	1.59	0.91	0.86	0.82
	6061-T6	1.61	0.93	0.58	0.58
8-ply	6061-0	—	0.94	0.84	0.80
	6061-T6	—	—	—	—

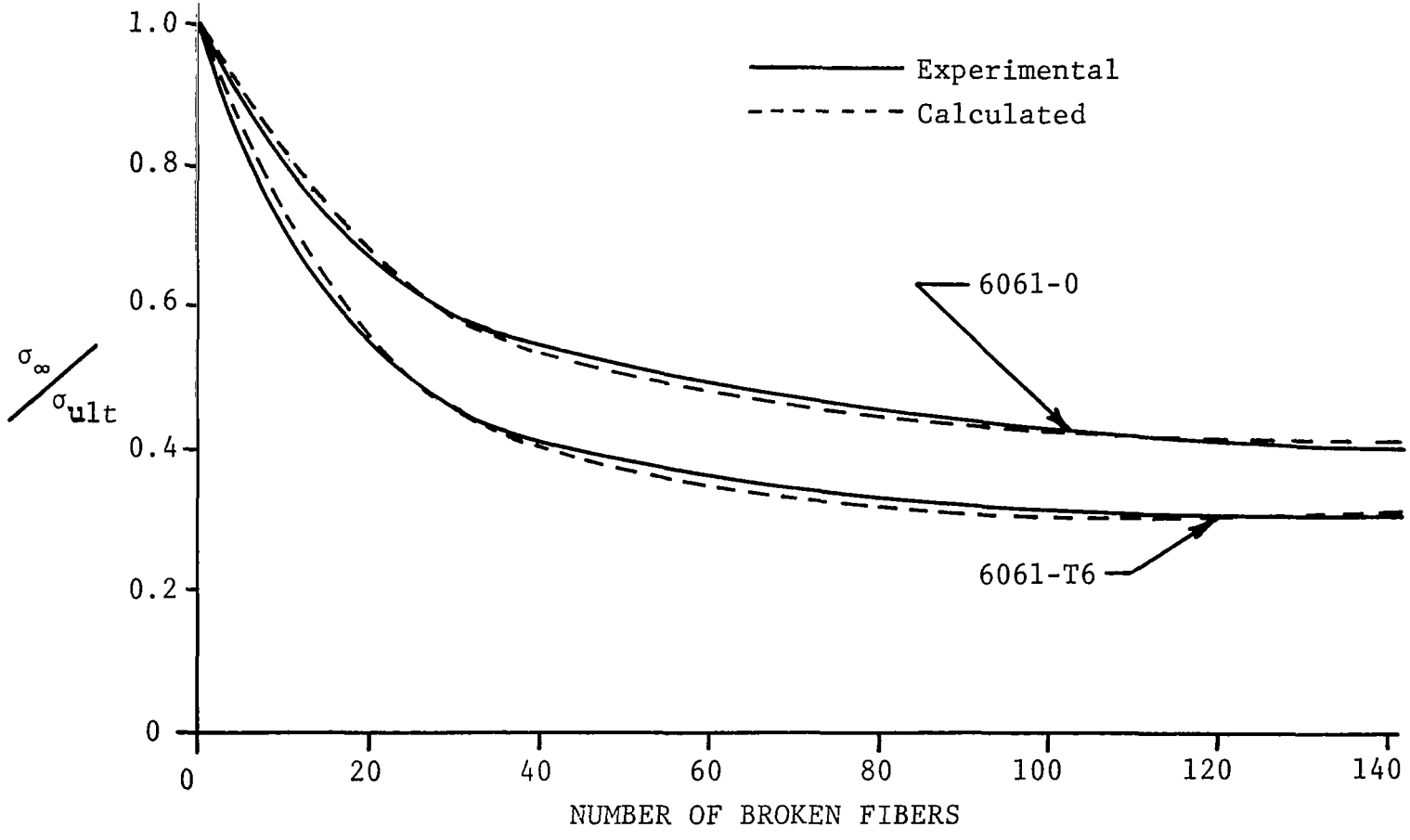

Figure 40. Strength curve: Applied stress as a function of the number of broken fibers; comparison of the different matrix tempers.

CHAPTER V

CONCLUSIONS

Results of this study indicate that the mathematical models presented in [2] based on the classical shear-lag assumption predict the displacements and stresses in a unidirectional fibrous composite laminate with very acceptable accuracy for a wide range of notch lengths, laminate widths, and laminate thicknesses. It is also shown that the crack opening displacement versus load curve predicted by the model is very close to the actual behavior, particularly in the early part of the load cycle before a large number of fibers have broken. The extent of the stable notch extension, that is, the number of broken but constrained fibers, predicted by the model is found to accurately represent that observed in all laminates tested. Also, the dimensions of the longitudinal damage region observed in the laboratory are found to agree well with those calculated by the shear-lag model, as were the notched strengths of the test specimens.

It is demonstrated that the thickness (number of plies) has very little effect on the damage growth and fracture behavior of a unidirectional composite laminate. Longitudinal damage regions and crack opening displacements measured for single-ply, two-ply, four-ply, and eight-ply specimens

are found to be almost identical for a given value of remote strain. The stable notch extension in the form of broken fibers and matrix yielding ahead of the notch is found to be present in the same quantities in specimens having various numbers of plies.

Finally, it is shown that heat-treating the matrix to increase the yield strength actually reduces the notched strength of the laminate. The stronger matrix transfers load to the unbroken fibers at a lower load than the fully annealed matrix, with a substantial reduction in the amount of matrix yielding. The results of these tests indicate that to increase the capability of a laminate to tolerate a defect during a load cycle, the matrix must be able to yield and thereby absorb some energy that would otherwise serve to propagate the notch and cause failure of the laminate.

REFERENCES

1. Goree, J. G., and Gross, R. S., "Analysis of a Unidirectional Composite Containing Broken Fibers and Matrix Damage," Engineering Fracture Mechanics, Vol. 13, (1979), pp. 563-578.

2. Goree, J. G., Dharani, L. R., and Jones, W. F., "Mathematical Modeling of Damage in Unidirectional Composites," NASA CR-3453, 1981.

3. Hedgepeth, J. M., "Stress Concentrations in Filamentary Structures," NASA TN D-882, May 1961.

4. Hedgepeth, J. M., and Van Dyke, P., "Local Stress Concentrations in Imperfect Filamentary Composite Materials," J. Composite Materials, Vol. 1, (1967), pp. 294-309.

5. Zweben C., "An Approximate Method of Analysis of Notched Unidirectional Composites," Engineering Fracture Mechanics, Vol. 6, (1964), pp. 1-10.

6. Awerbuch, J., and Hahn, H. T., "Fracture Behavior of Metal Matrix Composites," Proc. of the Soc. of Engr. Science, Recent Advances in Engineering Science, 1977, pp. 343-350.

7. Grandemange, J. M., and Street, K. N., "The Effect of Notch Root Radius and Thickness on the Static Fracture Toughness of B-Al Composites," Proc. of the 1975 Int. Conference on Composite Materials, Vol. 2, 1975, pp. 1019-1050.

8. Poe, C. C., Jr. and Sova, J. A., "Fracture Toughness of Boron/Aluminum Laminates with Various Proportions of 0^{o} and $\pm 45^{o}$ plies. NASA TP-1707, November 1980.

9. Reedy, E. D., Jr., "On the Specimen Dependence of Unidirectional Boron/Aluminum Fracture Toughness," J. Composite Materials, Supplement, Vol. 14, (1980), p. 118.

10. Rollins, F. R., Jr., "Acoustic Emission from Boron/Aluminum Composites during Tensile Fracture and Fatigue," Tech. Report No. 6, Office of Naval Research, October 1971. (Available from DTIC as AD 731 710.)

11. Grenis, A. F., and Levitt, A. P., "Acoustic Emission of Graphite and Boron Fiber-Reinforced Aluminum Composites During Deformation and Fracture," Army Matl. and Mech. Res. Center AMMRC-TR-75-15, June 1975.

12. Dharani, L. R., Jones, W. F., and Goree, J. G., "Mathematical Modeling of Damage in Unidirectional Composites," Engineering Fracture Mechanics, Vol. 17, (1983), pp. 555-573.

13. Dharani, L. R., "Analysis of a Hybrid, Unidirectional Composite Laminate with Damage," Ph.D. Dissertation, Engineering Mechanics, Clemson University, August 1982.

14. Yeow, Y. T., Morris, D. H., and Brinson, H. F., "The Fracture Behavior of Graphite/Epoxy Laminates," Experimental Mechanics, Vol. 19, (1979), pp. 1-8.

15. Chaturvedi, S. K., and Agarwal, B. D., "Brittle Coating Analysis of Orthotropic Materials," Int. J. of Engr. Science, Vol. 17, (1979), pp. 169-174.

16. Reedy, E. D., Jr., "Large Strain Shear Response of Unidirectional Boron/Aluminum," Proc. of the JSME/SESA Conference on Experimental Mechanics, Hawaii, May 1982.

17. Reedy, E. D., Jr., "Notched Unidirectional Boron/Aluminum: Effect of Matrix Properties," J. Composite Materials, Vol. 16, (1982), pp. 495-509.

18. Lekhnitskii, S. G., "Theory of Elasticity of an Anisotropic Body," Holden-Day, San Francisco, 1963.

19. Awerbuch, J., and Hahn, H. T., "Crack-Tip Damage and Fracture Toughness of Boron/Aluminum Composites," J. Composite Materials, Vol. 13, (1979), pp. 82-107.

1. Report No.	2. Government Accession No.	3. Recipient's Catalog No.
NASA CR-3753		

4. Title and Subtitle	5. Report Date
FRACTURE BEHAVIOR OF UNIDIRECTIONAL BORON/ ALUMINUM COMPOSITE LAMINATES	December 1983
	6. Performing Organization Code
7. Author(s)	8. Performing Organization Report No.
James G. Goree and Walter F. Jones	
	10. Work Unit No.
9. Performing Organization Name and Address	
Department of Mechanical Engineering Clemson University Clemson, SC 29631	11. Contract or Grant No. NSG-1297
	13. Type of Report and Period Covered
12. Sponsoring Agency Name and Address	Contractor report
National Aeronautics and Space Administration Washington, DC 20546	14. Sponsoring Agency Code

15. Supplementary Notes

Langley technical monitor: Clarence C. Poe, Jr.
Final Report

16. Abstract

An experimental investigation dealing with the fracture behavior of unidirectional boron/aluminum composite laminates was conducted in order to verify the results of mathematical models developed by the authors. These models predict the stresses and displacements of fibers and the amount of damage growth in a center-notched lamina as a function of the applied remote stress and the matrix and fiber material properties. The damage may take the form of longitudinal yielding and splitting in the matrix as well as stable transverse damage consisting of broken fibers and matrix yielding ahead of the notch. A brittle lacquer coating was used to detect the yielding in the matrix while X-ray techniques were used to determine the number of broken fibers in the laminate.

The notched strengths and the amounts of damage found in the specimens agree well with those predicted by the mathematical model. It was shown that the amount of damage and the crack opening displacement does not depend strongly on the number of plies in the laminate for a given notch width. By heat-treating certain laminates to increase the yield stress of the aluminum matrix, the effect of different matrix properties on the fracture behavior was investigated. It was demonstrated that the stronger matrix will actually weaken the notched laminate by decreasing the amount of matrix damage and thereby making the laminate more notch sensitive.

17. Key Words (Suggested by Author(s))	18. Distribution Statement
Composite laminate, Fracture, Crack growth, Boron/Aluminum	Unclassified-Unlimited Subject Category 24

19. Security Classif. (of this report)	20. Security Classif. (of this page)	21. No. of Pages	22. Price
Unclassified	Unclassified	112	A06

For sale by the National Technical Information Service, Springfield, Virginia 22161

NASA-Langley, 1983